Regulation of somatostatin secretion from pancreatic δ-cells

Elisa Vergari

Green Templeton College

A thesis submitted for the Degree of Doctor of Philosophy at the University of Oxford



OXION-Wellcome Trust DPhil Programme

Oxford Centre for Diabetes Endocrinology & Metabolism

University of Oxford

Michaelmas Term 2016

To my beloved family
and to my lifelong friends
Anna and Laura

“fatti non foste a viver come bruti,

ma per seguir virtute e canoscenza”

(Dante Alighieri – Inferno, Divina Commedia –)

(you were not born to live like brutes,

but to follow virtue and knowledge)

STATEMENT OF AUTHORSHIP

I hereby declare that this is entirely my own work with the following exceptions:

The data reported in Figure 6-2(A-B), Figure 6-4(A) and Figure 6-13(A-B) were generated by Dr. Albert Salehi at the University of Lund (in Malmö). The experiments summarised in Figure 6-11 and Figure 6-12 were performed together with Dr. Salehi at the University of Lund (in Malmö).

The data reported in Figure 4-10(A-B) were generated by Dr. Quan Zhang. They are included for the sake of completion.

The correlation analysis of time series, included in Chapter 5, was carried out in collaboration with Dr. Linford Briant, who created the script (Appendix 3).

The data included in Appendix 2 are entirely my work. They are included in the Appendices as they were not entirely pertinent with the content of the whole thesis. However, they do have an important bearing in some aspects.

ACKNOWLEDGMENTS

I wish to express my sincere gratitude to my supervisor Professor Patrik Rorsman. Thank you for involving me in such exciting and challenging projects. After all, it has been really a great experience!!! Thank you also for the independence and the freedom that you gave me to develop my ideas. Your enthusiasm and excitement for science have been extremely contagious!!!

I am deeply indebted to Dr. Julie Adam for having taught me everything about animal work and having kindly reviewed this thesis. Without your help, this thesis would have not been possible!! There are not enough words to thank you for all you have done for me during these years!!!

I owe many thanks to Dr. Margarita Chibalina for kindly assisting me at every stage of my DPhil. Thank you for the help with molecular biology issues and for being available anytime that I needed. I think that the day that I tried to dissolve the agar was epic!!!

I am grateful to Dr. Andrei Tarasov. The imaging techniques dramatically improved after you have joined the lab and I have benefited a lot from all your suggestions!! Thank you!!

I would like to express my greatest gratitude to Dr. Linford Briant. Finally, with your correlation analysis we have been able to explore the synchronization of δ-cells. Your help has been invaluable! Grazie mille!!!

Mahdieh, my lab buddy, it would have been not half as much fun without you. Thanks for the nice time inside and outside of the lab, as well as for the interesting scientific discussions while looking for our “glory”! I am really happy to have met you and have shared this experience with you!! Best of luck for your DPhil!!!

I am truly indebted to Mr. David Wiggins for having been a great source of support in many ways over the years. Many many thanks!!!

I want to thank Dr. Juris Galvanovski for having introduced me to live confocal imaging. Thank you for sharing your knowledge, for your wise advice and for all the interesting discussions!

I wish to thank Dr. Albert Salehi and Dr. Reshma Ramracheya for the collaboration with the insulin project and Dr. Quan Zhang for the collaboration with all the δ-cell projects.

Thanks to everyone in the Rorsman's lab for making it a nice place to work with a happy and joyful atmosphere!!!

Dr. Anne Clark, thank you very much for having encouraged me to write the δ-cells part in our review and for your interest in my research!!

Many thanks to Mr. Andrew Worth to help me out with the FACS experiments.

I am extremely indebted to my college advisor, Dr. Lindy Castell. Thank you very much for all your support during the difficult times and thank you very much for always caring about me.

A special thank goes to all the friends I met here in Oxford: Sara, Maria Pia, Alessandra, Astrid, Nicoletta, Fahd, Siddharth, Thanasis and Marc. Thanks for all the nice times we spent together!!!

Many thanks to all my friends back home especially my best friends Anna and Laura for always being there! Thank you very much for your visits to Oxford and for all the reunions in the "valleys". Amiche, infinitamente grazie!!!

Last but not least un ringraziamanto veramente speciale va alla mia amata famiglia per essermi sempre vicina, avermi sempre s(o)upportato e essere sempre stata fiera di me! Grazie al babbo, a Francesco e in particolare alla mamma che con il suo entusiasmo e ottimismo mi ha sempre incoraggiato e dato la forza di guardare avanti e superare le difficoltà. Vi voglio bene Grazie!

TABLE OF CONTENTS

ACKNOWLEDGMENTS **1**
ABSTRACT **7**
ABBREVIATIONS **9**
LIST OF FIGURES **11**
LIST OF TABLES **14**
1 INTRODUCTION **15**
1.1 Anatomy and physiology of the pancreas 15
1.2 Regulation of blood glucose levels and diabetes 16
1.3 Cellular arrangement of pancreatic islets 18
1.4 Pancreatic δ-cells 19
1.5 Somatostatin production and somatostatin receptors 20
1.6 Role of somatostatin in the islets 22
1.7 Regulation of δ-cells somatostatin secretion 23
1.8 Cross-talk between pancreatic islet cells 24
1.9 Somatostatin as a paracrine regulator of glucagon secretion 27
AIM OF THE THESIS **29**
2 MATERIALS AND METHODS **30**
2.1 Establishment of SST-Cre mouse colony 30
2.2 Mouse genotyping 32
2.3 Intraperitoneal glucose tolerance test (ipGTT) 36
2.4 Intraperitoneal insulin tolerance test (ipITT) 37
2.5 Pancreatic islets isolation and culture 38
2.6 Immunocytochemistry 38
2.7 FACS Analysis (flow cytometry) 39
2.8 RNA extraction, cDNA synthesis and quantitative PCR 41
2.9 Secretion assay 43
2.10 Intracellular [Ca^{2+}] measurements 45
2.11 Statistical analysis 47
3 CHARACTERIZATION OF SST-Cre-GCaMP3 MICE **48**
3.1 Introduction 48
3.2 Materials and Methods 50

3.2.1 Intracellular [Ca^{2+}] recording: parallel measurements of GCaMP3 and fura red 50
3.2.2 Simultaneous $[Ca^{2+}]_i$ imaging and hormone secretion measurements..... 51
3.3 Results..... 52
3.3.1 Physiological characterization of SST-Cre-GCaMP3 mice 52
3.3.2 Characterization of SST-Cre-GCaMP3 islets..... 54
3.3.3 Characterization of Ca^{2+} signalling in δ-cells..... 59
3.3.4 Problems with SST-Cre-mice..... 65
3.4 Discussion..... 67
3.4.1 Validation of SST-Cre-GCaMP3 mouse model..... 67
4 CONTROL OF SOMATOSTATIN SECRETION 70
4.1 Introduction 70
4.2 Materials and methods..... 73
4.2.1 Intracellular [Ca^{2+}] imaging..... 73
4.2.2 Dynamic hormone secretion measurements..... 74
4.2.3 Parallel measurement of membrane potential and $[Ca^{2+}]_i$ 75
4.3 Results..... 76
4.3.1 Glucose sensing in δ-cells 76
4.3.2 Effect of glucose and modulation of K_{ATP} channels on δ-cells $[Ca^{2+}]_i$ 78
4.3.3 Characterization of Ca^{2+} channels in δ-cells 82
4.3.4 Ca^{2+}-induced Ca^{2+} release mechanism regulates somatostatin secretion 85
4.3.5 Role of intracellular Ca^{2+} on somatostatin release 88
4.4 Discussion..... 97
4.4.1 Stimulus-secretion coupling in pancreatic δ-cells..... 97
5 HOMOLOGOUS INTERACTION BETWEEN δ-CELLS..... 103
5.1 Introduction 103
5.1.1 Connexins..... 103
5.1.2 Pannexins 104

5.2 Materials and methods 107
5.2.1 Intracellular [Ca^{2+}] imaging 107
5.2.2 Correlation analysis of [Ca^{2+}]$_i$ imaging time series in δ-cells 107
5.3 Results 108
5.3.1 Assessment of electrical coupling in δ-cells 108
5.3.2 Analysis of gap-junctions expression in δ-cells 116
5.3.3 Role of connexin-36 in δ-cells 118
5.3.4 Role of pannexins in δ-cells 119
5.4 Discussion 123
5.4.1 δ-cells crosstalk and its role on somatostatin secretion . 123
6 PARACRINE REGULATION OF GLUCAGON SECRETION BY INSULIN-INDUCED STIMULATION OF SOMATOSTATIN RELEASE 128
6.1 Introduction 128
6.2 Materials and methods 131
6.2.1 Generation of δ-cell specific insulin receptor knockout mice 131
6.2.2 Assessment of Cre recombination in pancreatic δ-cells from SIRKO mice 133
6.3 Results 135
6.3.1 Effect of exogenous insulin on somatostatin release 135
6.3.2 Endogenous insulin regulates somatostatin release 140
6.3.3 Validation of insulin receptor knockout in δ-cells from SIRKO mice 143
6.3.4 Physiological characterization of SIRKO mice 146
6.3.5 Reduced hypoglycaemic effect in female SIRKO mice .. 149
6.3.6 Insulin effect in vitro in SIRKO mice 151
6.3.7 Use of somatostatin receptor blocker 2 155
6.4 Discussion 157
6.4.1 Insulin potentiates somatostatin release 157
6.4.2 Glucagonostatic effect of insulin is mediated by somatostatin 159

6.4.3 Role of SSTR2 receptor antagonist 162
7 CONCLUSIONS 165
8 APPENDICES 168
8.1 Appendix 1: Generation of SST-Cre-GCaMP3 mice 168
8.2 Appendix 2: Characterization of the human somatostatinoma cell line QGP-1 170
8.2.1 Introduction 170
8.2.2 Materials and methods 170
8.2.3 Results 173
8.2.4 Discussion 179
8.3 Appendix 3: Correlation analysis of times series 181
8.3.1 Correlation analysis of times series 181
8.3.2 Example script for correlation analysis 183
9 REFERENCES 186

ABSTRACT

The somatostatin-secreting δ-cell is the least abundant cell type in the pancreatic islet and this may explain why very little is known about its role and function. In this thesis, I have characterized the SST-Cre-GCaMP3 mouse model in which the genetically encoded Ca^{2+} sensor GCaMP3 is expressed in somatostatin-expressing cells. Using these mice, glucose-induced somatostatin secretion was found to be inhibited by a K_{ATP} channel-dependent membrane depolarization and amplified by Ca^{2+}-induced Ca^{2+} release (CICR) mediated by activation of ryanodine receptor Ca^{2+} release channels.

Interestingly, glucose-induced $[Ca^{2+}]_i$ oscillations in δ-cells did not correlate with electrical activity and persisted also when the cells were clamped at -70 mV, consistent with an important role of CICR. In addition, this study led to the finding that $[Ca^{2+}]_i$ oscillations in different δ-cells display a synchronous behaviour upon glucose stimulation.

The role of somatostatin in the paracrine regulation of glucagon secretion was also addressed. Application of insulin inhibited glucagon secretion and stimulated somatostatin release. Using the SST-GCaMP3 mice, it was demonstrated that insulin exerts a direct stimulatory effect on δ-cells $[Ca^{2+}]_i$ oscillations. After δ cell-specific ablation of insulin receptor, insulin had no inhibitory effect on glucagon secretion. This was paralleled by the loss of insulin-induced stimulation of somatostatin secretion.

Collectively, these data suggest that insulin stimulates somatostatin release, which in turn inhibits glucagon secretion. This finding highlights the pivotal role of somatostatin in the regulation of glucagon secretion. It also raises the interesting possibility of using a somatostatin receptor antagonist as an adjunct to insulin therapy to minimize the risk of hypoglycaemia.

ABBREVIATIONS

AMP	Adenosine 5′-monophosphate
ADP	Adenosine 5′-diphosphate
ANOVA	Analysis of Variance
AUC	Area under the curve
ATP	Adenosine 5′-triphosphate
bp	Base pair(s)
BSA	Bovine serum albumin
Ca^{2+}	Calcium
$[Ca^{2+}]_i$	Intracellular free Ca^{2+} concentration
cAMP	Adenosine 3′,5′-cyclic monophosphate
CBX	Carbenoxolone
CICR	Ca^{2+}-induced Ca^{2+} release
Ctrl/CTRL	Control
DNA	Deoxyribonucleic acid
diH_2O	Deionized water with the resistivity 18.2 MΩ
ER	Endoplasmic reticulum
FACS	Fluorescence-activated cell sorting
FBS	Foetal Bovine Serum
fmol	Femtomolar
Glc	Glucose
h	Hour(s)
IR	Insulin receptor
ipGTT	Intraperitoneal glucose tolerance test
ipITT	Intraperitoneal insulin tolerance test
IP_3	Inositol 1,4,5-triphosphate
IP_3R	Inositol 1,4,5-triphosphate receptor
$[K^+]_o$	Extracellular K^+ concentration
K_{ATP} channel	ATP sensitive K^+-channel
Kir6.2	Inward rectifier potassium channel
min	Minute(s)

ml	Millilitre
mM	Millimolar
mRNA	Messenger ribonucleic acid
Na^+	Sodium
$[Na^+]_i$	Intracellular sodium concentration
NAADP	Nicotinic acid adenine dinucleotide phosphate
ng	Nanogram(s)
nM	Nanomolar
NS	Not significant
PBS	Phosphate-buffered saline
PCR	Polymerase chain reaction
PFA	Paraformaldehyde
RFP	Red fluorescent protein
RIA	Radioimmunoassay
RNA	Ribonucleic acid
ROI	Region of interest
RPMI	Roswell Park Memorial Institute
RT	Room temperature
RT-PCR	Reverse transcription PCR
RyR	Ryanodine receptor
s	Second(s)
SE	Standard error
SERCA	Sarco-endoplasmic reticulum ATPase
SST	Somatostatin
SST-Cre	Cre recombinase expressed exclusively in somatostatin-expressing cells
SSTR	Somatostatin receptor
TAE	Tris-acetate-EDTA
VGCC	Voltage-gated Ca^{2+} channel
µM	Micromolar
µm	Micrometre
µl	Microlitre

LIST OF FIGURES

Figure 1-1 Immunostaining of a mouse pancreatic islet. 16
Figure 2-1 Schematic of the generation of SST-Cre-RFP-GCaMP3 mice.... 31
Figure 2-2 Agarose gel electrophoresis of genotyping PCR products. 35
Figure 2-3 Representative FACS analysis of SST-Cre-RFP cells. 41
Figure 3-1 Physiological characterization of SST-Cre-GCaMP3 mice. 53
Figure 3-2 Confirmation of δ-cell specific GCaMP3 expression in SST-Cre-GCaMP3 islets. 55
Figure 3-3 Insulin, glucagon and somatostatin expression in SST-Cre-GCaMP3 and SST-RFP islet cells. 57
Figure 3-4 Hormones secretion measurements from SST-Cre-GCaMP3 islets. 58
Figure 3-5 Analysis of glucose-stimulated somatostatin release in SST-Cre-GCaMP3 islets. 60
Figure 3-6 Simultaneous imaging of $[Ca^{2+}]_i$ changes in intact islets recorded with fura red and GCaMP3. 62
Figure 3-7 Parallel measurements of hormone secretion and $[Ca^{2+}]_i$ imaging using SST-Cre-GCaMP3 islets. 64
Figure 3-8 Example of leakage in tissues isolated from a SST-Cre-GCaMP3 mouse. 66
Figure 4-1 Current model of glucose-induced somatostatin secretion in mouse δ-cells. 72
Figure 4-2 Procedure to determine the average duration of $[Ca^{2+}]_i$ oscillations. 74
Figure 4-3 Expression of genes involved in glucose metabolism in SST-negative and SST-positive fractions. 77
Figure 4-4 Effect of tolbutamide on $[Ca^{2+}]_i$ in δ-cells. 79
Figure 4-5 Effect of diazoxide on $[Ca^{2+}]_i$ and somatostatin secretion. 81
Figure 4-6 Expression levels of voltage-gated Ca^{2+} channels in SST-negative and SST-positive cells. 82

Figure 4-7 Effect of L-type and R-type Ca^{2+} channels inhibitors on somatostatin release. 84
Figure 4-8 Intracellular Ca^{2+} stores regulate somatostatin secretion..... 87
Figure 4-9 Effect of ryanodine and thapsigargin on δ-cells $[Ca^{2+}]_i$ oscillations. 89
Figure 4-10 Correlation between membrane potential and $[Ca^{2+}]_i$. 91
Figure 4-11 Effect of depolarizing K^+ concentration on $[Ca^{2+}]_i$ in δ-cells. 93
Figure 4-12 Effect of glucose in the presence of depolarizing K^+ concentration. 93
Figure 4-13 Effect of ryanodine and thapsigargin in the presence of depolarizing K^+ concentration..... 94
Figure 4-14 Effect of acidic endolysosomal Ca^{2+} stores on somatostatin secretion. 96
Figure 4-15 Revised model of glucose-induced somatostatin secretion. ... 102
Figure 5-1 Synchronous $[Ca^{2+}]_I$ oscillations between δ-cells..... 108
Figure 5-2 Correlation matrices obtained for δ-cell pairs of one recording. 111
Figure 5-3 The increase in correlation at high glucose does not depend on the choice of the size of the time-window (ΔT)..... 112
Figure 5-4 Correlation between δ-cells increases upon glucose stimulation. 114
Figure 5-5 Example of average correlations in two distinct experiments.... 115
Figure 5-6 Gap-junctions expression in SST-negative and -positive cells.. 117
Figure 5-7 Effect of the connexin-36 inhibitor mefloquine on δ-cells. 118
Figure 5-8 Effect of the gap-junctions inhibitor CBX on δ-cells. 120
Figure 5-9 Effect of the specific pannexin-1 inhibitor 10Panx on δ-cells. ... 122
Figure 6-1 Current model of paracrine regulation of glucagon secretion.... 129
Figure 6-2 Effect of exogenous insulin on glucagon and somatostatin secretion. 136
Figure 6-3 Insulin receptor expression and effect of insulin on $[Ca^{2+}]_i$ in SST-Cre-GCaMP3 islets 139
Figure 6-4 Effect of endogenous insulin on somatostatin release. 141

Figure 6-5 Correlation analysis in the presence of the insulin receptor blocker S961. 142
Figure 6-6 Assessment of insulin receptor recombination in SIRKO mice. 144
Figure 6-7 Sequence alignment demonstrating removal of exon 4 in δ-cells. 145
Figure 6-8 Physiological characterization of SIRKO male mice. 147
Figure 6-9 Physiological characterization of SIRKO female mice. 148
Figure 6-10 Insulin effect in vivo in SIRKO mice. 150
Figure 6-11 Effect of insulin at 1 mM glucose in control and SIRKO mice. 153
Figure 6-12 Effect of insulin at 4 mM glucose in control and SIRKO mice. 154
Figure 6-13 In vitro effect of CYN154806 and insulin on hormone secretion. 156
Figure 6-14 Revised model of regulation of glucagon secretion. 164
Figure 7-1 Revised model of regulation of somatostatin release. 167
Figure A2-1 Immunostaining of QGP-1 cells. 174
Figure A2-2 Somatostatin secretion from QGP-1 cells in response to glucose. 175
Figure A2-3 Membrane potential recording of a QGP-1 cell. 176
Figure A2-4 Glucokinase expression in QGP-1, human islets and EndoC-βH1 cells. 177
Figure A2-5 Effect of cAMP-elevating agent and Ca^{2+}-elevating agent on somatostatin secretion from QGP-1. 179

LIST OF TABLES

Table 2-1 Alleles contained in SST-Cre mice.....32
Table 2-2 SST-Cre-RFP-GCaMP3 genotyping primers.....36
Table 2-3 Quantitec primer assays used for qPCR experiments.....43
Table 6-1 Insulin receptor alleles.....132
Table 6-2 IRKO mice sequencing primers.....132
Table 6-3 IRex3-5 primers sequences to assess Cre recombination in SIRKO mice.....133

1 INTRODUCTION

1.1 Anatomy and physiology of the pancreas

The pancreas is a glandular organ located in the abdominal cavity next to the stomach and the duodenum. It is formed by exocrine and endocrine cells. The exocrine pancreas accounts for 98-99% of the total mass. The exocrine cells secrete enzymes that assist digestion and facilitate absorption of nutrients in the small intestine. The endocrine part represents the remaining 1-2% of the organ and plays a key role to maintain glucose homoeostasis. It consists of aggregates of endocrine cells named islets of Langerhans (after the German pathologist Paul Langerhans (Langerhans, 1869)). As shown in Figure 1-1, each islet is formed by at least three different cell types: the glucagon-producing alpha (α)-cells, the insulin-releasing beta (β)-cells, and the somatostatin-secreting delta (δ)-cells.

All endocrine cells are in close proximity with vascular endothelial and smooth muscle cells (Cabrera et al., 2006). Moreover, pancreatic islets are highly innervated by sympathetic, parasympathetic and sensory nerves (Ahren, 2000, Rodriguez-Diaz et al., 2012, Thorens, 2014). Importantly, human islets are less densely innervated than mouse islets (Rodriguez-Diaz et al., 2011).

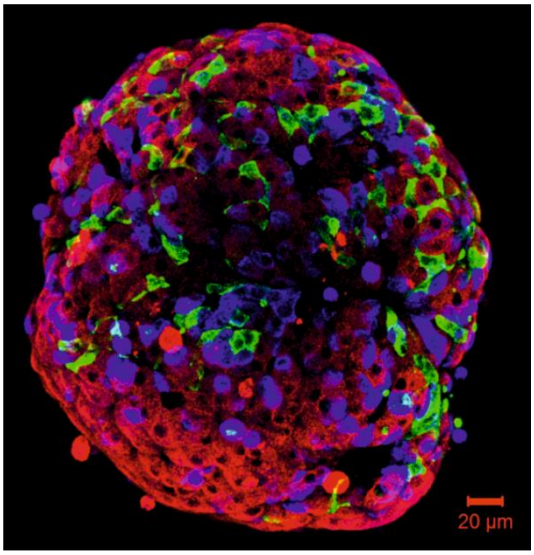

Figure 1-1 Immunostaining of a mouse pancreatic islet.
α-, β-, δ-cells are labelled as blue, red and green, respectively. In mice, β-cells account for 65-80% of the total islet mass while α- and δ-cells account for 10-25% and 5-10%, respectively. This 3D-picture is a reconstruction of a series of Z-stack confocal scanning images. This image was created by Elisa Vergari (Brereton et al., 2015).

1.2 Regulation of blood glucose levels and diabetes

The main function of pancreatic islets is to regulate blood glucose levels through the release of hormones insulin and glucagon into the bloodstream. Normally, an increase in the plasma glucose concentration stimulates insulin secretion from β-cells and inhibits glucagon release from α-cells. Conversely, decreasing plasma glucose levels suppresses insulin secretion and stimulates glucagon release. These events depend on both intrinsic (i.e. regulated by processes within the α- and β-cells) as well as paracrine cross-talk between the different endocrine cells within the islets (Hauge-Evans et al., 2009, Caicedo, 2013, Meda, 2013).

Diabetes mellitus, often referred to as diabetes, is a group of metabolic diseases associated with chronic hyperglycaemia, which results from defects in insulin secretion, insulin action, or both (American Diabetes Association, 2010). There are several types of diabetes, but the most common are type 1 and type 2. Type 1 diabetes (also known as insulin-dependent diabetes mellitus (IDDM) or juvenile diabetes) is regarded as an autoimmune disease. In this type of diabetes, the plasma cells of the immune system produce antibodies, which mark insulin-producing β-cells for destruction by T-cells. Type 2 diabetes (referred to as non-insulin-dependent diabetes mellitus (NIDDM) or adult-onset diabetes) is characterized by a combination of insulin resistance and relative (rather than absolute) insulin deficiency.

However, it is now well accepted that diabetes is a bihormonal disease (Lefebvre and Luyckx, 1979, Unger and Orci, 1982) where the metabolic consequences of impaired insulin secretion from β-cells are often exacerbated by dysregulation of glucagon release from α-cells. The resulting hyperglycaemia induces long-term damage and dysfunction of many organs, especially the eyes, kidneys, nerves, heart, and blood vessels.

The role of somatostatin (SST) in the regulation of plasma glucose homeostasis remains largely unknown. Abnormalities in islet δ-cell morphology in diabetes, in man and in rat, were described already 40 years ago (Orci et al., 1976, Gerich, 1981) and at that time it was speculated that over-secretion of somatostatin from the pancreatic δ-cell might play a role in diabetes (Unger and Orci, 1977). Thus, diabetes is perhaps best described as

a multihormonal disorder with dysfunction of all three major cell types of the islet of Langerhans. In fact, it has been reported that streptozotocin-induced diabetic animals display higher plasma somatostatin levels compared to controls (Patel et al., 1980, Yue et al., 2012). A more detailed understanding of the control of somatostatin secretion and its function in the islets is clearly required in order to establish the role of somatostatin in the pathophysiology of diabetes.

1.3 Cellular arrangement of pancreatic islets

Pancreatic islets function as micro-organs where signalling between different cell types is tightly coordinated. Orci and Unger (1975) showed that the arrangement of islet cells, where a core of β-cells is surrounded by a mantle of α- and δ-cells, was conserved in various species, including man. A few years later, Grube and Bohn (1983) reported that in humans, α-cells are distributed in the peripheral mantle of the islets, but δ-cells are primarily located next to intra-insular capillaries and are infrequently found at the periphery of the islets.

Although controversies still persist in terms of cells islet cytoarchitecture, more recently, a study highlighted substantial differences between human and rodents (Cabrera et al., 2006). In rodent islets, a core of β-cells, accounting for 65-85%, is surrounded by a mantle of α- and δ-cells (accounting for 10-25% and 5-10% respectively, see Figure 1-1). In human islets, β-cells account only for 50-60% of the total islet mass and the percentage of α-cells is higher than

in mouse (~35-45%). Moreover, α- and δ-cells are evenly distributed throughout the pancreatic islet. This particular structure is likely to favour cross-talk between islets cells.

1.4 Pancreatic δ-cells

Pancreatic δ-cells were originally identified using Mallory-Heidenhain azan trichrome technique, as they stained differently from α- and β-cells and referred to as δ-cells (Bloom, 1931). Later, an islet cell type was identified by an argyrophil reaction, using a novel silver staining method (Hellerstroem and Hellman, 1960). These cells were named α_1 to distinguished from them α_2 (later named α-cells). Finally, it was suggested that α_1-cells were identical to the δ-cells (Fujita, 1968).

In mammals (including man), δ-cells feature moderately electron-opaque secretory granules that tend to be smaller than those found in α- and β-cells. Interestingly, δ-cells exhibit a peculiar neurone-like morphology with cytoplasmic processes abutting directly on islet capillaries (Baskin et al., 1984). These dendrite-like protrusions may allow also paracrine cross-talk with several neighbouring α- and β-cells. Another distinctive feature of δ-cells, observed in both human and rodent islets is their tendency to be juxtaposed to other δ-cells. Such an arrangement has been defined as “homologous” interaction while “heterologous” interaction describes contact between δ- and α- or β-cells (Grube and Bohn, 1983). One can speculate that “homologous”

interaction between δ-cells allows substantial and synchronous somatostatin secretion.

1.5 Somatostatin production and somatostatin receptors

Somatostatin, also known as growth hormone-inhibiting hormone (GHIH) or somatotropin release-inhibiting hormone (SRIF), was originally discovered in ovine hypothalamus (Brazeau et al., 1973). Somatostatin is found in the brain (in the hypothalamus, the deeper layers of the cortex, all limbic structures, the striatum, the periaqueductal central gray) (Patel, 1992), in pancreatic δ-cells (Arimura et al., 1975), in peripheral neurones (Hökfelt et al., 1975) and in the gastrointestinal tract (Polak et al., 1975).

Somatostatin is synthesised as a precursor called preprosomatostatin (PPSST, 116 amino acids). This molecule is rapidly cleaved into pro-somatostatin (PSST, 92 amino acids). Then, a protein convertase (PC), probably PC2 (Marcinkiewicz et al., 1994) processes PSST enzymatically at its C-terminal to yield several mature products including the two bioactive forms: SST-14 (14 amino acids) and SST-28 (28 amino acids) (Patel, 1992, Patel et al., 2010).

Pancreatic δ-cells produce mainly SST-14 (Arimura et al., 1975, Hobart et al., 1980, Patel et al., 1981). Somatostatin has a very short half-life in plasma (1-3 min) due to enzymatic degradation and endocytosis (Brazeau et al., 1974,

Sheppard et al., 1979). Both SST-14 and SST-28 bind to five somatostatin receptor subtypes (SSTR1- SSTR5) (Kumar et al., 1999).

SSTRs belong to the family of G-protein coupled receptors, coupled to inhibition of adenylyl cyclase (Patel and Srikant, 1997) or of voltage-gated Ca^{2+} channels (Fujii et al., 1994) and to activation of inwardly rectifying K^{+} channels (Kreienkamp et al., 1997). Somatostatin receptors are widely expressed in the brain (Breder et al., 1992, Thoss et al., 1996), heart (Smith et al., 2005), lungs (Varecza et al., 2009), exocrine (Srikant and Patel, 1986) and endocrine (Kumar et al., 1999, Ludvigsen et al., 2004) pancreas, spleen (Ferone et al., 2012), kidney (Bates et al., 2003), adrenal gland (Ueberberg et al., 2005) and gastrointestinal tract (Schafer et al., 1998).

Using SST-14-selective and SST-28-selective radioligands, it was demonstrated that β- and α-cells possess SST-28-preferred sites and SST-14-preferred sites, respecitvely (Amherdt et al., 1987). It was later suggested that SST-14 binds preferentially to SSTR2 expressed on the α-cells, while SST-28 binds to SSTR5 present on the β-cells (Strowski et al., 2000, Strowski et al., 2003). However, two recent papers reporting transcriptomic profiling of pancreatic islet cells (Adriaenssens et al., 2016, Di Gruccio et al., 2016) have shown that in mouse islets, α-cells express mainly SSTR2 and SSTR3 while β-cells possess mainly SSTR3 with little or any SSTR5. In human islets, it has been demonstrated that SSTR2 is the functionally dominant receptor present in both α- and β-cells (Kailey et al., 2012), but RNAseq data suggest that

SSTR1 and SSTR3 are also expressed at significant levels in adult human α- and β-cells (Blodgett et al., 2015).

1.6 Role of somatostatin in the islets

The role of somatostatin released by δ-cells in the pancreatic islet is poorly understood. Interestingly, somatostatin inhibits both glucagon (Koerker et al., 1974) and insulin release (Alberti et al., 1973) as well as its own secretion through an autofeedback mechanism (Ipp et al., 1979). In somatostatin-deficient mice (Low et al., 2001), insulin and glucagon release were increased compared to control mice, but only in response to nutrient stimuli (Hauge-Evans et al., 2009). In rodents, somatostatin inhibits exocytosis from singles α-cells (Gromada et al., 2001) and isolated β-cells by a late effect on exocytosis (Renström et al., 1996). Likewise, application of exogenous somatostatin inhibited exocytosis in human α- and β-cells (Kailey et al., 2012). Studies on somatostatin-deficient and wild type mice suggest that in intact islets, endogenous somatostatin exerts a tonic inhibition of islet hormone secretion and application of exogenous somatostatin was only effective in the KO islets (Hauge-Evans et al., 2009).

In rodents, like in humans, somatostatin is secreted in a glucose-dependent and in a Ca^{2+}-dependent manner (Grill and Efendić, 1984, Berts et al., 1996, Zhang et al., 2007, Braun et al., 2009). It remains mysterious why somatostatin (an inhibitor of insulin secretion) is released at glucose concentrations where

insulin secretion is required. We have proposed that somatostatin is released to prevent over-secretion of insulin or glucagon (Brereton et al., 2015). The fact that there are so few δ-cells ensures that excessive inhibition of insulin or glucagon does not happen at glucose concentrations where either hormone is required. It is also possible, that the architecture of the islet is such that somatostatin released from δ-cell at high glucose levels inhibits primarily glucagon release rather than insulin secretion.

1.7 Regulation of δ-cells somatostatin secretion

While stimulus-secretion coupling in β-cells is relatively well understood (Ashcroft and Rorsman, 1989, Ashcroft et al., 1994, Maechler and Wollheim, 1999, Henquin, 2004), the molecular mechanisms controlling somatostatin secretion from pancreatic δ-cells remain obscure. Two studies have described cytoplasmic Ca^{2+} oscillations in mouse δ-cells in pancreatic islets identified *in situ* (Nadal et al., 1999, Quesada et al., 1999). These were followed by a characterization of the electrophysiological properties of mouse pancreatic δ-cells (Göpel et al., 2000) but a limitation of this study was that δ-cells were identified by their electrophysiological "signature" rather than by immunostaining.

Glucose-stimulated somatostatin secretion requires the following steps: uptake and metabolism leading to an increased ATP/ADP ratio, closure of ATP-sensitive K^+ (K_{ATP}) channels, membrane depolarization, opening of the

voltage-gated Ca^{2+} channels (VGCC), Ca^{2+} influx and initiation of somatostatin granules release (Göpel et al., 2000). In addition, a K_{ATP} channel-independent pathway has been described (Zhang et al., 2007). This pathway involves Ca^{2+}-induced Ca^{2+} release (CICR) mediated by R-type Ca^{2+} channels and ryanodine receptors (Zhang et al., 2007), which are intracellular Ca^{2+} release channels located in the membrane of the endoplasmic reticulum (ER) (Nagasaki and Fleischer, 1988, Zimanyi et al., 1992). CICR is required for glucose-induced somatostatin release as closure of the K_{ATP} channels by sulphonylureas is not sufficient to elicit the full response of high glucose (Zhang et al., 2007).

In human δ-cells, somatostatin secretion is regulated in a similar manner as in mouse δ-cells but the importance of the CICR component remain less well characterized (Braun et al., 2009). However, human δ-cells exhibit a slow component of exocytosis (Braun et al., 2009), which reflects CICR-dependent secretion in mouse δ-cells (Zhang et al., 2007).

1.8 Cross-talk between pancreatic islet cells

Cell-cell communication within any given tissue is an important characteristic for proper organ function. Pancreatic islets, composed of several types of endocrine cells, function like micro-organs and co-operative interaction between islet cells is likely to be essential for the fine-tuning of islet hormone release and systemic glucose homoeostasis. In both human and mouse islets,

cells can influence each other by both gap-junctions and paracrine signalling (Meda et al., 1982, Serre-Beinier et al., 2009, Short et al., 2014).

Pancreatic hormones are secreted in a Ca^{2+}-dependent manner and in a pulsatile fashion. In the case of insulin, the hypothesis that glucose-induced Ca^{2+} oscillations underlie pulsatile insulin secretion was validated by parallel measurements of $[Ca^{2+}]_i$ and insulin release from superfused mouse islets (Bergsten et al., 1994, Hellman, 2009). The evidence that pulsatile hormone release is mediated by synchronous $[Ca^{2+}]_i$ dynamics regulated by gap-junctions came from experiments using connexin-36 knockout mice, the major gap-junction expressed in pancreatic β-cells (Ravier et al., 2005). In this study, it was demonstrated that pulsatile insulin release and $[Ca^{2+}]_i$ synchronization are lost in mice lacking connexin-36.

Gap-junctions are electrical “synapses”, which were first discovered in the myocardium and in crayfish nervous system, due to their ability to transmit electrical signals between adjacent cells (Weidmann, 1952, Furshpan and Potter, 1957). In conventional electron micrographs, gap-junctions appear as a small area where a uniform narrow gap of about 2-4 nm separate the membranes of two adjacent cells. By means of dye injection experiments, the pore size of the connecting channels has been estimated to be around 15 Å. This implies that coupled cells can share only small molecules (such as inorganic ions, sugars, amino acids, nucleotides, vitamins, the intracellular mediators cyclic AMP (cAMP) and inositol 1,4,5-triphosphate (IP_3)) less than 1 kDa in size (Alberts et al., 2002).

Gap-junctions in the endocrine cells of the islets of Langerhans were first identified in 1973 (Orci et al., 1973). At that time, it was suggested that they might play a role in the control of insulin secretion. Indeed, isolated β-cells secrete less insulin than re-aggregated or intact islets, demonstrating that inter-cellular communication enhances insulin secretion (Halban et al., 1982, Bosco et al., 1989). Interestingly, somatostatin is also released in a pulsatile fashion. In human islets, insulin pulses coincide with those of somatostatin, while glucagon pulses are anti-synchronous to both of them (Hellman et al., 2009). In rodents, somatostatin pulses are anti-synchronous to those of glucagon but are synchronous and slightly delayed relative to those of insulin (Salehi et al., 2007).

Although previous ultrastructural (Orci et al., 1975) and dye-coupling studies (Michaels and Sheridan, 1981, Meda et al., 1982) demonstrated the existence of gap-junctions between non-β-cells, there is little evidence that non-β-cells are electrically coupled. However, it has to be acknowledged that electrical coupling is more efficient than dye-coupling (Quesada et al., 2003). Therefore, the lack of this evidence could be attributed to the lack of a reliable method to investigate electrical coupling between α- or δ-cells.

It has been reported that $[Ca^{2+}]_i$ oscillations in non-β-cells are completely asynchronous (Nadal et al., 1999). However, in the case of δ-cells, this conclusion was drawn using a very limited number of cells. In fact, the

observation that glucagon and somatostatin release are pulsatile suggests that non-β-cells may also be electrically coupled.

Type-2 diabetes is associated with loss of pulsatile insulin release (O'Rahilly et al., 1988, Menge et al., 2011). Thus, exploring synchronization and pulsatility of pancreatic hormone may provide clues to the causes of diabetes.

1.9 Somatostatin as a paracrine regulator of glucagon secretion

In the late 60s, based on the observation that in diabetic patients lack of insulin release correlated with over-secretion of glucagon, it was postulated that glucagon is under paracrine control of insulin (Aguilar-Parada et al., 1969). The observation that insulin may inhibit glucagon secretion was later confirmed (Samols et al., 1972, Samols and Harrison, 1976). The subsequent discovery that somatostatin strongly inhibits insulin and glucagon (Alberti et al., 1973, Koerker et al., 1974) bolstered the idea that there exists a "paracrine" system where islet cells may interact with one another locally (Unger and Orci, 1977).

Although somatostatin is a strong inhibitor of insulin and glucagon release, the condition under which somatostatin plays its role as a paracrine messenger is not yet known. The limited knowledge about the regulation of somatostatin secretion and its role as a paracrine regulator of pancreatic hormone section

illustrates the importance of further studies of the mechanisms regulating somatostatin release.

AIM OF THE THESIS

The aim of this thesis is to explore the regulation of somatostatin secretion from pancreatic δ-cells.

The specific objectives were to:

1. validate a mouse model, which allows identification of δ-cells *in situ*;
2. explore the stimulus-secretion coupling in pancreatic δ-cells;
3. assess how homologous interaction between δ-cells modulates somatostatin release; and
4. determine the role of somatostatin in the paracrine regulation of glucagon secretion.

2 MATERIALS AND METHODS

In this Chapter, the general methods used for the whole thesis are described. The specific methods relevant for each of the Results Chapters are included in the separate Materials and Methods section for the respective Chapters.

2.1 Establishment of SST-Cre mouse colony

Mice, which express fluorescent markers under the somatostatin promoter were used to facilitate identification of living δ-cells. The SST-Cre mouse model (Chera et al., 2014) was generated by Dr. Frank Reimann (University of Cambridge), as described in Appendix 1. SST-Cre mice were crossed with ROSA26tdRFP (Luche et al., 2007) and or ROSA26GCaMP3 (Zariwala et al., 2012) to generate SST-Cre-RFP, SST-Cre-RFP-GCaMP3 and SST-Cre-GCaMP3 (Figure 2-1). The details of the alleles of each genotype are reported in Table 2-1.

These resulting mice express either only the tandem red fluorescent protein (tdRFP, for simplicity here called SST-Cre-RFP), or the genetically encoded Ca^{2+} indicator (GCaMP3, SST-Cre-GCaMP3), or both (SST-Cre-RFP-GCaMP3). This strategy ensures that RFP and GCaMP3 are expressed specifically in the somatostatin-secreting δ-cells.

GCaMP3 is a fluorescent Ca^{2+} indicator created by the fusion of a circularly permuted enhanced green fluorescent protein (cpEGFP, so that the N- and C-termini are fused), calmodulin (CaM), and the Ca^{2+}/CaM-binding "M13" domain of a myosin light chain kinase (Nakai et al., 2001). When the intracellular Ca^{2+} level rises, the CaM domain undergoes a conformational change that induces an increase of GFP fluorescence. Whereas, GFP fluoresces very dimly in the absence of Ca^{2+} (Nakai et al., 2001, Tian et al., 2009, Zariwala et al., 2012).

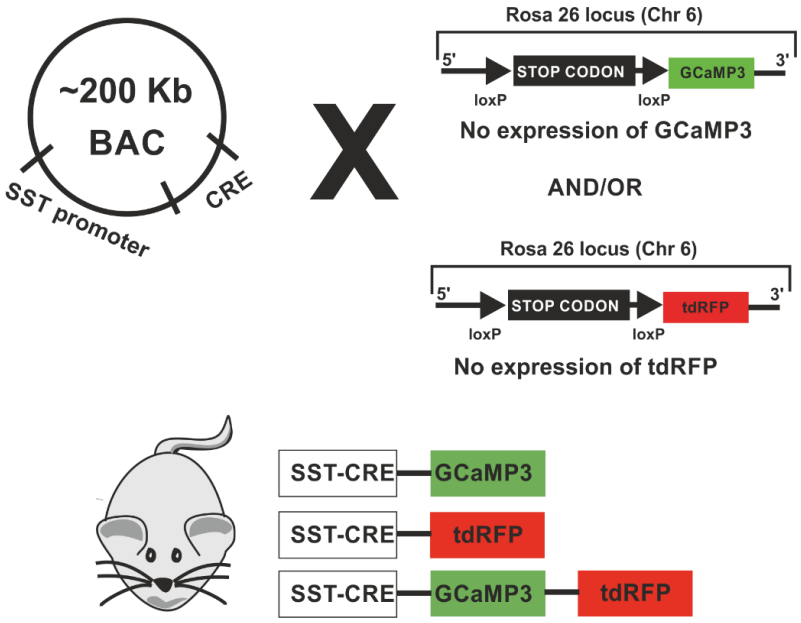

Figure 2-1 Schematic of the generation of SST-Cre-RFP-GCaMP3 mice.

SST-Cre mice contain Cre recombinase under control of the somatostatin promoter. When bred to ROSA26GCaMP3 or ROSA26tdRFP, Cre recombinase excises the STOP cassette located upstream of the fluorescent marker. This event occurs exclusively in somatostatin-expressing tissues to enable tissue-specific expression of GCaMP3 or RFP (or both).

Mouse model	Alleles
SST-Cre-RFP-GCaMP3	*Sst-mCherry-2A-iCre* *Gt(ROSA)26Sor^{tm1Hjf}* *Gt(ROSA)26Sor$^{tm38(CAG-GCamp3)Hze}$*
SST-Cre-RFP	*Sst-mCherry-2A-iCre* *Gt(ROSA)26Sor^{tm1Hjf}*
SST-Cre-GCaMP3	*Sst-mCherry-2A-iCre* *Gt(ROSA)26Sor$^{tm38(CAG-GCamp3)Hze}$*

Table 2-1 Alleles contained in SST-Cre mice.

2.2 Mouse genotyping

Genomic DNA (gDNA) was isolated from ear clip samples (2-3 mm in diameter) taken from 3-4 weeks old mice, using a ChargeSwitch® gDNA Micro Tissue Kit (Invitrogen CS11203) according to manufacturer's instructions. ChargeSwitch® is a magnetic bead-based technology where nucleic acid purification is facilitated by a switchable surface charge, dependent on the pH. Earclips were digested and genomic DNA was extracted and eluted in 300 µl of elution buffer using the magnetic rack MagnaRack (Invitrogen CS15000). For genotyping, polymerase chain reaction (PCR) was carried out using BioMix Red (Bioline BIO-25006). BioMix Red is a ready-to-use 2x reaction mix containing dNTPs, 5 mM $MgCl_2$ (2.5 mM final concentration) and a stable Taq DNA polymerase. In addition, it contains an inert red dye that permits easy visualisation and direct loading onto an agarose gel.

For each sample, the 25 µl PCR mix contained:

- 2X BioMix Red 12.5 µl
- 500 nM Forward primer (from 10 µM stock) 1.25 µl
- 500 nM Reverse primer (from 10 µM stock) 1.25 µl
- diH_20 9 µl
- DNA template 1 µl

The primers used for genotyping SST-CRE-GCaMP3 mice were β-catenin, iCre, SST-mCherry, tdRFP and GCamP3 (Table 2-2). Amplification of iCre and β-catenin resulted in 2 products of 537 bp (iCre) and 220 bp (β-catenin). Amplification of SST-mCherry generated a product of 725 bp while tdRFP and GCaMP3 generated products of 726 bp and 500 bp, respectively (see example reported in Figure 2-2). In every PCR, a negative control (genomic DNA from a C56Bl/6J mouse), a positive control (genomic DNA from a mouse expressing iCre, SST-mCherry, tdRFP and GCaMP3) and water (as a blank to exclude primer contamination) were always included.

The following PCR program was used for all genotypes:

- denaturation step 94°C for 3 min,
- amplification step consisting of
    - denaturation 94°C for 30 s,
    - annealing 58°C for 30 s,
    - extension 72°C for 45 s
    - repeated for 39 cycles
- final extension at 72°C 5 min
- holding at 8°

After PCR, samples were loaded onto 2-2.5% agarose gel (3-4.5 g agarose (Sigma) in 150 ml 1X Tris-acetate-EDTA (TAE) buffer (Sigma)) containing ethidium bromide (3 µl per 100 ml gel, Sigma) and visualised using ChemiDoc™ XRS + System with Image Lab Software (Bio-Rad, Hercules, CA, USA).

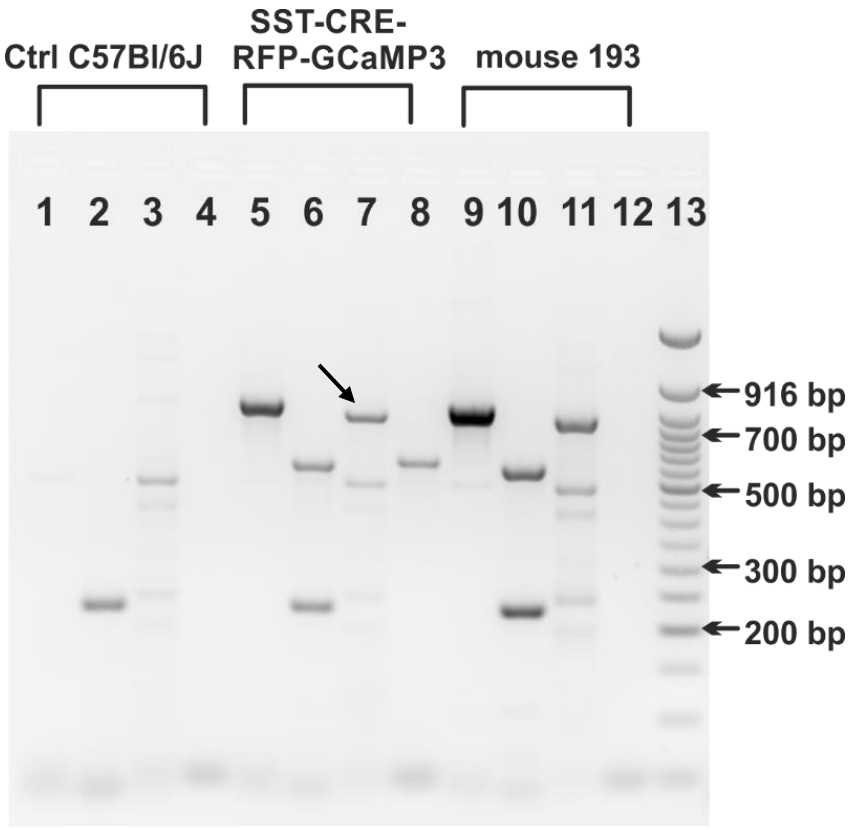

Figure 2-2 Agarose gel electrophoresis of genotyping PCR products.

Lanes 1, 5, 9: represent the SST-mCherry band (725 bp)

Lanes 2, 6, 10: represent the β-catenin band (220 bp) and iCRE band (537 bp)

Lanes 3, 7, 11: represent the tdRFP band (726 bp)

Lanes 4, 8, 12: represent the GCaMP3 band (500 bp)

Lane 13: 50 bp ladder

This is a representative gel showing the genotype of (lanes 1-4) a negative control (C57Bl/6J mouse), (lanes 5-8) a positive control SST-Cre-RFP-GCAMP3 mouse and (lanes 9-12) mouse 193, which was genotyped and resulted to be SST-Cre-RFP. tdRFP primers, as reported in this gel, could give multiple bands, (even in the negative control). However, the only specific band is the thick band of 726 bp (lane 7, arrow), which is absent in the control (lane 3).

Primer	Primer sequences
β-catenin	Fwd: AAGGTAGAGTGATGAAAGTTGTT Rev: CACCATGTCCTCTGTCTATTC
iCre	Fwd: GACAGGCAGGCCTTCTCTGAA Rev: CTTCTCCACACCAGCTGTGGA
SST-mCherry	Fwd: GGGAGACCGTGGAGAGCTC Rev: TCCACGATGGTGTAGTCCTCG
tdRFP	Fwd: CTGTTCCTGGGGCATGGC Rev: CTACAGGAACAGGTGGTGG
GCamP3	Fwd: CTTCAAGATCCGCCACAACATCG Rev: TTGAAGAAGATGGTGCGCTCCTG

Table 2-2 SST-Cre-RFP-GCaMP3 genotyping primers.

Forward (Fwd) and reverse (Rev) primer sequences of each gene used for genotyping SST-Cre-RFP-GCaMP3 mice.

2.3 Intraperitoneal glucose tolerance test (ipGTT)

The ipGTT measures the clearance of an intraperitoneally injected glucose bolus. Blood glucose levels were measured using the Accu-Check Aviva from a drop of blood obtained by a tail vein nick. For these experiments, 12-20 weeks old mice were used. Mice were fed *ad libitum* and fed blood glucose levels were measured prior to fasting. For the GCaMP3 experiments, mice were fasted overnight (16 h), whereas for the SIRKO experiments mice were fasted only 6 h (due to amendments of the project licence).

However, some important aspects need to be considered when performing long-term (overnight) or short-term fasting (6h). As nocturnal animals, mice consume primarily at night. Thus, overnight fasting (~16 h) produces low,

stable blood glucose and insulin levels. It also depletes liver glycogen stores and enhances insulin sensitivity. Conversely, 6h fasting (usually performed from early morning till early afternoon) does not reduce blood glucose and insulin levels (Muniyappa et al., 2008, Ayala et al., 2010). Therefore, studies using overnight fasting have the advantage of assessing insulin sensitivity and glucose utilisation, while 6h fast is adequate to determine insulin sensitivity in a more physiological context (Ayala et al., 2010).

After fasting, a bolus of glucose (2g per kg of body weight, Sigma) was injected intraperitoneally (ip) with a 25-gauge needle at time 0. Blood glucose levels were measured at intervals of 0, 15, 30, 60, 90, 120, 150 min after intraperitoneal glucose administration.

2.4 Intraperitoneal insulin tolerance test (ipITT)

The ipITT is a diagnostic procedure performed to assess the peripheral response to insulin. The intraperitoneal injected insulin acts to decrease blood glucose levels by stimulating organ (primarily adipose tissue and muscle) glucose uptake. For these experiments, 12-20 weeks old mice were used. Fed blood glucose levels (data point before fasting) were measured from a blood drop obtained by a tail vein nick using the Accu-Check Aviva exactly as for the ipGTT described above. The mice were then fasted for 3-4 h prior to the experiments. Fast-acting human insulin (Actrapid, Novo Nordisk) was injected intraperitoneally with a 25-gauge needle at time 0. Blood glucose levels were

measured at intervals of 0, 15, 30, 60, 90 min post intraperitoneal insulin injection.

2.5 Pancreatic islets isolation and culture

Mice (16-24 weeks old) were killed by cervical dislocation, using a Schedule 1 method approved by the Home Office. Pancreatic islets were isolated following injection of collagenase (type V, Sigma) or liberase (Liberase TL, Roche) into the common bile duct. The pancreas was then excised and digested in a shaking water bath at 37 ºC, for 10-11 min (collagenase digestion) or 12-14 min (liberase). The islets were handpicked and cultured up to 2 days, but most of the experiments were done within 24 h from the isolation. The islets were cultured in RPMI 1640 medium (Gibco 11879-020) supplemented with 10% foetal bovine serum (FBS, Sigma), 1% penicillin-streptomycin (Gibco), 5 mM glucose (Sigma).

2.6 Immunocytochemistry

For immunocytochemistry, islets were fixed in 4% paraformaldehyde for at least 30 min and then permeabilized with 0.1% Triton X-100 in phosphate-buffered saline (PBS) containing 5% goat serum for 20-25 min. Permeabilization was followed by blocking of non-specific binding in 5% goat serum for 30 min. The islets were then incubated in primary antibodies for 1 h

at room temperature. The antibodies used in this study were: rabbit anti-insulin receptor (1:75, Santa Cruz), rabbit anti-somatostatin (Sigma, 1:250), guineapig anti-insulin (Sigma, 1:3000), mouse anti-glucagon (Sigma, 1:4000), chicken anti-GFP (Invitrogen, 1:500). The islets were then incubated in secondary antibodies (1:500, all from Invitrogen) for 1 h at room temperature. Samples were visualised with a Zeiss LSM 510 META confocal microscope using appropriate lasers and filters.

2.7 FACS Analysis (flow cytometry)

Pancreatic islets from either SST-Cre-GCaMP3, or SST-Cre-RFP, or SIRKO mice (see Chapter 6) were dissociated into single cells by trypsin digestion and mechanical dissociation. Briefly, following isolation as described above, the islets were incubated in 1 ml of trypsin (TrypLE, Gibco) at 37 ºC for 5 min. Enzymatic digestion was stopped by adding 9 ml of RPMI 1640 medium supplemented with 10% FBS, 1% penicillin-streptomycin and 5 mM glucose. The islets were centrifuged for 5 min at 400 g at room temperature. The supernatant was removed, and the islet pellet was re-suspended in 600 µl of RPMI 1640 supplemented with 2% FBS, 1% penicillin-streptomycin and 10 mM glucose. The islets were mechanically dissociated into single cells by trituration and filtered through a 30 µm filter to remove remaining clumps of cells.

Single cells were passed through a FAC sorter (MoFlo Legacy from Beckman Coulter). GCaMP3 or RFP-positive cells were purified by combining several narrow gates. Forward and side scatter were used to isolate small cells (R1) and to exclude cell debris (R5). Cells were then gated on pulse width to exclude doublets or triplets (R2). GCaMP3 positive cells were excited with a 488 nm laser and the fluorescent signal was detected through a 530/40 bandpass filter (*i.e.* in the range 510-550 nm). RFP was excited with the 488 nm laser and the fluorescent signal was detected through a 580/30 bandpass filter (*i.e*. in the range 565-595 nm) (R4). GCaMP3- or RFP-negative cells were collected separately (R3) (Figure 2-3A-C). For the SST-Cre-GCaMP3 or SST-Cre-RFP sorted samples, 3 mice were used for each sample, while for the SIRKO mice a single mouse was counted as an individual sample.

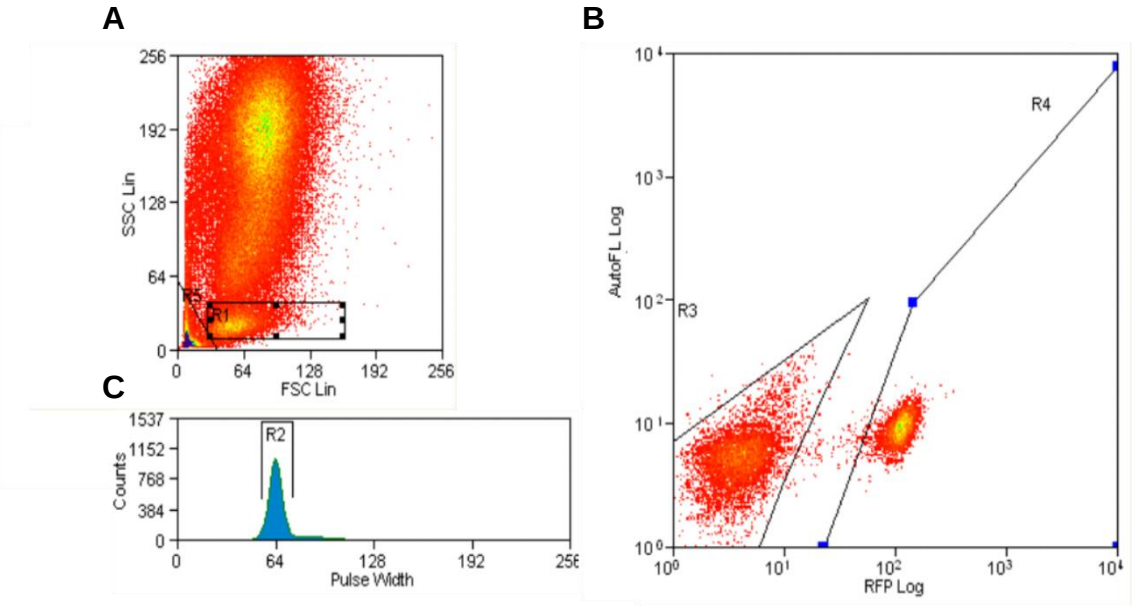

Figure 2-3 Representative FACS analysis of SST-Cre-RFP cells.

A Small cells were selected using R1 gate for forward and side scatter **B** RFP-positive cells (gated in R4) were collected separately from RFP negative cells (gated in R3). **C** To exclude doublets or triplets cells were then gated on pulse width R2.

2.8 RNA extraction, cDNA synthesis and quantitative PCR

The levels of gene expression in the positive and in the negative FAC-sorted fractions were determined using real-time quantitative PCR (qPCR). Total RNA was extracted using RNeasy Micro Kit (Qiagen) following the manufacturer's instructions. The RNA yield of the positive fraction was always very low (RNA concentration ~1-10 ng/µl), while the yield of the negative fraction varied between 30-40 ng/µl. cDNA was then synthesised by reverse transcription carried out using High Capacity RNA-to-cDNA™ Kit (Applied biosystem). For cDNA synthesis, ~10-20 ng RNA were used (due to the limited amount of RNA obtained from the positive sorted fraction).

qPCR was performed using SYBR Green kit (QuantiFast SYBR Green PCR Kit, Qiagen) and ABI 7900HT Sequence Detection System (Applied Biosystems). Primers used were QuantiTect Primer Assays (Qiagen, Table 2-3). Each sample was run in duplicate or triplicate. Expression of selected targets was compared with that of β-actin (*Actb*) measured for the same sample in parallel on the same plate. ΔCt values were obtained by subtracting the Ct value of Actb from the Ct value of the target gene. Ct values greater than 36 were not considered. Differences in expression of target genes in the RFP-positive/negative or GCaMP3 positive/negative were calculated using the $2^{-\Delta CT}$ method (Schmittgen and Livak, 2008).

Gene name	Gene symbol	Primer ID
β-actin	Actb	QT00095242
Glyceraldehyde 3-phosphate dehydrogenase	Gapdh	QT01658692
Insulin	Ins2	QT00114289
Glucagon	Gcg	QT00124033
Somatostatin	Sst	QT00239295
Glucose transporter 1	Slc2a1	QT01044953
Glucose transporter 2	Slc2a2	QT00103537
Glucose transporter 3	Slc2a3	QT00159691
Glucokinase	Gck	QT00140007
Hexokinase-1	Hk1	QT01039598
L-type calcium channel/$Ca_v1.2$	Cacna1c	QT00150752
L-type calcium channel/$Ca_v1.3$	Cacna1d	QT00112238
P/Q-type calcium channel/$Ca_v2.1$	Cacna1a	QT00170632
N-type calcium channel/$Ca_v2.2$	Cacna1b	QT00098287
R-type calcium channel/$Ca_v2.3$	Cacna1e	QT01057672
T-type calcium channel/$Ca_v3.1$	Cacna1g	QT02378922
T-type calcium channel/$Ca_v3.2$	Cacna1h	QT02524830
Ryanodine receptor 1	Ryr1	QT00145628
Ryanodine receptor 2	Ryr2	QT00153223
Ryanodine receptor 3	Ryr3	QT01043805
Inositol 1,4,5-trisphosphate receptor type 1	Itpr1	QT01539573
Pannexin-1	Panx1	QT00138845
Pannexin-2	Panx2	QT01773737
Pannexin-3	Panx3	QT00139958
Connexin-36	Gjd2	QT00165711
Connexin-43	Gja1	QT00173635
Insulin receptor	Insr	QT01540840

Table 2-3 Quantitec primer assays used for qPCR experiments.

2.9 Secretion assay

Freshly isolated islets were used in static secretion experiments. The islets were cultured briefly in RMPI supplemented with 10% FBS, 1% penicillin-streptomycin and 5 mM glucose for 1-2 h to allow recovery after the isolation.

For experiments in Chapter 6, a Krebs buffer containing in (mM) 120 NaCl, 4.7 KCl, 2.5 CaCl2, 25 $NaHCO_3$, 1.2 KH_2PO_4, 1.2 MgSO4, 10 HEPES, and 0.1% BSA was used (called Krebs buffer A) exclusively for all the secretion experiments reported in Chapter 6. This solution was adjusted to pH=7.4 with NaOH and bubbled with carbogen (O_2:CO_2, 95:5%) for 4 min at room temperature. For all other experiments, a Krebs buffer containing in (mM) 140 NaCl, 4.7 KCl, 2 $NaHCO_3$, 0.5 NaH_2PO_4, 0.5 MgSO4, 5 HEPES, 2.6 CaCl2 and 0.1% BSA (called Krebs buffer B). The pH of the solution was adjusted to 7.4 with NaOH at room temperature. All chemicals were from Sigma.

All experiments were carried out in a shaking water bath at 37 ºC. Islets from at least 3 mice were pooled together for each experiment. Groups of 15-20 islets, in at least 4 replicates (*i.e.* technical replicates) per condition, were used in each experiment. Each batch of islet was preincubated for 1 h in 500 µl Krebs buffer supplemented with 1 mM glucose. After the preincubation, the supernatant was removed and islets were then stimulated with 500 µl Krebs buffer containing glucose and other compounds as indicated for 1 h. The secretion experiments reported in Chapter 6 were carried out using 1 ml of Krebs buffer instead of 500 µl (for both preincubation and stimulation conditions).

For radioimmunoassay (RIA), 300 µl of supernatant from each tube were collected. To prevent degradation of the hormones, 25 µl of aprotinin (from 0.5 mM stock solution, Sigma) was added to the collected supernatants. Samples were stored at -20 ºC pending analysis. The islet pellets were lysed with 250

µl acid-ethanol (containing ethanol, diH_20 and HCl in a ratio of 52:17:1), sonicated and stored at -20 ºC. Somatostatin, insulin and glucagon concentrations in both pellet and supernatant fractions were determined using RIA kits (Eurodiagnostica for somatostatin and glucagon and Millipore for insulin and glucagon).

Data were analysed and were expressed as either as percent of content or as pg/islet/h (glucagon) or fmol/islet/h (somatostatin). Before normalising data to content, it was ascertained that islet hormone content did not change between groups.

2.10 Intracellular [Ca^{2+}] measurements

To investigate $[Ca^{2+}]_i$ signals in δ cells, SST-Cre-RFP-GCaMP3 or SST-Cre-GCaMP3 islets were used. Prior to all the experimental recordings, the islets were perfused with Krebs-Ringer Buffer consisting of (mM) 139 NaCl, 4.7 KCl, 0.5 $MgSO_4$, 2.6 $CaCl_2$, 5 Hepes, 0.5 NaH_2PO_4, 2 $NaHCO_3$ and 1 mM glucose, for at least 20 min. The solutions were always compensated for osmolality (i.e. in the Krebs buffer with 1 mM glucose, 19 mM of mannitol (Sigma) was added to have the same osmolarity as the Krebs buffer with 20 mM glucose). The average osmolality of the media was 310-315 mOsm. Glucose and drugs were added as reported in each experiment.

Islets were imaged in a heated chamber at 37 ºC placed on an inverted LSM 510 confocal microscope (Zeiss; Oberkochen, Germany) using a 40X oil objective (NA 1.4). The software used for the recording was ZEN 2009. Some of the initial experiments were run on an upright LSM 510 confocal microscope (Zeiss; Oberkochen, Germany) using a 40X water immersion objective (NA 0.8). During the recording, the islets were continuously superfused using a peristaltic pump with Krebs buffer containing glucose and other compounds as indicated. GCaMP3 was excited at 488 nm and fluorescence emission was recorded at 510-535 nm. The pinhole diameter was kept constant, and frames of 256x256 pixels were taken every 1-3 s.

The recordings were replayed off-line and regions of interest (ROI) were selected and analysed using the ZEN 2009 software and OriginPro 8.5 (OriginLab). Background fluorescence (if any) was subtracted from the fluorescence intensity (F) of each ROI. Raw data were normalized to initial fluorescence (F_0 *i.e*. expressed as F/F_0). Each single ROI of each recording was analysed and corrected for linear baseline changes, using the baseline function of OriginPro 8.5. Traces containing extensive motion artefacts were rejected and not used for the analysis.

Data are reported as frequency or as an average time duration (Chapter 4). Ca^{2+} oscillations were detected by the peak analyser tool of OriginPro 8.5. The frequencies were calculated as numbers of Ca^{2+} oscillations divided by the duration (in minutes) of each condition. The percentage of active δ-cells was

calculated as the number of cells showing Ca^{2+} oscillations over the total number of GCaMP3-expressing cells in the field of view.

2.11 Statistical analysis

GraphPad Prism 6.0 software was used for statistical analysis. Unless otherwise stated, data are represented as the mean ± standard error (S.E.) of at least three independent experiments. For normally distributed data, differences between two groups were assessed by two-tailed unpaired Student's t-test while for differences between more groups one-way ANOVA or two-way ANOVA followed by a *post hoc* test were used.

For comparison of non-normal distributed data, Mann-Whitney U-test or non-parametric ANOVA (Friedman's test) followed by a *post hoc* test were used. For ipGTT and ipITT experiments one-way or two-way ANOVA followed by *post hoc* test were used.

3 CHARACTERIZATION OF SST-Cre-GCaMP3 MICE

3.1 INTRODUCTION

Pancreatic δ-cells have not been studied much because of their small numbers in the pancreatic islets and due to the lack of a reliable model that allows identification of living δ-cells. Our current knowledge about δ-cell physiology is as the result of few original and arduous studies. Until a few years ago, the only way to unequivocally establish cell identity was to perform immunocytochemistry after the experiment (Berts et al., 1996, Nadal et al., 1999, Quesada et al., 1999, Zhang et al., 2007, Braun et al., 2009). Studies on δ-cells would have been facilitated if a δ-cell line had been available. The somatostatin-secreting cell line QGP-1, established from a human somatostatinoma, was generated in the early 1990s (Iguchi et al., 1990). The possibility of using this cell line was tested (see Appendix 2: Characterization of the human somatostatinoma cell line QGP-1). However, the lack of a physiological response to glucose makes the QGP-1 cells an unsuitable tool to investigate the regulation of somatostatin secretion.

More recently, identification of living human δ-cells was accomplished with a genetically encoded fluorescent sensor expressed under the human somatostatin promoter (Molina et al., 2014). However, human islets are not widely accessible and the variation between preparations is an important factor that needs to be taken into account. Therefore, the possibility of using a mouse model as an alternative to cell lines, or human islets, was evaluated. Although

data from mouse islets should not be assumed to reflect the situation in man, mouse islets remain a useful tool. In fact, mouse models play an increasingly important role in the study of islet physiology and pathophysiology, especially because of the ability to manipulate them genetically. Studies using mouse models can guide future work using human tissues. Recently, genetically engineered mouse models were generated to allow identification of δ-cells (Chera et al., 2014, Adriaenssens et al., 2015, van der Meulen et al., 2015, Adriaenssens et al., 2016, Di Gruccio et al., 2016). In this thesis, the usefulness of the SST-Cre-RFP and SST-Cre-GCaMP3 mouse models was evaluated.

3.2 MATERIALS AND METHODS

3.2.1 Intracellular [Ca^{2+}] recording: parallel measurements of GCaMP3 and fura red

Ca^{2+}-binding fluorescent dyes (indo1, fluo-4, fura red) are considered to be the gold standard for measurements of the cytoplasmic Ca^{2+} concentration and have been historically used in Ca^{2+} imaging experiments of intact islets (Asada et al., 1998, Nadal et al., 1999, Speier et al., 2008). When this study was initiated the SST-Cre-GCaMP3 mouse model was a relatively novel tool. Thus, the use of these mice was first validated by comparing [Ca^{2+}] dynamics detected by the Ca^{2+}-binding dye fura red, with those detected by GCaMP3, in δ-cells. Islets from SST-Cre-GCaMP3 mice were loaded with the membrane permeable Ca^{2+} indicator fura red AM (7μM; Molecular Probes) and 0.1% F127-Pluronic (Molecular Probes) in RPMI-1640 medium (supplemented with 10% FBS, 1% penicillin-streptomycin, 5 mM glucose) for >1 h at room temperature. Both Ca^{2+} indicators (GCaMP3 and fura red) were excited at 488 nm, and fluorescence emissions were recorded simultaneously at 510-535 nm (GCaMP3) and 640-680 nm (fura red), respectively. Fura red is a dual-excitation Ca^{2+} indicator. This property has allowed ratiometric confocal Ca^{2+} imaging, using 457 nm and 488 nm lasers, to measure the ratio between Ca^{2+}-bound and Ca^{2+}-free forms (Lohr, 2003). When excited only with the 488 nm laser, the fluorescence of the fura red indicator decreases once it binds Ca^{2+} (as it measures only the Ca^{2+}-free form) (Oheim et al., 2014). Thus, for representative purposes, Ca^{2+} recordings performed with fura red are

expressed as F_0/F, while those with GCaMP3 are reported as F/F_0 so that an increase in $[Ca^{2+}]_i$ is represented as an upward deflection.

3.2.2 Simultaneous $[Ca^{2+}]_i$ imaging and hormone secretion measurements

To measure changes in $[Ca^{2+}]_i$, and hormones secretion simultaneously, mouse islets (between 85 and 100 islets) from SST-Cre-GCaMP3 were introduced into an imaging micro-chamber (containing ~100 µl of the buffer used for experiments) mounted on an inverted confocal microscope (LSM 510, Zeiss). The islets were continuously superfused with Krebs buffer (Section 2.10) containing 1 mM glucose, at 37 ºC for 45 min. During the experiment, the islets were stimulated with glucose (20 mM), tolbutamide (0.2 mM) or high-$[K^+]_o$ (30 mM) as indicated. When islets were stimulated with 30 mM K^+, NaCl was equimolarly replaced by KCl to maintain iso-osmolarity. Islets were imaged using Plan-Apochromat 20X/NA 0.75 objective, allowing the imaging of 15-20 islets at the same time. The superfusate was manually collected at an interval of 5 min and stored on ice. The total volume of each collected fraction was ~360 µl. Aprotinin (25 µl; from 0.5 mM stock, Sigma) was added to prevent degradation of somatostatin.

3.3 RESULTS

3.3.1 Physiological characterization of SST-Cre-GCaMP3 mice

To ascertain that expression of exogenous proteins (such as Cre and GCaMP3) in somatostatin-containing tissues does not adversely affect the physiology of SST-Cre-GCaMP3 mice, several functional parameters were tested. All the mice used in these sets of experiments were 16-24 weeks old. No differences in body weight were observed between control littermates and SST-Cre-GCaMP3 mice (Figure 3-1A, p=0.8). To establish that pancreatic δ-cell function remains unaltered, fed and fasting blood glucose levels were compared. SST-Cre-GCaMP3 and control mice did not exhibit any significant differences in fed blood glucose levels or after 4 h fasting (Figure 3-1B). Short fasting (4 h) did not affect glucose homoeostasis and blood glucose levels decreased by 50% (compared to fed blood glucose levels) in both groups only after 16 h fasting. However, also in this condition no relevant differences between the control and the SST-Cre-GCaMP3 group were detected (Figure 3-1B). To assess glucose clearance and insulin sensitivity, ipGTT and ipITT were performed on SST-Cre-GCaMP3 mice and control littermates. No significant differences were observed in the two groups in response to administration of glucose (Figure 3-1C) or insulin (Figure 3-1D).

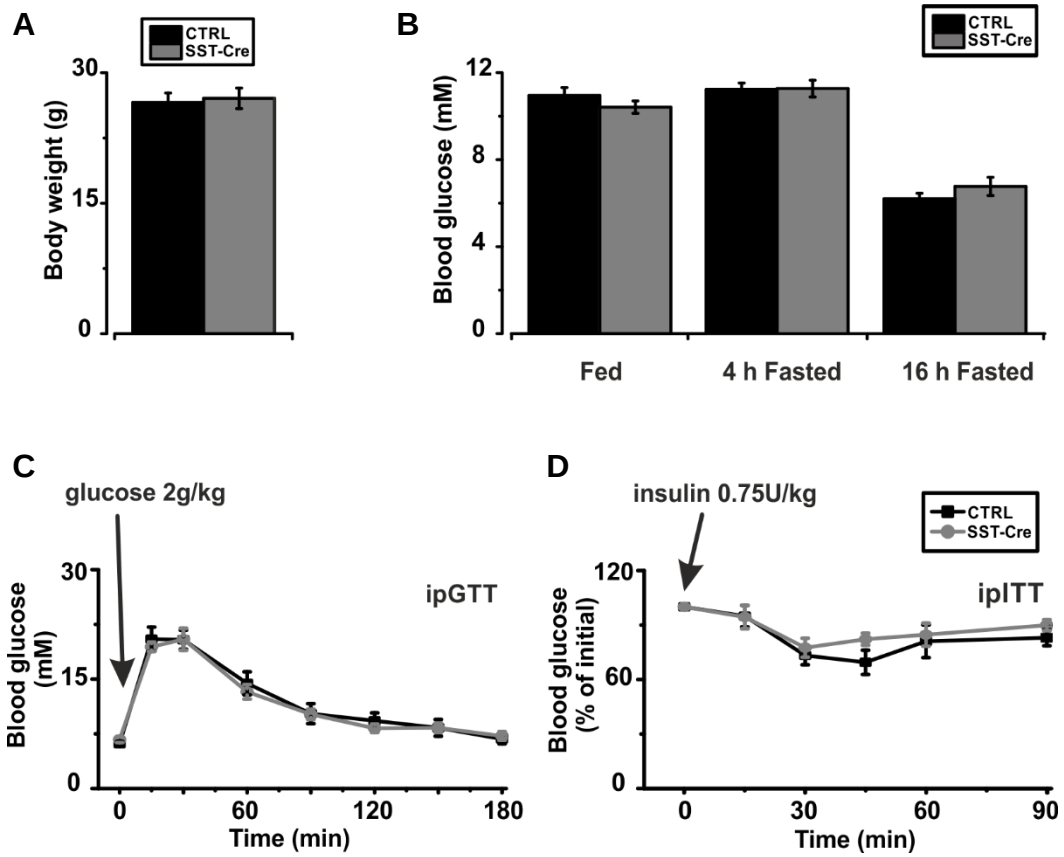

Figure 3-1 Physiological characterization of SST-Cre-GCaMP3 mice.

A-B Biological parameters measured in control (CTRL) and SST-Cre mice: **A** body weight in fed state **B** blood glucose levels in fed, 4 h fasted and 16 h fasted mice. **A-B** Data generated using n=12-13 SST-Cre-GCaMP3 and control mice, respectively. Data were statistically analysed with unpaired Student's t-test. No significant differences were observed. **C** ipGTT (2g/kg glucose injected at t=0 min). Mice were fasted for 16 h prior to the test. **D** ipITT (0.75U/kg insulin, injected at t=0 min). **C-D** Data generated using n=6 mice for each genotype. Data were statistically analysed by two-way ANOVA followed by Sidak's *post hoc.* No significant differences were observed between CTRL and SST-Cre mice (including the data point t=45 in **D**).

3.3.2 Characterization of SST-Cre-GCaMP3 islets

Specific localisation of GCaMP3 to the δ-cells in the pancreatic islets was confirmed by immunocytochemistry and qPCR analysis of FACS-purified GCaMP3 cells. Immunocytochemistry in intact islets showed that 84% of the somatostatin-expressing cells were immunoreactive for GCaMP3, while 6% of the cell that contained somatostatin did not express detectable GCaMP3 (Figure 3-2). The GCaMP3-positive but somatostatin-negative may represent either non-δ-cells or δ-cells in which the somatostatin granules were polarized and not detected in the confocal segment. The somatostatin-positive but GCaMP3-negative cells may be δ-cells in which recombination did not happen and thus, the expression of GCaMP3 was prevented.

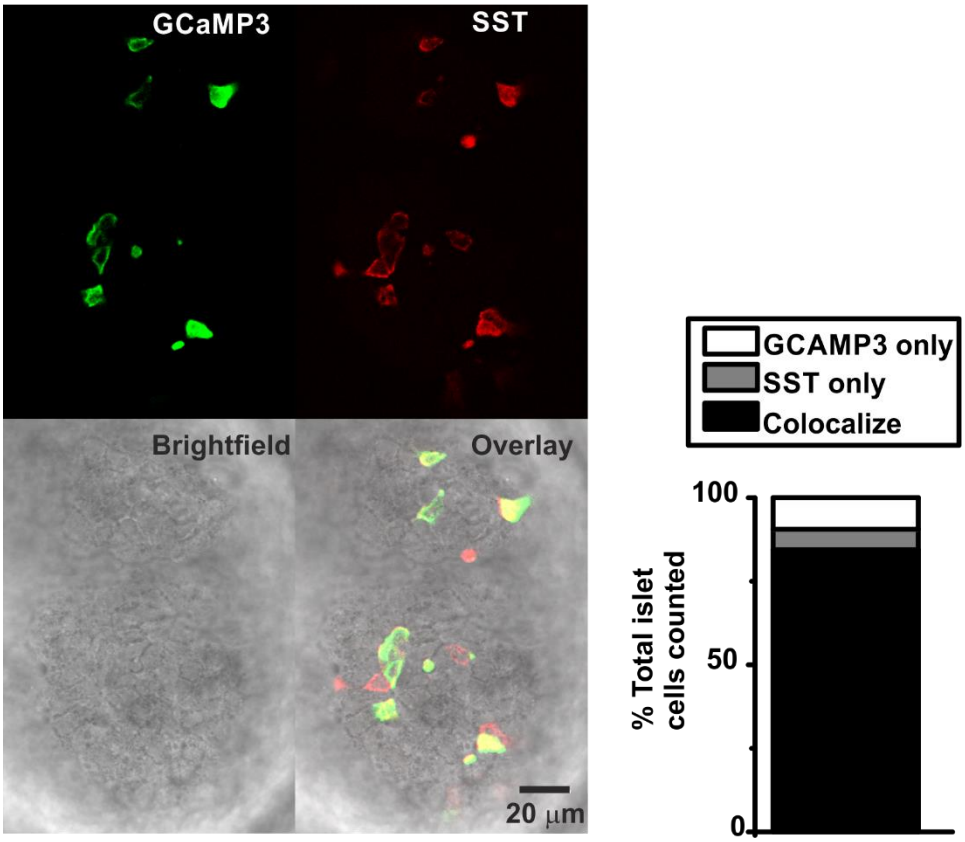

Figure 3-2 Confirmation of δ-cell specific GCaMP3 expression in SST-Cre-GCaMP3 islets.

Immunostaining of a pancreatic islet demonstrating co-localization of GCaMP3 (green) and somatostatin (red). Within a population of cells either somatostatin and/or GCaMP3 positive (100%), the majority (~85%) co-expressed somatostatin and GCaMP3 (yellow in the overlay picture), 6% stained only for somatostatin while 10% of cells stained only for GCaMP3 Percentages calculated in n=212 cells from 14 islets from 7 mice.

FACS purification and qPCR of mRNA levels demonstrated that GCaMP3-negative cells contained mainly insulin- and glucagon-expressing cells (Figure 3-3A) while the GCaMP3-positive cells were highly enriched in somatostatin-expressing cells with almost no contamination by glucagon- or insulin-containing cells (Figure 3-3B). For the gene expression experiments both SST-Cre-GCaMP3 and SST-Cre-RFP mice were used. To verify that in terms of gene expression SST-Cre-RFP and SST-Cre-GCaMP3 samples were comparable, the expression of insulin, glucagon and somatostatin mRNAs was quantified in both RFP-negative and -positive fractions. No significant differences were observed between insulin, glucagon and somatostatin levels in GCaMP3-negative compared to RFP-negative (Figure 3-3A, C) or in GCaMP3-positive compared to RFP-positive (Figure 3-3B, D). Thus, both GCaMP3- and RFP-negative and -positive fractions were enriched in insulin- and glucagon-containing cells (SST-negative) and in somatostatin-containing cells (SST-positive), respectively. In the following chapters, the terms non-δ-cells and δ-cells are used to indicate SST-negative and SST-positive cells, respectively, regardless of the fluorescent marker used for sorting the samples.

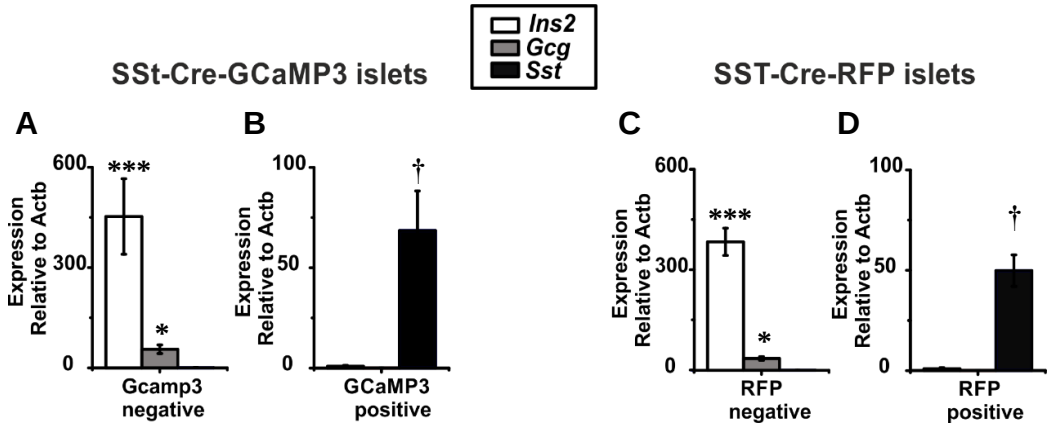

Figure 3-3 Insulin, glucagon and somatostatin expression in SST-Cre-GCaMP3 and SST-RFP islet cells.

Expression of insulin (*Ins2*), glucagon (*Gcg*) and somatostatin (*Sst*) was assessed by qPCR in **A** GCaMP3-negative, **B** Gcamp3-positive cells, **C** RFP-negative and **D** RFP-positive cells. n= 3 or 4 in **A-B** and **C-D**, respectively. Data were analysed by two-way ANOVA followed by Sidak's *post hoc*. *: p<0.05, ***: p< 0.001 vs GCaMP3-positive or RFP-positive; †: p<0.05 GCaMP3-negative or RFP-negative. No significant differences in the expression of insulin (*Ins2*), glucagon (*Gcg*) and somatostatin (*Sst*) were observed between GCaMP3 negative/RFP negative cells and between GCaMP3 positive/RFP positive cells.

A series of secretion experiments were performed to confirm that pancreatic islets from SST-Cre-GCaMP3 mice maintain normal physiological response to glucose, after expression of exogenous proteins. An increase in glucose from 1 to 20 mM, stimulated insulin and somatostatin secretion by 40- and 6-fold, respectively (Figure 3-4A, C, $p<0.001$), whereas glucagon secretion was inhibited by 60% (Figure 3-4B, $p<0.05$).

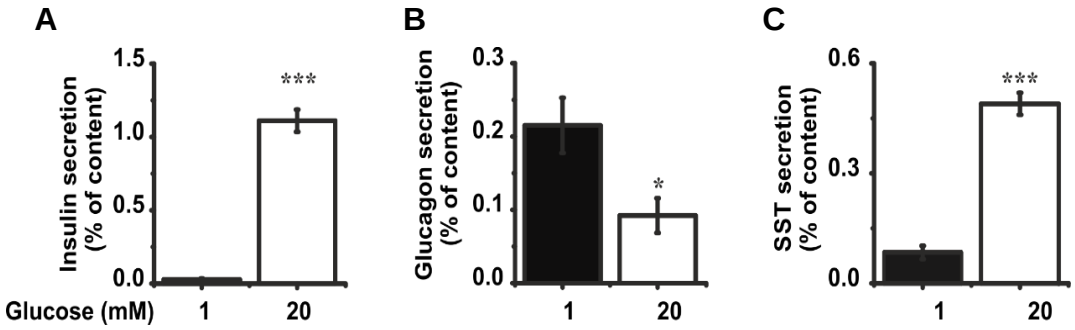

Figure 3-4 Hormones secretion measurements from SST-Cre-GCaMP3 islets.

A Insulin, **B** glucagon and **C** somatostatin secretion in SST-Cre-GCaMP3 mice were measured at 1 mM and 20 mM glucose. Islet hormone content did not change between groups. Results were obtained using 9 mice, n=10-15 replicates. Data were statistically analysed by unpaired Student's t-test. *: $p<0.05$, ***: $p<0.001$ *vs* 1 mM glucose.

3.3.3 Characterization of Ca^{2+} signalling in δ-cells

As somatostatin is released in a glucose-dependent manner, the effects of increasing glucose concentration (1 mM, 4 mM and 20 mM) on somatostatin secretion were tested. An increase in glucose from 1 mM to 4 mM, stimulated somatostatin release by 100% (Figure 3-5A, $p<0.05$). At 20 mM glucose, somatostatin release was stimulated by >1000% in this experiment (Figure 3-5A). $[Ca^{2+}]_i$ imaging in the presence of 2.6 mM extracellular $[Ca^{2+}]$ (see Section 2.10), in islets from SST-Cre-GCaMP3 mice revealed the occurrence of spontaneous $[Ca^{2+}]_i$ oscillations in 27±3% of the cells at 1 mM glucose. Increasing glucose concentration to 4 mM and 20 mM, increased the percentage of active cells to 48±7% and 82±5%, respectively (Figure 3-5B, D). Similar to secretion data, at 4 mM and 20 mM glucose, the frequency of $[Ca^{2+}]_i$ oscillations increased by 2- and 10-fold, respectively, compared to basal (Figure 3-5C-D).

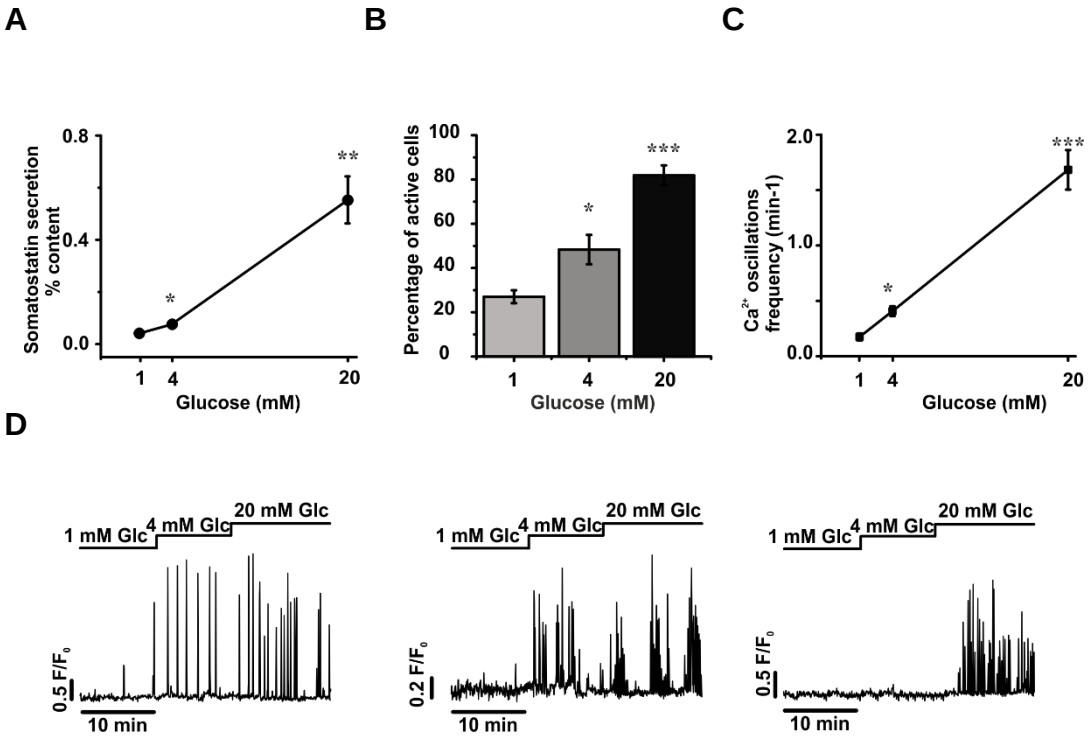

Figure 3-5 Analysis of glucose-stimulated somatostatin release in SST-Cre-GCaMP3 islets.

A Somatostatin secretion measured in response to 1 mM, 4 mM, and 20 mM glucose. Somatostatin content did not differ between groups. Data were obtained using 6 mice and n=4-6 replicates per condition. **B** Percentage of active cells at 1, 4 and 20 mM glucose (Glc). Data were obtained from n=79 cells from 7 islets from 7 mice. **C** Three representative $[Ca^{2+}]_i$ recordings showing different types of Ca^{2+} response at 1, 4 and 20 mM glucose (Glc) in **A-B**. Data were analysed by unpaired Student's t-test for statistical differences *vs* 1 mM glucose condition.*: p<0.05, **: p<0.005, ***: p<0.001.

To validate the use of the genetically encoded Ca^{2+} sensor GCaMP3 Ca^{2+}, changes in intracellular [Ca^{2+}] were measured in parallel using GCaMP3 and fura red (as outlined in the Methods section 3.2.1). β-cells imaged within an islet can be easily identified by their characteristic $[Ca^{2+}]_i$ dynamics generated in response to high glucose stimulation (Asada et al., 1998, Nadal et al., 1999). The objective of parallel measurements of GCaMP3 and fura red was two-fold: first, it enabled a comparison to be made between the Ca^{2+} signals detected using the GCaMP3 with those detected by fura red in δ-cells; second it allowed simultaneous $[Ca^{2+}]_i$ measurements of δ- and β-cells. As shown in Figure 3-6A (and inset), GCaMP3 and fura red detected the same Ca^{2+} events. However, the responses in δ-cells were quite different from the typical $[Ca^{2+}]_i$ dynamics detected by fura red in β-cells (Figure 3-6B).

These measurements confirmed the occurrence of $[Ca^{2+}]_i$ oscillations in δ-cells at 1 mM glucose and their frequency was increased by glucose. Importantly, the $[Ca^{2+}]_i$ oscillations were superimposed on a plateau of elevated $[Ca^{2+}]_i$, which was more pronounced in the fura red recordings than in the simultaneous GCaMP3 recordings.

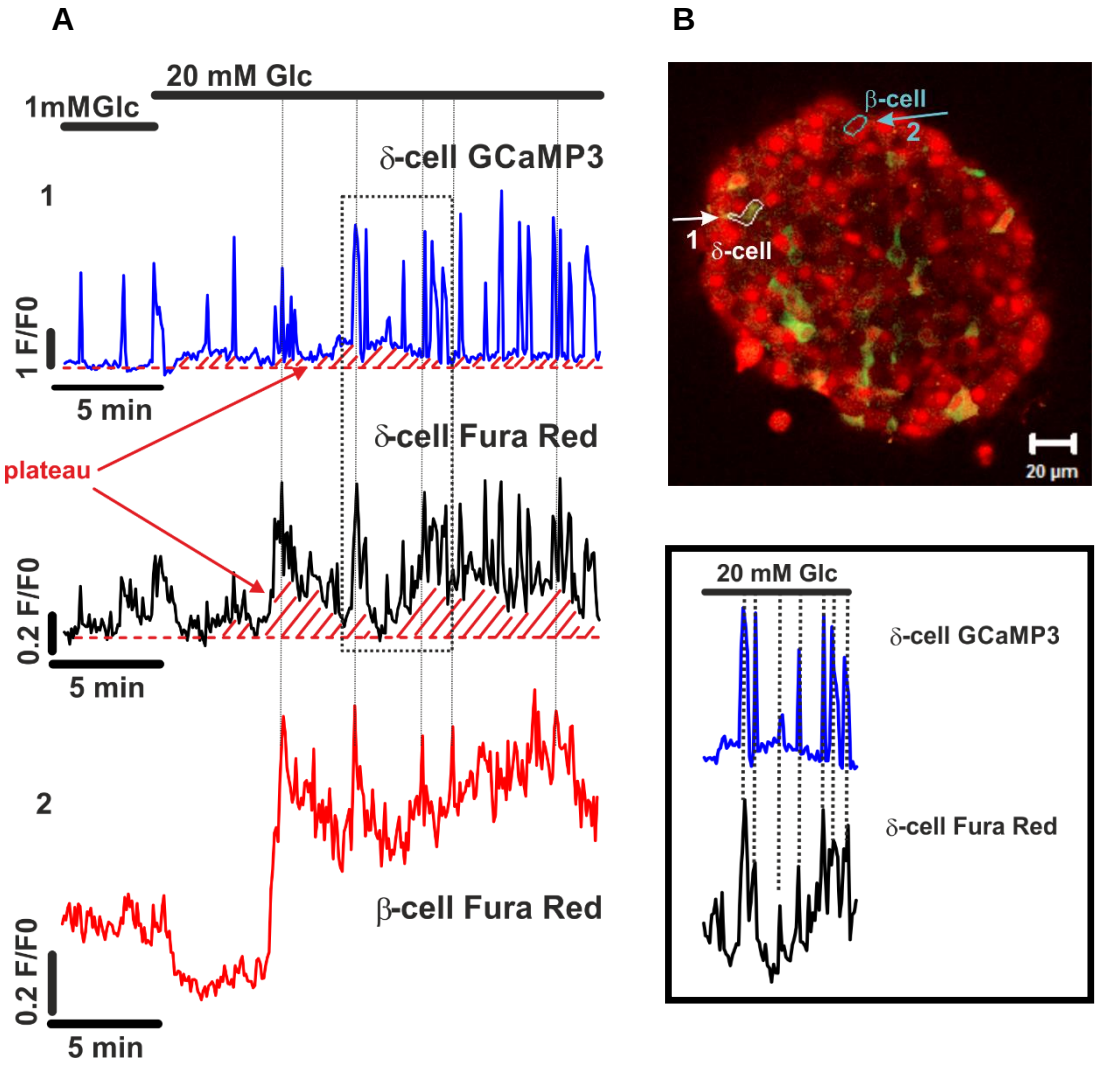

Figure 3-6 Simultaneous imaging of $[Ca^{2+}]_i$ changes in intact islets recorded with fura red and GCaMP3.

A Representative traces from δ-cells imaged using GCaMP3 and fura red (first two traces from the top and inset) and a β-cell imaged with fura red. The inset shows the period indicated by the rectangle in **A** on an expanded time base. **B** Position of the δ- (1) and β-cell (2) presented in **A**.

Changes in $[Ca^{2+}]_i$ and hormone release in GCaMP3 islets were measured in parallel to confirm that glucose-induced $[Ca^{2+}]_i$ oscillations correlate with somatostatin secretion. Figure 3-7A shows that increasing glucose concentrations from 1 to 20 mM, application of the K_{ATP} channel blocker tolbutamide (0.2mM, Sigma) or membrane depolarization produced by high-$[K^+]_o$ (30 mM) increased both insulin and somatostatin release. The stimulation of somatostatin secretion correlated with the induction of $[Ca^{2+}]_i$ oscillations in the δ-cells in response to glucose, tolbutamide and 30 mM $[K^+]_o$.

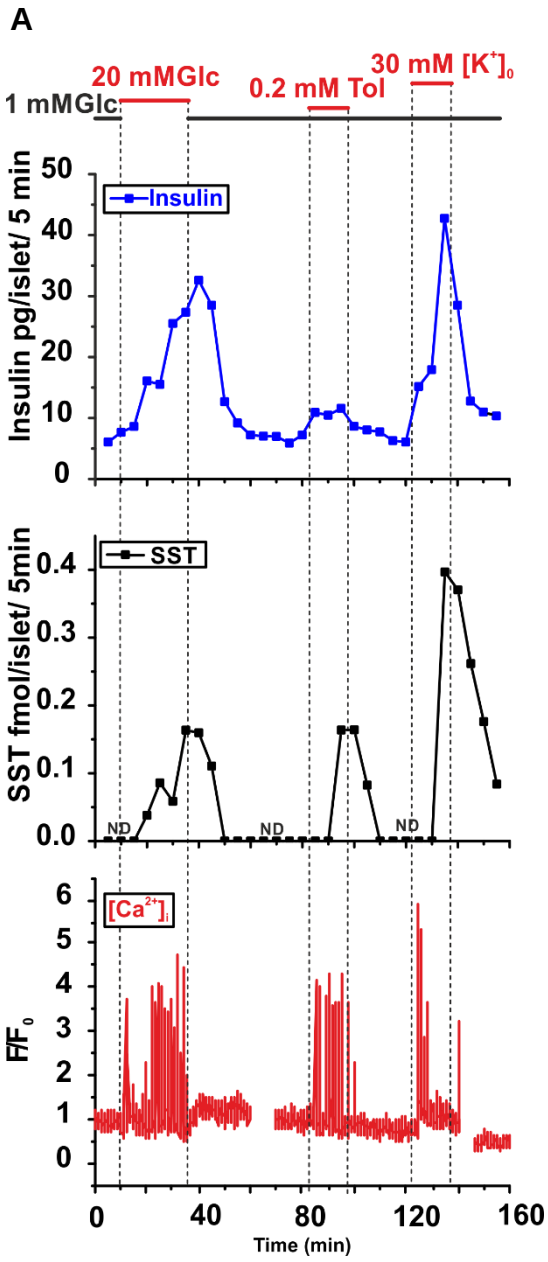

Figure 3-7 Parallel measurements of hormone secretion and $[Ca^{2+}]_i$ imaging using SST-Cre-GCaMP3 islets.

A Parallel measurment of insulin, somatostatin and changes in $[Ca^{2+}]_i$ in response to glucose (Glc), tolbutamide (Tol) and 30 mM $[K^+]_o$, in SST-Cre-GCaMP3 islets. 87 islets were used for this experiment. The Ca^{2+} trace is the representative recording in a single δ-cell. The recording was interrupted for 10 min at 60 and at 140 min due to the inability of the software to handle long recordings. **B** Confocal image of some of the SST-Cre-GCaMP3 islets present in the chamber. Green represents GCamP3 fluorescence.

3.3.4 Problems with SST-Cre-mice

Although the SST-Cre-GCaMP3 mouse represents a useful model to address questions regarding the regulation of somatostatin secretion, its use is not unproblematic. Occasionally, the fluorescent markers can "leak" [1]. In a leaky mouse, GCaMP3 is expressed almost in every islet cells (Figure 3-8A) as well as other tissues, including exocrine cells (Figure 3-8B) and hepatocytes (Figure 3-8C). This non-specific fluorescence was not restricted to GCaMP3; RFP was occasionally "leaky" too. The causes underlying this problem are still unknown. Initially, it was hypothesized that the leakage was due to unspecific Cre recombinase activity in tissues which do not express somatostatin. However, this theory was not supported when it was observed that mice which did not express Cre recombinase but which expressed only GCaMP3 or RFP alleles (*i.e.* ROSA26-GCaMP3 or ROSA26-RFP) were also leaky. Therefore, it was hypothesized that the leakiness was due to the loss or mutation in the flox-stop cassette in the ROSA26 locus. Under these circumstances, the stop elements are unable to restrict the expression of the fluorescent protein to SST-Cre-expressing cells, and fluorescence will be observed in any other tissue (as the ROSA26 locus in ubiquitously expressed). Moreover, it was observed that if "leaky" mice were used for mating, all the offspring displayed a "leaky" phenotype (including the ROSA26-GCaMP3 or ROSA26-RFP mice).

[1] A mouse where the fluorescent protein is expressed in many other tissues other than the somatostatin-expressing tissues was defined as a "leaky mouse".

Therefore, based on this evidence it was reasoned that the flox-stop cassette may have already been deleted from previous generations.

An alternative hypothesis is that Cre recombinase is activated in the germ line of female mice (Dr. Ben Davies personal communication based on evidence reported in (Schmidt-Supprian and Rajewsky, 2007, Zhang et al., 2013a)). If this is the case, to prevent the leakage, mating with females carrying the Cre transgene should be avoided. Currently, this possibility is being tested.

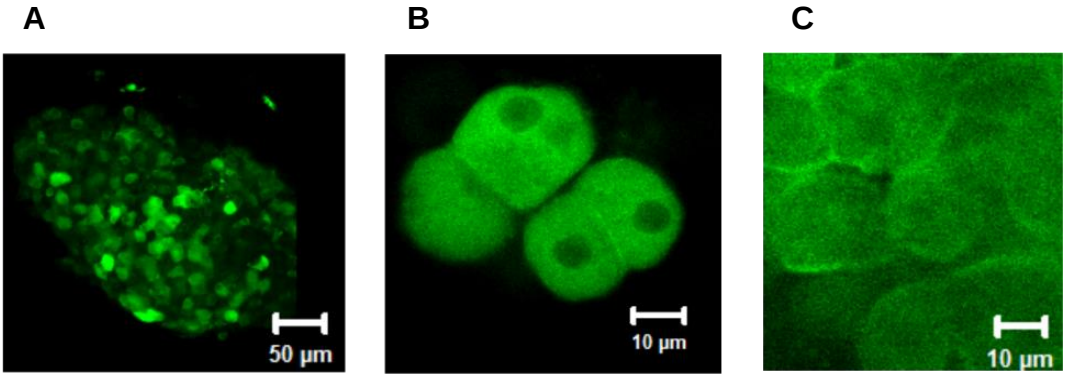

Figure 3-8 Example of leakage in tissues isolated from a SST-Cre-GCaMP3 mouse.

A 3D reconstruction of a leaky pancreatic islet obtained by confocal imaging. GCaMP3 is not confined only to δ-cells but it is spread throughout the whole islet. **B** Exocrine cells isolated from the same mouse expressing GCaMP3. **C** Hepatocytes from a liver slice displaying GCaMP3 fluorescence. Measurements in **A-C** were obtained in the presence of 10 mM $CaCl_2$ to increase $[Ca^{2+}]_i$ and enhance the brightness of GCaMP3.

3.4 DISCUSSION

3.4.1 Validation of SST-Cre-GCaMP3 mouse model

Studies to investigate the role of somatostatin in islets and the mechanisms, which regulate its secretion have been hampered by the difficulties to identify δ-cells. The δ-cells are present only in small numbers in islets (5-10%) and this has prevented more detailed molecular analysis. In the past few years, two transgenic mouse models (SST-ires-Cre (Taniguchi et al., 2011) and Sst-Cre (Chera et al., 2014)) were generated to allow easy identification of somatostatin-expressing cells (Adriaenssens et al., 2015, van der Meulen et al., 2015, Adriaenssens et al., 2016, Di Gruccio et al., 2016).

In this study, the usefulness of SST-Cre-GCaMP3 and SST-Cre-RFP mouse models (Adriaenssens et al., 2015, Adriaenssens et al., 2016) as tools to explore somatostatin secretion from pancreatic δ-cells was explored. Expression of exogenous proteins such as RFP or GCaMP3 in δ-cells did not affect mouse physiology as SST-Cre mice displayed similar physiological parameters (blood glucose levels, body weight, insulin and glucose sensitivity) as control littermates. *In vitro* experiments confirmed that δ-cell function in SST-Cre-GCaMP3 islets was not altered and somatostatin secretion in such islets largely confirmed previous observations (Grill and Efendić, 1984, Berts et al., 1996, Zhang et al., 2007).

It was also demonstrated that glucose stimulates somatostatin secretion in a concentration-dependent manner not only by recruiting more δ-cells but

primarily by increasing the frequency of $[Ca^{2+}]_i$ oscillations (Figure 3-5). The interplay between glucose-induced somatostatin secretion and Ca^{2+} will be addressed more in detail in the next Chapter.

Parallel measurements using GCaMP3 and fura red demonstrated that GCaMP3 is a valid sensor to investigate Ca^{2+} signalling in δ-cells. Although the Ca^{2+} affinity of the two calcium indicators is different (GCaMP3 K_d=405 nM (Akerboom et al., 2012), while fura red K_d=140 nM (Oheim et al., 2014)) the responses detected using the two indicators are nearly superimposable. Notably, $[Ca^{2+}]_i$ oscillations in the presence of 1 mM glucose were detected by both indicators. These results confirm the reliability of the GCaMP3 recordings. To date, no study has reported that δ-cells display Ca^{2+} oscillations in the presence of low glucose (1 mM). In this thesis, although several hundreds of δ-cells were analysed, 27% of the δ-cells displayed spontaneous Ca^{2+} oscillations at 1 mM glucose. Moreover, due to the higher Ca^{2+} affinity of fura red, the recordings made with this indicator highlighted that $[Ca^{2+}]_i$ oscillations are superimposed on a plateau of elevated $[Ca^{2+}]_i$, which was not so clear in the GCaMP3-measurements.

It is acknowledged that Ca^{2+} indicators act as Ca^{2+} buffers and they can perturb the kinetics and the levels of Ca^{2+} signalling within cells (Takahashi et al., 1999, Paredes et al., 2008). Therefore, it cannot be excluded that the presence of two Ca^{2+} indicators (GCaMP3 and fura red) may have contributed to the different Ca^{2+} responses between β- and δ-cells (Figure 3-6).

Nevertheless, further validation of the performance of GCaMP3 came from parallel $[Ca^{2+}]_i$ imaging and hormone secretion measurements. Stimulation of somatostatin secretion induced by glucose, tolbutamide and high-$[K^+]_o$, correlated with an increase in intracellular $[Ca^{2+}]_i$ in SST-Cre-GCaMP3 δ-cells. This observation reinforces previous data indicating that somatostatin secretion is a Ca^{2+}-dependent process (Berts et al., 1996, Zhang et al., 2007). Moreover, the expression of fluorescent markers under the somatostatin promoter was demonstrated to be specific and a very useful tool that enabled isolation of a fraction of somatostatin-positive cell.

4 CONTROL OF SOMATOSTATIN SECRETION

4.1 INTRODUCTION

Compared with the fairly detailed knowledge about the regulation of glucagon (Vieira et al., 2007, Cheng-Xue et al., 2013, Zhang et al., 2013b) and (in particular) insulin secretion (Ashcroft et al., 1994, Henquin, 2000, Braun et al., 2008), the understanding of the control of somatostatin secretion from the δ-cells remains rudimentary.

In previous work (Zhang et al., 2007), it was noted that islets from K_{ATP} channel-deficient mice (Kir6.2 STOP) retain almost normal glucose-induced somatostatin secretion. A thorough analysis revealed that most of the stimulatory effect of glucose on somatostatin secretion is mediated distally to membrane depolarization *via* CICR triggered by Ca^{2+} influx *via* R-type Ca^{2+} channels. Blockers of CICR, such as dantrolene and ryanodine, inhibited glucose-induced somatostatin secretion. This model (Figure 4-1) suggests that although K_{ATP} channel closure is required for glucose-induced somatostatin secretion, its effect is 'permissive'. The model is consistent with the observation that membrane depolarization as such (induced by either the K_{ATP} channel blocker tolbutamide or increasing the extracellular K^+ concentration) is a fairly weak stimulus in comparison with the much stronger stimulatory effect of glucose.

It must be acknowledged, however, that this model is not to be taken as definitive and there remain many unknowns. These include the link between glucose and CICR, the role of membrane depolarization and the cross-talk between the δ-cells and the other endocrine cells within the pancreatic islets. As already alluded to in previous chapters, mechanistic studies of the metabolic regulation of somatostatin secretion are hamstrung by the scarcity of δ-cells within the pancreatic islets (approx. 5-10%). Some of these limitations may be overcome by cell-specific expression of genetically encoded reporter proteins in the δ-cells. Using SST-Cre-GCaMP3 mice, a more detailed characterization of the mechanisms regulating glucose-induced somatostatin secretion became feasible. In this Chapter, the role of membrane depolarization, the mechanisms regulating CICR and the relationship between membrane potential and CICR during glucose-induced somatostatin secretion were investigated.

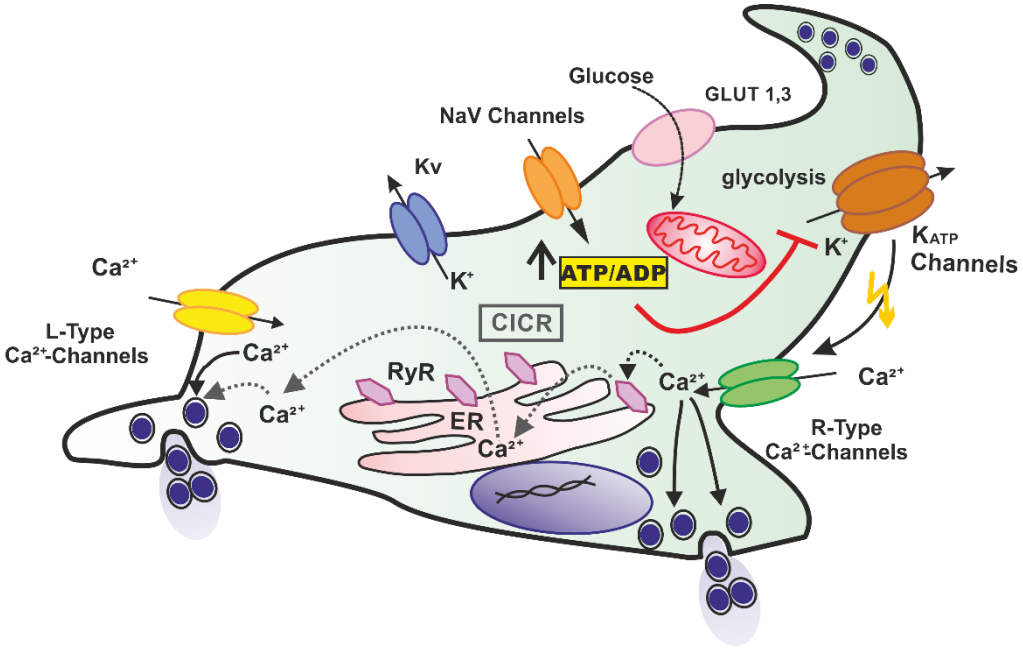

Figure 4-1 Current model of glucose-induced somatostatin secretion in mouse δ-cells.

Glucose-stimulated somatostatin secretion involves the following steps: glucose uptake into the cells, glucose metabolism which increases ATP/ADP ratio leading to the closure of K_{ATP} channels, membrane depolarization, opening of the voltage-gated Ca^{2+} channels and Ca^{2+} influx which triggers somatostatin granules release. In addition, a K_{ATP} channel-independent pathway, which involves Ca^{2+}-induced Ca^{2+} release (CICR) mediated by R-type Ca^{2+} channels and ryanodine receptors has been described (Zhang et al., 2007). CICR is required for glucose-induced somatostatin release, as closure of the K_{ATP} channels is not sufficient to produce the entire glucose-induced stimulation of somatostatin release.

4.2 MATERIALS AND METHODS

4.2.1 Intracellular [Ca^{2+}] imaging

Ca^{2+} imaging and analysis were performed as reported in Section 2.10. However, some experiments reported in this Chapter were performed under high-$[K^+]_o$ condition (70 mM). In these experiments, in Buffer B (as reported in Section 2.10) NaCl was equimolarly replaced by KCl to maintain iso-osmolarity.

In this Chapter the frequency and the duration of $[Ca^{2+}]_i$ oscillations was quantified. The frequency was determined as described above (Section 2.10). The duration of $[Ca^{2+}]_i$ oscillations was calculated in a semi-automated way. First, for each δ-cell (identified as a separate ROI) Ca^{2+} oscillations were automatically detected by the peak analyser tool of OriginPro 8.5 (Figure 4-2A). This tool identifies also the beginning and the end of each identified 'peak' (oscillation) (Figure 4-2B). The duration of a $[Ca^{2+}]_i$ oscillation was determined by subtracting the end point from the starting point (in time). The average duration of the $[Ca^{2+}]_i$ oscillations was calculated in each different condition and for each δ-cells (ROI).

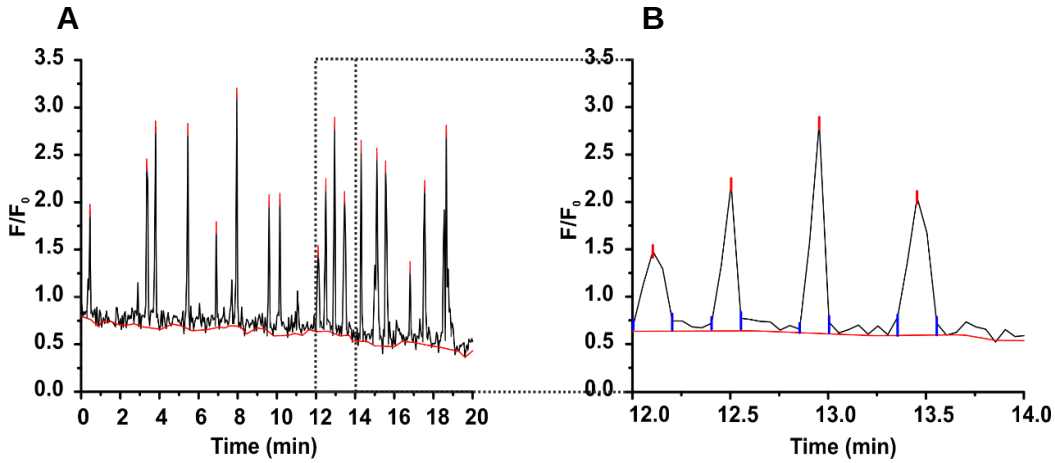

Figure 4-2 Procedure to determine the average duration of $[Ca^{2+}]_i$ oscillations.

A Ca^{2+} oscillations were automatically identified by the peak analyser tool of OriginPro 8.5 (red tags indicate the identified peaks) **B** Zoom-in of recording showed in **A** between 12 and 14 min. Blue tags indicate the beginning and the end time of each oscillation detected by the peak analyser tool of OriginPro 8.5.

4.2.2 Dynamic hormone secretion measurements

Dynamic secretion measurements were carried out as described in Section 3.2.2.

Somatostatin secretion was normalized to the content (*i.e.* amount of somatostatin in the group of islets used in each experiment). Because of the interexperimental variation, data have been further normalized to the maximum value of each experiment. After these normalization procedures, the area under the curve (AUC) was calculated using OriginPro 8.5 and then normalized to the duration of each condition. Data are expressed as AUC/t.

4.2.3 Parallel measurement of membrane potential and $[Ca^{2+}]_i$

Membrane potential recordings were performed as described previously (Zhang et al., 2013b) using the perforated-patch whole-cell technique. The pipette-filling medium contained in (mM) 76 K_2SO_4, 10 NaCl, 10 KCl, 1 $MgCl_2$, 5 HEPES (pH 7.35 with KOH) and 60 µg/ml of the pore-forming antibiotic amphotericin B. In these experiments, the extracellular solution consisted of (mM) 140 NaCl, 3.6 KCl, 0.5 $MgSO_4$, 0.5 NaH_2PO_4, 2 $NaHCO_3$, 5 HEPES and 1.5 $CaCl_2$ (pH=7.4 with NaOH). Glucose and diazoxide were included in the medium as indicated. δ-cells were identified by the expression of GCaMP3. All electrophysiological experiments were carried out at 34 ºC, using an EPC10 amplifier (HEKA Electronik, Lambrecht/Pfalz, Germany) controlled by the Pulse software (version 8.53 HEKA Electronik). Parallel measurements of $[Ca^{2+}]_i$ and membrane potential were performed using an Axioskop 2FS microscope (Zeiss, Oberkochen, Germany) equipped with a 40x/0.8 objective, Lambda DG-4 exciter (Sutter Instruments, USA) and Orca-R2 cooled CCD camera (Hamamatsu, Japan). GCaMP3 was excited at a wavelength of 490 nm and emitted light was collected at 515 nm. Images were acquired using an open-source Micromanager software (developed at Ron Vale's lab, UCSF, San Francisco, USA). Images were processed using ImageJ (Rasband, 1997-2016) and data analysis was performed in Igor Pro (Wavemetrics). Fluorescence (F) was normalized to the initial fluorescence (F_0).

4.3 RESULTS

4.3.1 Glucose sensing in δ-cells

Glucose stimulates somatostatin secretion following its metabolism and degradation. Metabolism of glucose is preceded by the uptake into the cell. To better understand how these mechanisms are regulated, the expression of glucose transporters and hexokinases was investigated by qPCR. Glucose transporter 2 (*Slc2a2*), the major isoform expressed in mouse β-cells (Thorens et al., 1988, Johnson et al., 1990), was less abundant in the δ-cells compared to the non-δ-cells fraction (Figure 4-3A, $p<0.005$). However, the expression of the glucose transporter 1 (*Slc2a1*), the most prominent isoform in rodent α-cells (De Vos et al., 1995), was slightly higher in the δ-cells than in non-δ-cells, but this did not attain statistical significance (Figure 4-3A, $p=0.06$). Glucose transporter 3 (*Slc2a3*) was also significantly more expressed in δ-cells compared to non-δ-cells (Figure 4-3A, $p< 0.05$).

Next, it was examined which isoforms of hexokinase are expressed in δ-cells. Glucokinase (also known as hexokinase-4) is the key glucose-sensor in pancreatic β-cells (Matschinsky, 1990). While glucokinase was expressed at comparable levels in δ- and non-δ-cells (Figure 4-3B, $p=0.8$), hexokinase-1 was significantly less expressed in δ-cells (Figure 4-3B, $p<0.05$). The expression of hexokinase-2 and hexokinase-3 was not tested as it has been reported that they are expressed at very low levels in rodent islets (Heimberg et al., 1996, Schuit et al., 1999).

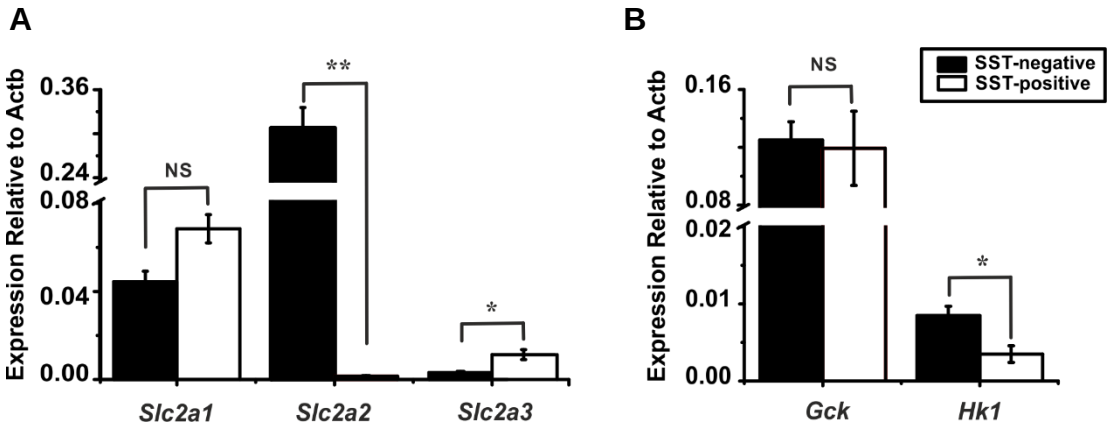

Figure 4-3 Expression of genes involved in glucose metabolism in SST-negative and SST-positive fractions.

A Expression of glucose transporters Glut1 (*Slc2a1*), Glut2 (*Slc2a2*) and Glut3 (*Slc2a3*). Data obtained from n=3 FAC-sorted samples **B** Expression of glucose sensors glucokinase (*Gck*) and hexokinase-1 (*Hk1*). Data generated using n=5 FAC-sorted samples. Statistical significance for each gene was calculated using unpaired Student's t-test between SST-negative and SST-positive cells. NS: not significant; *: $p<0.05$, **: $p<0.005$.

4.3.2 Effect of glucose and modulation of K_{ATP} channels on δ-cells $[Ca^{2+}]_i$

Both glucose and sulphonylureas stimulate somatostatin secretion (Berts et al., 1996, Zhang et al., 2007) and trigger electrical activity (Göpel et al., 2000), but the effects on $[Ca^{2+}]_i$ have not been extensively investigated (but see (Berts et al., 1996)). Increasing glucose from 1 mM to 20 mM enhanced the frequency of $[Ca^{2+}]_i$ oscillations by ~10-fold (Figure 4-4A-B, $p<0.001$). Application of the K_{ATP} channel blocker tolbutamide (0.2 mM) at 1 mM glucose, also increased the frequency of $[Ca^{2+}]_i$ oscillations in δ-cells by ~5-fold (Figure 4-4C-D, $p<0.001$). Notably this effect was weaker than that exerted by 20 mM glucose (Figure 4-4A *vs* C, $p<0.001$).

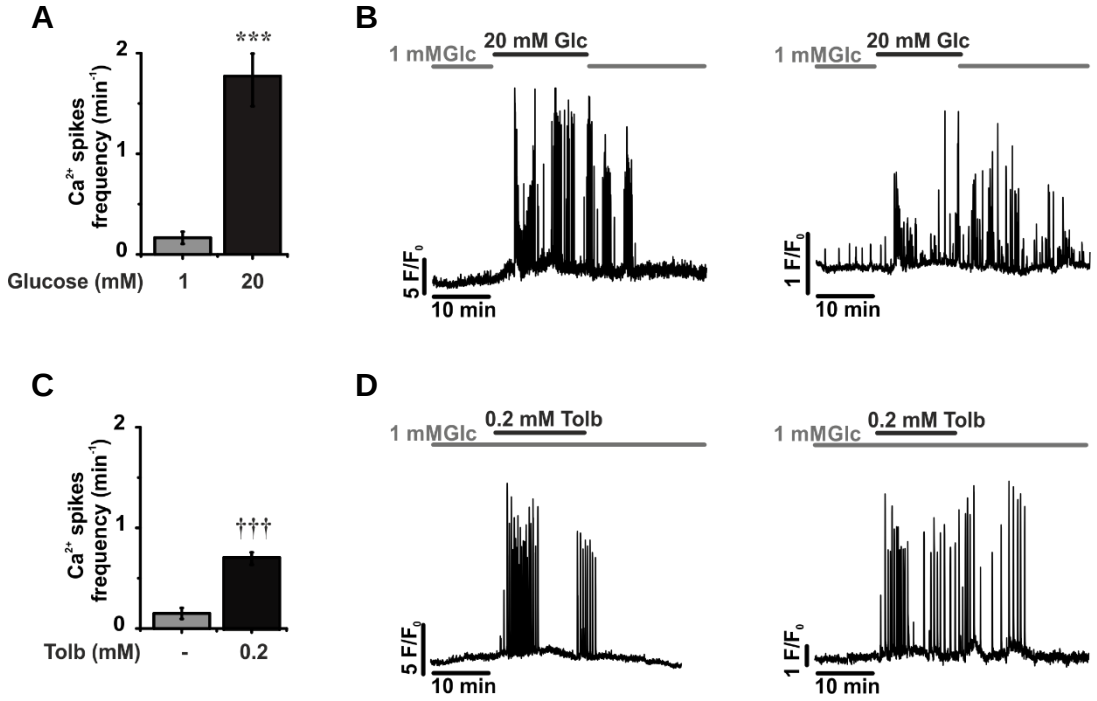

Figure 4-4 Effect of tolbutamide on $[Ca^{2+}]_i$ in δ-cells.

A Frequency of $[Ca^{2+}]_i$ oscillations in response to 1mM and 20 mM glucose (Glc), in SST-Cre-GCaMP3 islets. **B** Representative recordings of $[Ca^{2+}]_i$ of n=46 cells from 3 islets from 3 mice. **C**-**D** as in **A-B** but instead testing the effect of tolbutamide (Tolb, 0.2 mM). Data are representative of n=48 cells from 4 islets from 3 mice. Data were analysed statistically by two-way ANOVA followed by Tukey's *post hoc*. ***: p<0.001 *vs* 1 mM glucose; †††: p<0.001 *vs* 20 mM glucose.

The effect of diazoxide, which opens the K_{ATP} channels, was also tested. When applied at 20 mM glucose, diazoxide (100 µM, Sigma) reversibly lowered $[Ca^{2+}]_i$ and the frequency of the oscillations was reduced to basal levels (Figure 4-5A-B, $p<0.001$). The inhibitory effect of diazoxide on δ-cells $[Ca^{2+}]_i$ oscillations correlated with a decrease in somatostatin release: 20 mM glucose stimulated somatostatin release ~10-fold [2] (Figure 4-5C), an effect that was completely reversed by 100 µM diazoxide (Figure 4-5C-D, $p<0.05$). The same inhibitory effect of diazoxide was observed using islets isolated from NMRI mice, an outbred strain unrelated to C57BL/6 mice (Figure 4-5E).

[2] It is noteworthy that during dynamic secretion experiments glucose does not constantly stimulate somatostatin release. The trough occurring in the presence of stimulatory glucose concentration may underlie reduction of somatostatin secretion following depletion of the readily releasable pool (RRP) of granules (Zhang Q and Rorsman P, unpublished). Somatostatin release is promptly restored, probably after replenishment of this pool of vesicles.

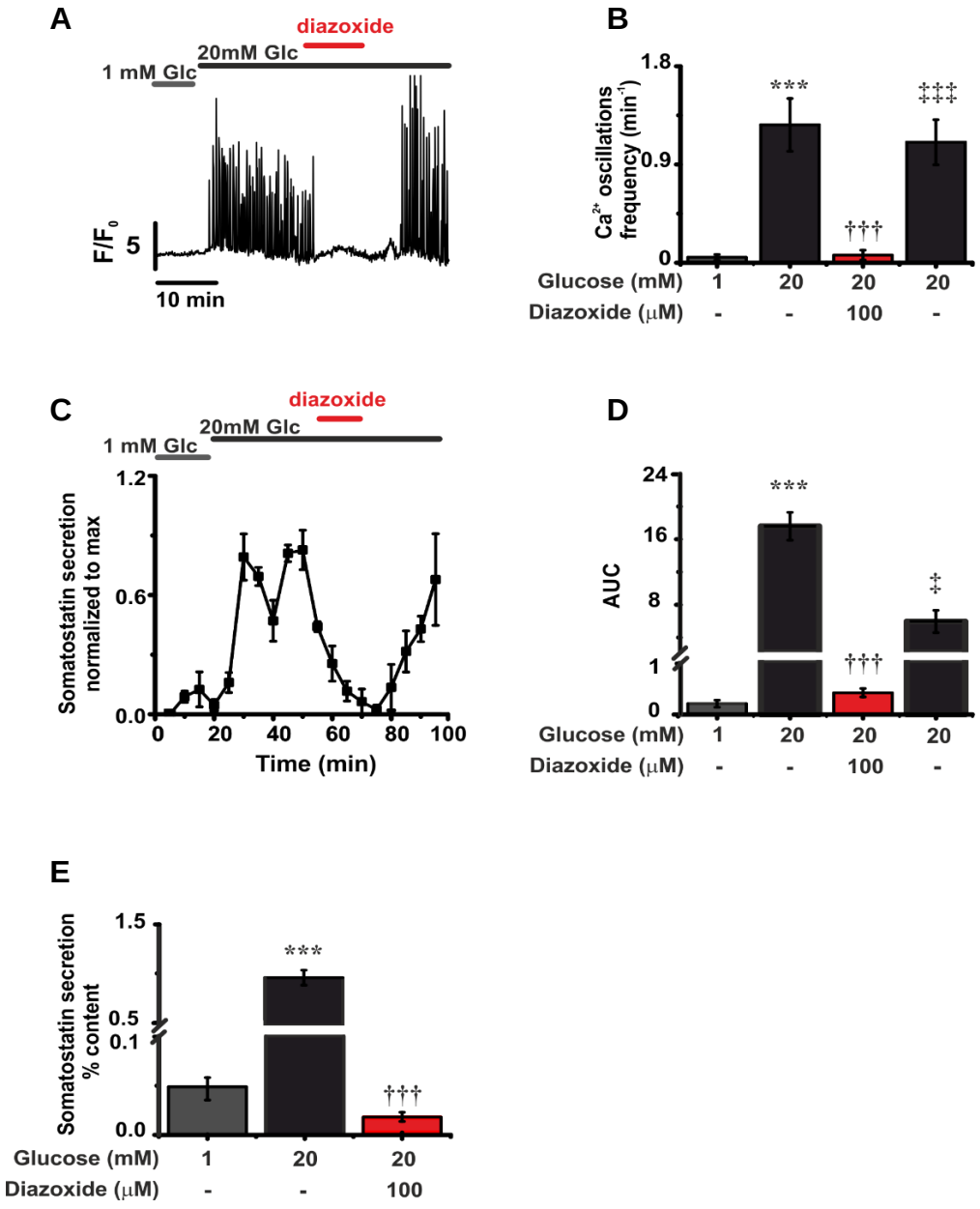

Figure 4-5 Effect of diazoxide on $[Ca^{2+}]_i$ and somatostatin secretion.

A-B Effect of diazoxide on $[Ca^{2+}]_i$ oscillations in SST-Cre-GCaMP3 islets. Data collected from n=13 cells from 3 islets from 3 mice. **C-D** Diazoxide strongly but reversibly inhibited somatostatin secretion in dynamic secretion experiments. Data obtained from n=3 experiments from 3 mice. **E** The inhibitory effect of diazoxide was observed using islet isolated from NMRI mice (measured in static incubations). Somatostatin content did not change between groups. This result is representative of 3 mice (n=4-6 replicates per condition). Data were analyzed by one-way ANOVA followed by Tukey's *post hoc*. ***: p<0.001 *vs* 1 mM glucose; †††: p<0.001 *vs* 20 mM glucose; ‡: p<0.05, ‡‡‡: p<0.001 *vs* 20 mM glucose in the presence of 100 µM diazoxide.

4.3.3 Characterization of Ca^{2+} channels in δ-cells

Ca^{2+} is an important regulator of somatostatin secretion and earlier electrophysiological analyses suggested that mouse δ-cells express R- and L-type Ca^{2+} channels (Zhang et al., 2007). The analysis of FACS purified cells by qPCR showed that L-type, R-type, N-type, P/Q type and T-type Ca^{2+} channels are variably expressed in SST-negative and SST-positive cells (Figure 4-6). Compared to non-δ-cells, δ-cells expressed higher levels of R-type Ca^{2+} channels (*Cacna1e,* p=0.06) and very high levels of T-type Ca^{2+} channels (*Cacna1h, p*<0.05).

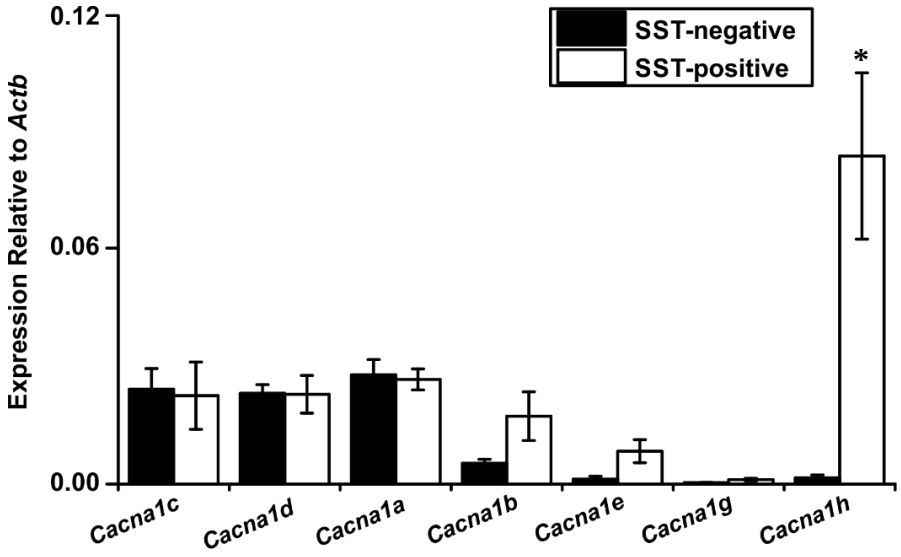

Figure 4-6 Expression levels of voltage-gated Ca^{2+} channels in SST-negative and SST-positive cells.

Gene and corresponding encoded protein: *Cacna1c* →Cav1.2/ L-type, alpha 1C subunit; *Cacna1d* →Cav1.3/ L-type, alpha 1D subunit; *Cacna1a* →Cav2.1/ P/Q type; *Cacna1b* →Cav2.2/ N-type; *Cacna1e* →Cav2.3/ R-type; *Cacna1g* →Cav3.1/ T-type, alpha 1G subunit; *Cacna1h* →Cav3.2/ T-type, alpha 1H subunit. *: p<0.05 vs SST-negative.

The functional role of L-type and R-type Ca^{2+} channels in the regulation of somatostatin release was addressed using selective blockers. Application of the L-type Ca^{2+} channel blocker isradipine (2.5 µM, Alomone) abolished glucose-induced somatostatin secretion at 20 mM glucose to levels below that at 1 mM glucose (Figure 4-7A, $p<0.005$). Likewise, the R-type Ca^{2+} channels antagonist SNX-482 (100 nM, Alomone) inhibited somatostatin release but the effect was limited to 55% (Figure 4-7A, $p<0.05$).

The differential roles of R-type and L-type Ca^{2+} channels in somatostatin secretion was further addressed by $[Ca^{2+}]_i$ imaging experiments. Application of isradipine (2.5 µM) in the presence of 20 mM glucose completely and irreversibly stopped $[Ca^{2+}]$ activity in all δ-cells (Figure 4-7B-C, $p<0.001$). Addition of SNX-482 (100 nM) reduced the frequency of $[Ca^{2+}]_i$ oscillations by ~50% (Figure 4-7D-E, $p<0.05$). These results show that both L-type and R-type Ca^{2+} channels play an important role in the control of somatostatin release.

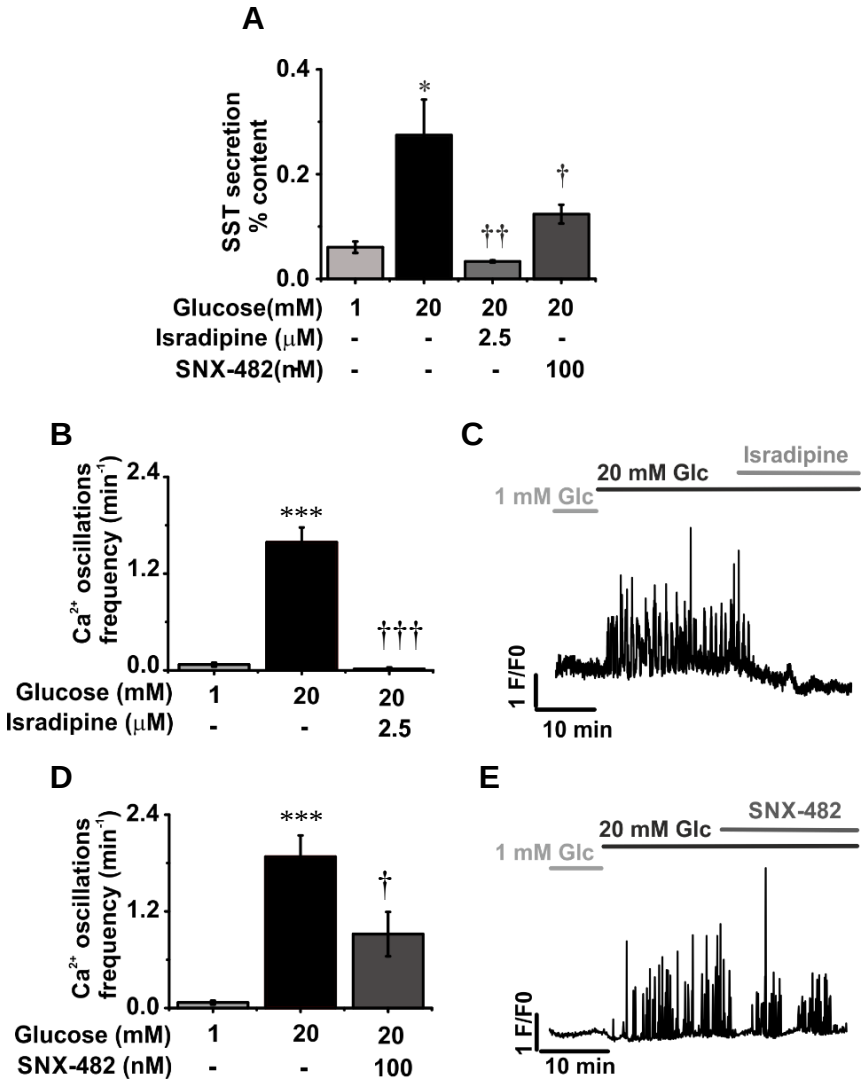

Figure 4-7 Effect of L-type and R-type Ca^{2+} channels inhibitors on somatostatin release. **A** Effect of the L-type Ca^{2+} channels blocker (isradipine) and R- type Ca^{2+} channels blocker (SNX-482) in the presence of 20 mM glucose on somatostatin secretion. Somatostatin content did not change between groups. Data from 3 mice with n=4-6 replicates per condition. **B-C** Isradipine (2.5 µM) abolished $[Ca^{2+}]_i$ oscillations in δ-cells (n=22 cells from 3 islets from 3 mice). **D-E** SNX-482 (100 nM) reduced the frequency of Ca^{2+} oscillations in SST-GCaMP3 islets (n=18 cells from 3 islets from 3 mice). Data were analysed by one-way ANOVA followed by Dunnett's *post hoc* test. *: p< 0.05, ***: p< 0.001 *vs* 1mM Glc; †: p<0.05, ††: p<0.005, †††: p<0.001 *vs* 20 mM Glucose.

4.3.4 Ca^{2+}-induced Ca^{2+} release mechanism regulates somatostatin secretion

Ca^{2+}-induced Ca^{2+} release (CICR) is the mechanism by which elevation of intracellular Ca^{2+} stimulates Ca^{2+} release from internal stores (Fabiato and Fabiato, 1975, Endo, 1977). To investigate whether Ca^{2+} released from the ER affects somatostatin secretion in SST-Cre-GCaMP3 mice, thapsigargin (a well-established inhibitor of the sarco/endoplasmic reticulum Ca^{2+} ATPase, SERCA) (Thastrup et al., 1990) was used. Thapsigargin (10 µM, Tocris), reduced glucose-induced somatostatin secretion by ~60% (after subtraction of basal, Figure 4-8A, $p<0.05$), confirming the involvement of intracellular Ca^{2+} stores in the regulation of somatostatin secretion.

CICR may be mediated by ryanodine but also IP_3 receptors (Bootman et al., 2002). Hence, the expression of IP_3 and ryanodine receptors (RyRs) was investigated. Low levels of ryanodine type 1 (*Ryr1*) and ryanodine type 2 (*Ryr2*) were detected in non-δ-cells. However, ryanodine type 3 (*Ryr3*) was exclusively expressed in δ-cells (Figure 4-8B, $p<0.05$). IP_3 receptor (IP_3R) type 1 (*Itpr1*) was likewise more expressed in the SST-positive cells compared to the SST-negative (Figure 4-8C, $p<0.05$). The expression of IP_3R type 2 and type 3 was not tested, as it was reported previously that *Itpr1* is the major isoform expressed in pancreatic islets (De Smedt et al., 1994, Lee and Laychock, 2001).

Next, ryanodine and xestospongin C were used to investigate whether Ca^{2+}-induced Ca^{2+} release is mediated by either or both RyRs and IP_3Rs.

Ryanodine was used at high concentration (50 µM, Tocris) to lock the channel in a closed state (Nagasaki and Fleischer, 1988, Zimanyi et al., 1992). Xestospongin C (10 µM, Cayman Chemical) was used to inhibit the IP_3 receptors (Gafni et al., 1997, Oka et al., 2002). Glucose-stimulated somatostatin secretion was reduced by 45% (after subtraction of basal) in the presence of ryanodine but was unaffected by xestospongin C (Figure 4-8D).

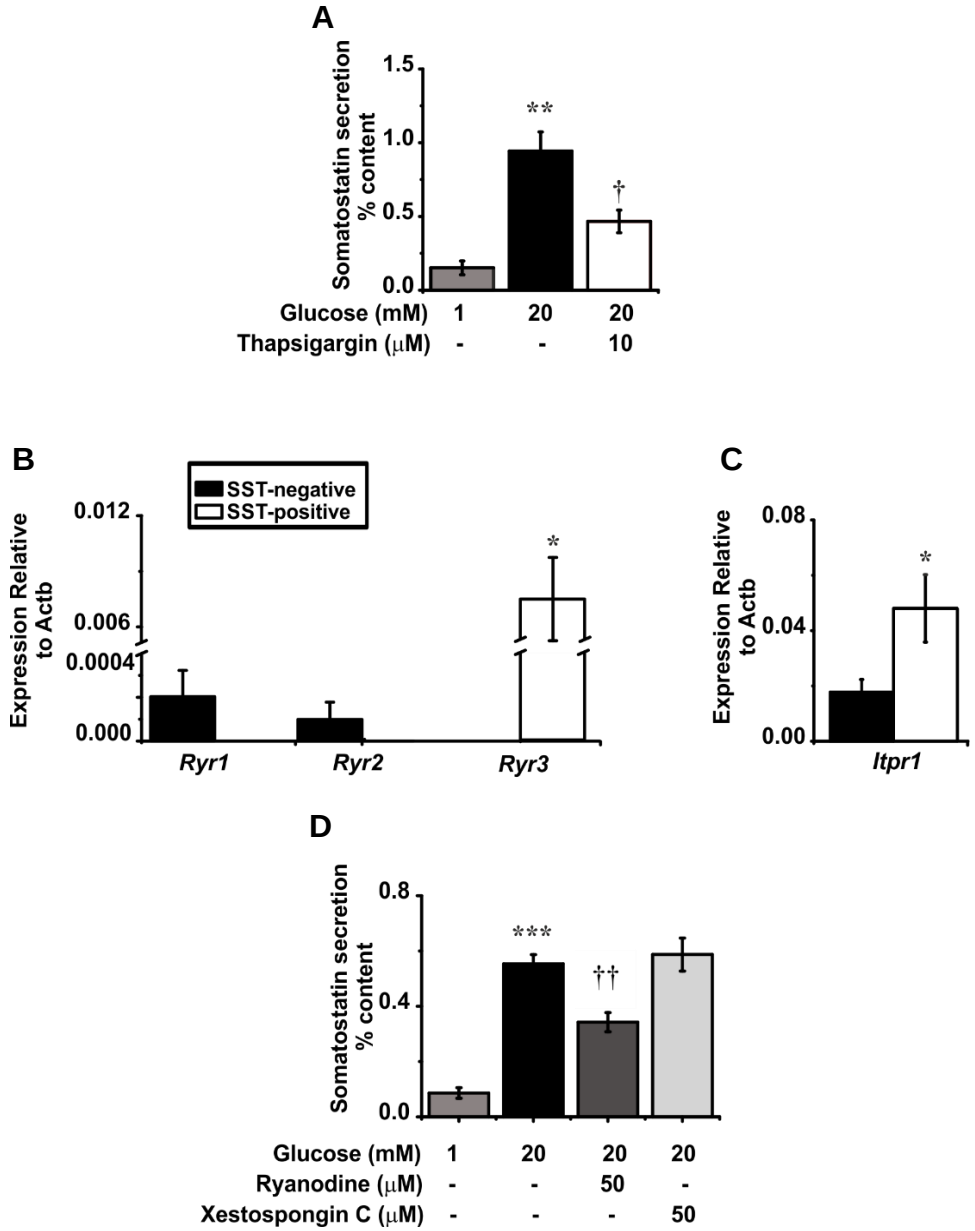

Figure 4-8 Intracellular Ca^{2+} stores regulate somatostatin secretion.

A Effect of thapsigargin on somatostatin secretion. Data obtained from 3 mice n=4 replicates per condition. Somatostatin content did not change between groups. Data were analysed by one-way ANOVA followed by Tukey's post hoc. **: p<0.005, *vs* 1 mM glucose; †: p<0.05, *vs* 20 mM glucose. **B-C** Expression of ryanodine receptor type 1, 2 and 3 (*Ryr1, Ryr2, Ryr3*) and IP_3 receptor type 1 (*Itpr1*) assessed by qPCR (n= 7 preparations). Data were analysed by unpaired Student's t-test. *: p<0.05 *vs* SST-negative cells. **D** Effect of ryanodine and xestospongin C on somatostatin secretion. Data obtained from 3 mice n=5 replicates per condition. Data were analysed by one-way ANOVA followed by Tukey's post hoc. ***: p< 0.001 *vs* 1 mM glucose; ††: p<0.005 vs 20 mM glucose.

4.3.5 Role of intracellular Ca^{2+} on somatostatin release

The secretion experiments support the concept that glucose-stimulated somatostatin release involves ryanodine-sensitive CICR from intracellular thapsigargin-sensitive Ca^{2+} stores. The role of CICR was next explored by monitoring $[Ca^{2+}]$ in δ-cells using islets from SST-Cre-GCaMP3 mice. Addition of ryanodine (50 µM) in the presence of 20 mM glucose, did not affect the frequency or the duration of $[Ca^{2+}]_i$ oscillations (Figure 4-9A-B, D). However, in the presence of thapsigargin (10 µM), the frequency of $[Ca^{2+}]_i$ oscillations was reduced by 30 % (Figure 4-9A-B, E, $p<0.05$); no effect on the duration of the $[Ca^{2+}]_i$ oscillations was observed. The results obtained by thapsigargin in the $[Ca^{2+}]_i$ experiments are consistent with the secretion data. However, the failure of ryanodine to affect $[Ca^{2+}]_i$ was unexpected given that somatostatin release was significantly inhibited by this CICR inhibitor.

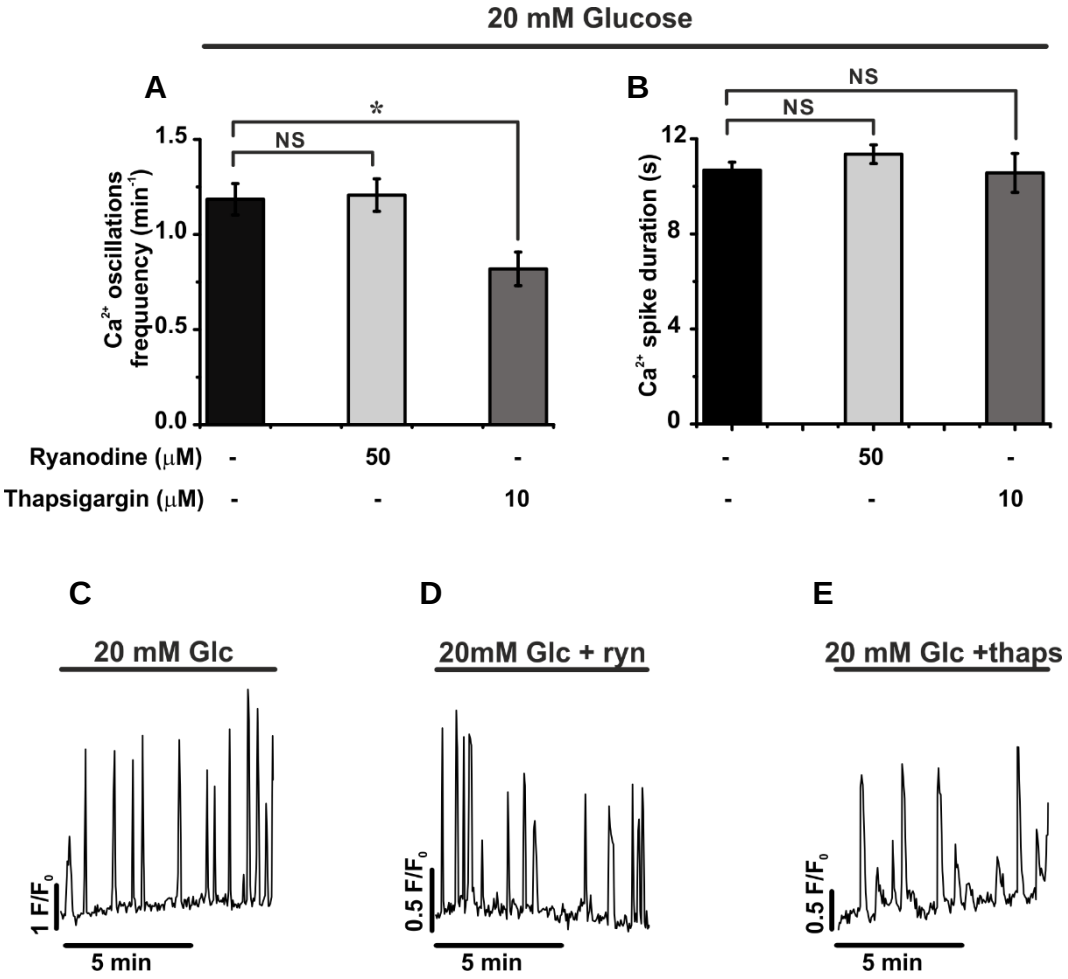

Figure 4-9 Effect of ryanodine and thapsigargin on δ-cells $[Ca^{2+}]_i$ oscillations.

A Effect of ryanodine (ryn, 50 µM) and thapsigargin (thaps, 10 µM) on the frequency of $[Ca^{2+}]_i$ oscillations, in δ-cells exposed to 20 mM glucose. **B** As in **A** but the duration was measured. **C-E** Representative recordings of data summarized in **A**-**B**. **C** n=66 cells from 3 islets from 3 mice; **D** n=60 cells from 3 islets from 3 mice, **E** n=68 cells from 3 islets from 3 mice. Data were analysed by one-way ANOVA followed by Tukey's *post hoc*. NS: not significant; *: $p<0.05$ *vs* 20 mM glucose alone.

To understand the relationship between electrical activity and $[Ca^{2+}]_i$, parallel measurements of intracellular $[Ca^{2+}]$ and membrane potential were conducted. These measurements revealed a surprisingly weak correlation between $[Ca^{2+}]_i$ and electrical activity (Figure 4-10A); $[Ca^{2+}]_i$, oscillations persisted even in δ-cells voltage-clamped at -70 mV, which is too negative for activation of R-type or L-type voltage-gated Ca^{2+} channels (Figure 4-10B). A voltage clamp depolarization evoked a large $[Ca^{2+}]_i$ transient. This shows that the $[Ca^{2+}]_i$ measurements were obtained from the voltage-clamped cell. Notably, the oscillations were reduced when the K_{ATP} channel activator, diazoxide (100 µM) was applied (Figure 4-10B).

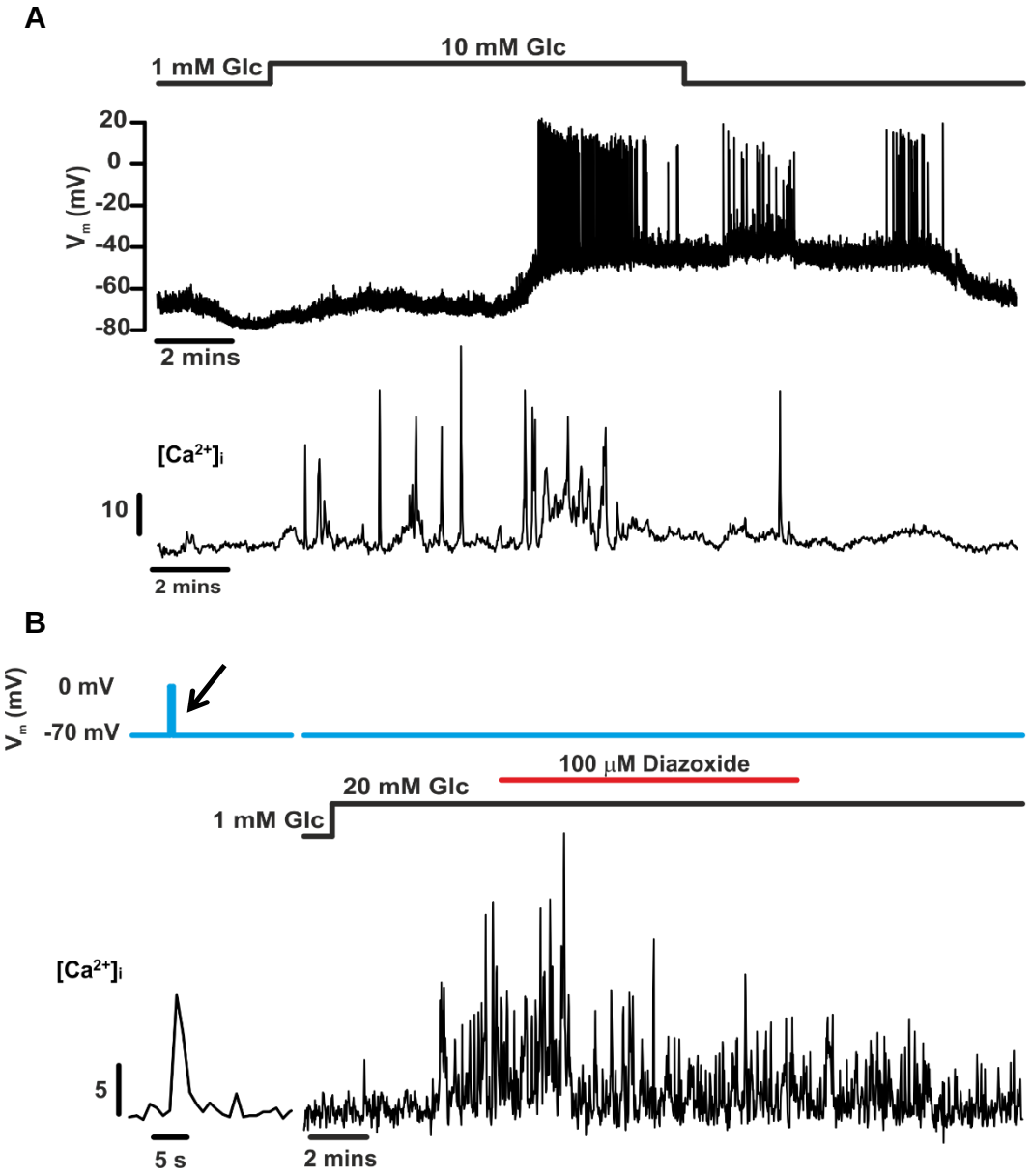

Figure 4-10 Correlation between membrane potential and $[Ca^{2+}]_i$.

A Parallel measuments of membrane potential recording and changes in intracellular $[Ca^{2+}]_i$ evoked by 20 mM glucose in a δ-cell recorded within a SST-Cre-GCaMP3 islet. **B** Measurements of changes in intracellular $[Ca^{2+}]$ in a δ-cell clamped at -70 mV with a patch pipette. It was ascertained by application of a voltage-clamp pulse (arrow) that the $[Ca^{2+}]_i$ measurments reflect the voltage-clamped cells.

To test the role of CICR under experimental conditions avoiding the confounding effect of δ-cells electrical activity, the effect of thapsigargin and ryanodine were next tested in the presence of a depolarizing K^+ concentration (70 mM). Under these experimental conditions, the membrane potential is clamped at -10 mV, thus bypassing any effect these compounds might have on the membrane potential. This allows the role of Ca^{2+} released from the intracellular compartment to be studied in isolation. Membrane depolarization evoked a large $[Ca^{2+}]_i$ transient that reflects the opening and subsequent inactivation of the voltage-gated Ca^{2+} channels (illustrated in Figure 4-11). $[Ca^{2+}]_i$ was measured at steady-state, 10 min after the onset of the high-$[K^+]_o$ depolarization (Figure 4-11).

Under depolarizing conditions, the frequency of $[Ca^{2+}]_i$ oscillations in the presence of 20 mM glucose was increased by 40% compared to 1 mM glucose (Figure 4-12A-C, $p<0.005$). In the presence of 20 mM glucose and 70 mM $[K^+]_o$, thapsigargin abolished the $[Ca^{2+}]_i$ oscillations (Figure 4-13A-B, E) while ryanodine was without effect on the frequency of $[Ca^{2+}]_i$ oscillations, but their duration was reduced by 30% [3] (Figure 4-13A-B, D).

[3] It is acknowledged that the sampling frequency we used is insufficient to make any reliable estimates of the true duration of the $[Ca^{2+}]_i$ oscillations. According to the Nyquist sampling theorem, the sampling frequency should be at least twice that of the lifetime of the event. We are currently repeating the experiments in individual δ-cells using a sampling frequency of 3 samples/s (*i.e.* 10/fold higher than used previously).

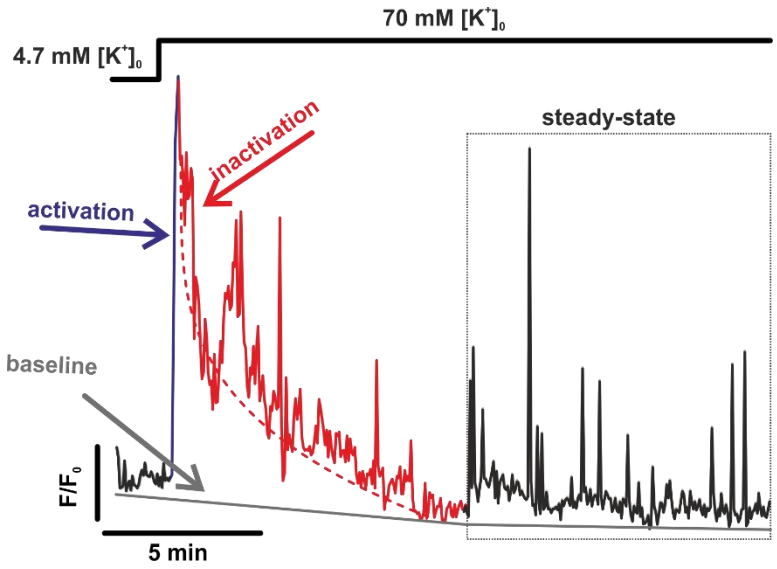

Figure 4-11 Effect of depolarizing K^+ concentration on $[Ca^{2+}]_i$ in δ-cells.
Activation (blue) and inactivation (red) phases of voltage-gated Ca^{2+} channels in response to 70 mM $[K^+]_o$. Steady-state after depolarization (dashed area).

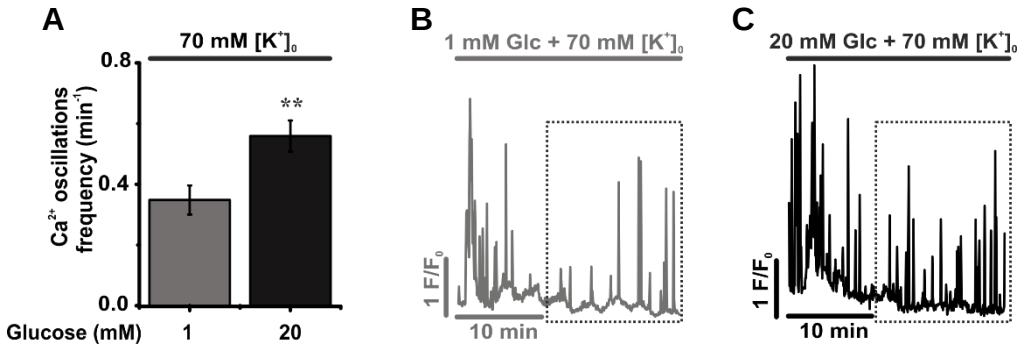

Figure 4-12 Effect of glucose in the presence of depolarizing K^+ concentration.
A The frequency of $[Ca^{2+}]_i$ oscillations in δ-cells measured under depolarizing K^+ conditions (70 mM $[K^+]_o$), in the presence of 1mM glucose (Glc) or 20 mM glucose. **B** Representative recording of n= 63 cells from 4 islets from 3 mice at 1mM or **C** As in **B** but at 20 Mm glucose. n=66 cells from 3 islets from 3 mice. Data were anlysed with unpaired Student's t-test. **: $p<0.005$ *vs* 1mM glucose. The frequency of $[Ca^{2+}]_i$ oscillations was measured at steady-state (dashed area in **B-C**).

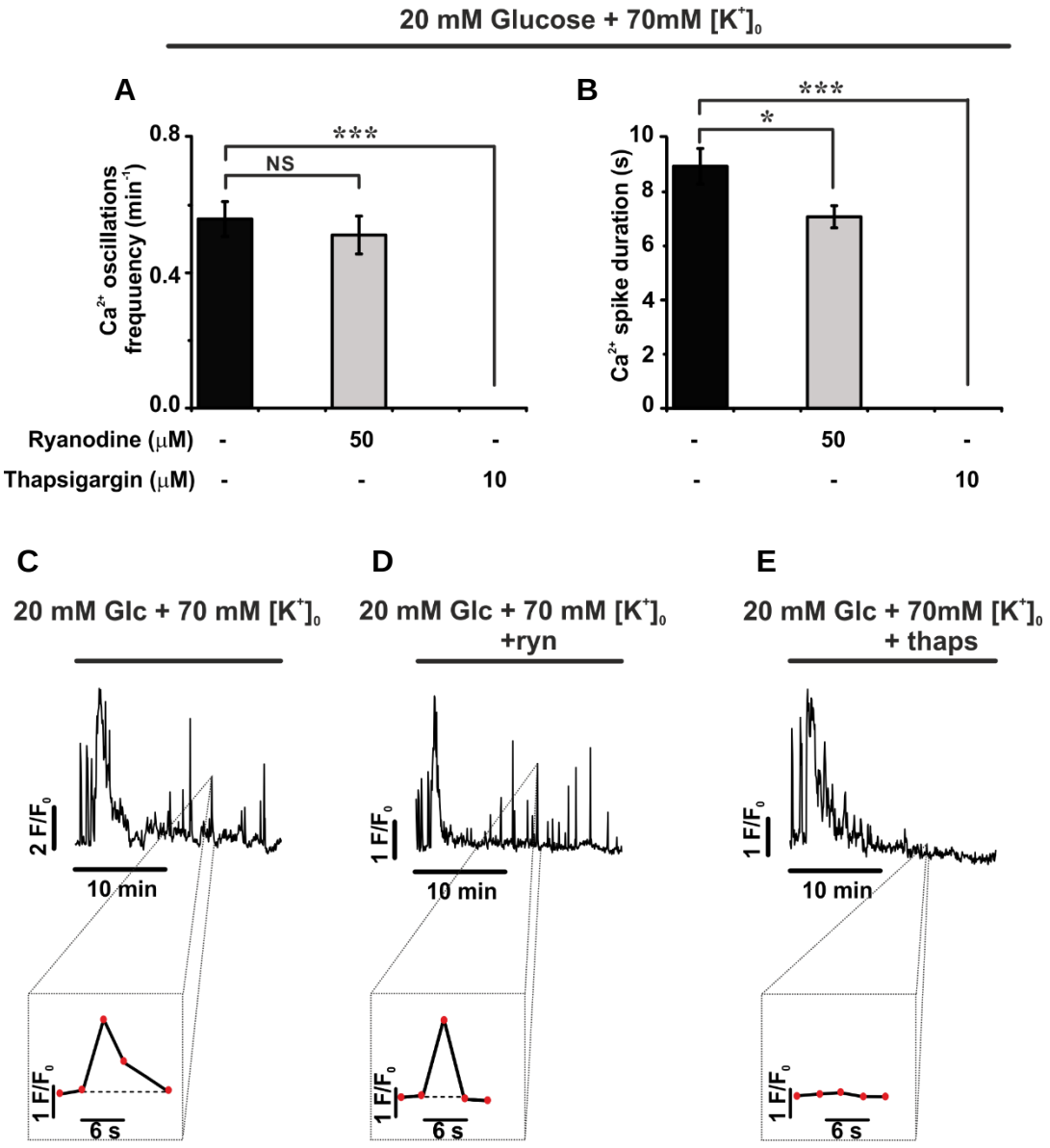

Figure 4-13 Effect of ryanodine and thapsigargin in the presence of depolarizing K^+ concentration.

A Effect of ryanodine (ryn, 50 µM) and thapsigargin (thaps, 10 µM) on the frequency of $[Ca^{2+}]_i$ oscillations in the presence of 70 mM $[K^+]_o$. **B** As in **A** but measuring the duration of $[Ca^{2+}]_i$ oscillations. **C-E** Representative recordings of data summarized in **A**-**B**. **Insets** Zoom-in images of single $[Ca^{2+}]_i$ oscillations. Data points in red are connected by black lines. **C** n=66 cells from 3 islets from 3 mice; **D** n=60 cells from 3 islets from 3 mice, **E** n=68 cells from 3 islets from 3 mice. Data were analysed by one-way ANOVA followed by Tukey's *post hoc*. NS: not significant; *: $p<0.05$, ***: $p<0.001$ *vs* 20 mM glucose in the presence of 70 mM $[K^+]_o$.

The persistence of Ca^{2+} oscillations in the presence depolarizing K^+ concentration and ryanodine suggested that other Ca^{2+} stores may be involved in glucose-induced somatostatin secretion. Acidic endolysosomal Ca^{2+} stores have been reported to regulate insulin secretion in pancreatic β-cells (Arredouani et al., 2015). More recently, unpublished observations from our laboratory have suggested that they are involved also in the control of glucagon secretion (Hamilton A, Tarasov AI, Galione A and Rorsman P, manuscript). NAADP mediates Ca^{2+} release from acidic Ca^{2+} stores *via* interaction with TPC1 and TPC2, two members of the endolysosomal two-pore channel family (Churchill et al., 2002, Calcraft et al., 2009). To test whether acidic Ca^{2+} stores may regulate glucose-induced somatostatin secretion, the membrane-permeable NAADP antagonist, Ned-19 (Naylor et al., 2009) was used. However, Ned-19 (100 µM, Tocris) was without any effect on glucose-induced (20 mM) somatostatin secretion (Figure 4-14), thus excluding the possible involvement of acidic stores in the regulation of somatostatin secretion.

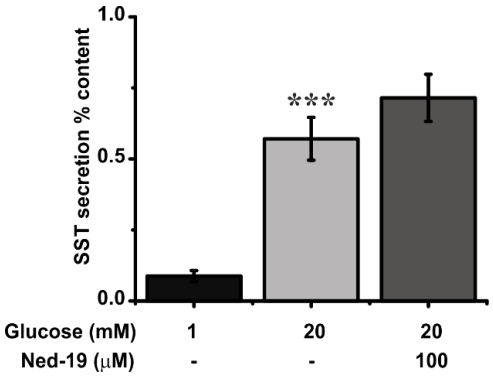

Figure 4-14 Effect of acidic endolysosomal Ca^{2+} stores on somatostatin secretion.
Effect of the NAADP antagonist Ned-19 on glucose-induced somatostatin release. Data were obtained using 6 mice n=7-10 replicates. Somatostatin content did not change between groups. Data were statistically analysed by one-way ANOVA followed by Tukey's *post hoc.* ***: p<0.005 vs 1 mM glucose.

4.4 DISCUSSION

4.4.1 Stimulus-secretion coupling in pancreatic δ-cells

The SST-Cre-GCaMP3 mouse model enables easy identification of δ-cells and thus allows detailed investigation of the regulation of glucose-induced somatostatin secretion. When this study was initiated, there were no data available about the expression of the metabolic regulators involved in glucose metabolism, in δ-cells. However, recently two independent but similar studies reported transcriptomic characterization of α-, β- and δ- cells (Adriaenssens et al., 2016, Di Gruccio et al., 2016). According to the data presented in this thesis, which are in agreement with both studies, glucose uptake in mouse δ-cells may be mediated by the glucose transporter GLUT1 (the major subtype identified) and GLUT3. GLUT2, the major subtype expressed in β-cells (Thorens et al., 1988), was expressed at very low levels in SST-positive δ-cells. GLUT1 and GLUT3 display higher affinity for glucose (K_m for 2-deoxyglucose 6.9 and 1.4 respectively) than GLUT2 (K_m=11.2) (Gould and Holman, 1993). Therefore, the high expression of GLUT1 and GLUT3 in δ-cells may explain why somatostatin secretion is triggered at lower concentrations of glucose than insulin release, with thresholds at 3 and 6 mM glucose, respectively (Walker et al., 2011). The “glucose sensor” involved in glucose metabolism in δ-cells is most probably glucokinase, although low levels of hexokinase-1 were also detected in δ-cells (Figure 4-3B).

The relatively weak stimulatory effect of tolbutamide compared to 20 mM glucose (Figure 4-4) does not mean that K_{ATP} channel closure in not required

for somatostatin secretion. Closure of K_{ATP} channels, which causes initiation of electrical activity and increase in $[Ca^{2+}]_i$ (Zhang et al., 2007), is presumably one of the signals triggering CICR that in turn leads to stimulation of somatostatin secretion. This concept is in good agreement with the strong inhibitory effect of both diazoxide (Figure 4-5C-D) and isradipine (Figure 4-7A) on somatostatin secretion and may explain why glucose-induced somatostatin release is maintained at nearly normal levels in K_{ATP} channels deficient (Kir6.2 STOP) islets (Zhang et al., 2007). This scenario is also in keeping with data from human islets that showed inhibition of glucose-induced somatostatin secretion in the presence of isradipine or diazoxide (Braun et al., 2009).

$[Ca^{2+}]_i$ imaging experiments revealed that somatostatin release is regulated by both R-type and L-type Ca^{2+} channels, which . belong to the family of high voltage-activated Ca^{2+} channels (Snutch et al., 2000-2013). However, R-type are activated at a lower voltage compared to L-type with threshold at -40 mV and -20 mV, respectively. Notably, it has been proposed that L-type and R-type are not evenly distributed in the plasma membrane of δ-cells (Zhang et al., 2007). Although the precise respective role of these two types of channels remain to be addressed, based on their electrophysiological properties, we postulate that R-type may regulate CICR, as previously reported (Zhang et al., 2007), while L-type might be involved in the initiation of electrical activity.

The effects of blocking L-type Ca^{2+} channels (using isradipine) and activation of K_{ATP} channels (using diazoxide) are different than previously observed (Zhang et al., 2007). Differences in mouse strain can be excluded (Figure

4-5E). However, the data presented in this thesis agree with the observations reported recently by other researchers (van der Meulen et al., 2015). Further studies are required to resolve these discrepancies.

Inhibition of SERCA pumps with thapsigargin demonstrated the importance of intracellular Ca^{2+} stores in glucose-induced somatostatin secretion (Figure 4-8A). Pancreatic δ-cells express IP_3R1, RyR3 (Figure 4-8B-C) but also IP_3R3 and low levels of IP_3R2, according to RNAseq data (Adriaenssens et al., 2016, Di Gruccio et al., 2016). However, the secretion data suggest that CICR mechanism in δ-cells is regulated primarily *via* RyRs (Figure 4-8D).

Ryanodine inhibited somatostatin secretion by 40%, similar to what was observed previously (Zhang et al., 2007), but it was without detectable effect on glucose-induced $[Ca^{2+}]_i$ oscillations. An inhibitory effect was seen only in cells depolarized with high-$[K^+]_o$ (Figure 4-12B, D). There was also a paradoxically weak effect of thapsigargin on $[Ca^{2+}]_i$ oscillations evoked by high glucose (Figure 4-9A, E). However, in the case of thapsigargin, a very strong effect was observed in depolarized islets (Figure 4-13A-B, E). It is possible that other intracellular stores regulate somatostatin release form δ-cells but the lack of effect of the NAADP antagonist Ned-19 suggests that acidic stores are not be involved in the regulation of glucose-stimulated somatostatin secretion. However, Ca^{2+} released from the mitochondria may regulate somatostatin secretion from δ-cells, analogously to insulin secretion from β-cells (Nita et al., 2012).

The findings that $[Ca^{2+}]_i$ oscillations do not correlate with changes in membrane potential support the hypothesis of Ca^{2+} released from intracellular stores independently of membrane depolarization (Figure 4-10A). Further evidence for this idea came from Ca^{2+} imaging experiments of voltage-clamped cells. The findings that $[Ca^{2+}]_i$ oscillations are maintained in voltage-clamped cells provide further evidence for membrane potential-independent mechanism (Figure 4-10B). It was therefore surprising that these oscillations disappear in the presence of diazoxide.

Remarkably, δ-cells express high levels of low-voltage activated (Snutch et al., 2000-2013) T-type Ca^{2+} channels (Figure 4-6). Thus, it is tempting to hypothesise that when a δ-cell is voltage-clamped at -70 mV, entry of extracellular Ca^{2+} through these channels can trigger Ca^{2+} release from the intracellular stores (Figure 4-10B). Probably, in the presence of the hyperpolarizing agent diazoxide, which inhibits both somatostatin secretion (Figure 4-5C, E) and $[Ca^{2+}]_i$ oscillations (Figure 4-5A and Figure 4-10B), the membrane potential of δ-cells become more negative than -70 mV, the threshold voltage required for opening of the T-Type Ca^{2+} channels to elicit CICR. Future experiments either in the presence of a T-type Ca^{2+} channels inhibitor or where a single δ-cell is voltage-clamped (by means of the amplifier) at a voltage lower than -70 mV, to mimic the effect of diazoxide, are required to validate this hypothesis. Nevertheless, the secretion data make it quite clear that glucose-induced somatostatin secretion relies also on CICR (Figure 4-8).

Another hypothesis is that the divergent results obtained when a δ-cell was hyperpolarized by voltage-clamping (when a single δ-cell is controlled) and diazoxide (which hyperpolarizes all the cells in the islets) reflects paracrine signalling. For example, glucose uptake *via* the sodium-dependent glucose transporter SGLT1 and 2, which are both expressed in δ-cells, albeit at low levels (Adriaenssens et al., 2016) may increase $[Ca^{2+}]_i$ (*e.g*. secondary to increased $[Na^+]_i$ and inhibition of the plasmalemmal Na^+/Ca^{2+} antiporter) sufficiently to trigger CICR.

To account for the inhibitory effects of diazoxide and isradipine, we postulate that a secretory product from the β-cells may augment the effect of glucose transport. Indeed, it has been reported that insulin stimulates SGLT-2 mediated glucose and Na^+- transport. (Ghezzi and Wright, 2012).

In conclusion, using GCaMP3-expressing δ-cells it has been possible to demonstrate that the regulation of somatostatin release by intracellular Ca^{2+} is complex. Based on the data presented in this thesis a revised model of glucose-induced somatostatin secretion that builds on the work of Zhang et al. (2007) may be proposed (Figure 4-15). In this model, CICR remain central stage but a more direct role of K_{ATP} channel closure is indicated. The revised model also suggests a more direct role of the L-type Ca^{2+} channels and raise the interesting possibility that SGLT1 and 2 are involved.

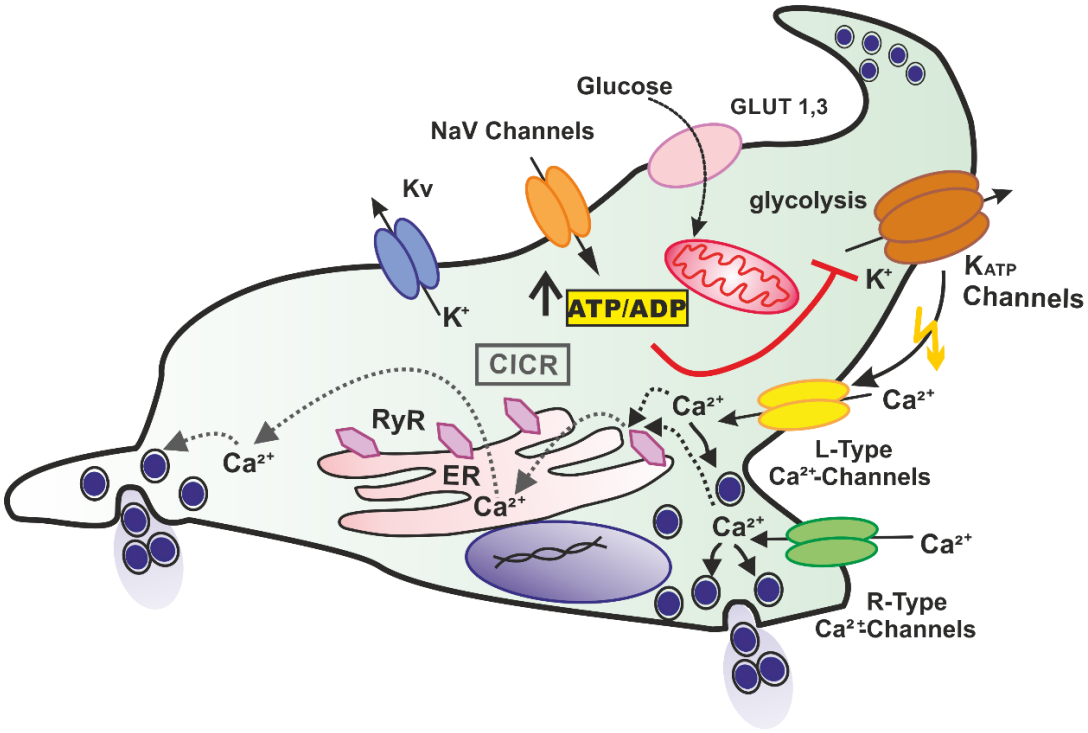

Figure 4-15 Revised model of glucose-induced somatostatin secretion.

According to the data here reported, glucose enters into the δ-cells *via* Glut1 or Glut3. Glucokinase enables glycolysis to generate metabolic signals including ATP. Increase ATP/ADP ratio leads to closure of the K_{ATP} channels, followed by membrane depolarization. This leads to opening of the R- and L-type Ca^{2+} channels. The resultant increase in $[Ca^{2+}]_i$ triggers CICR and results in a large $[Ca^{2+}]_i$ oscillation *via* activation of ryanodine receptors type 3 present in the ER.

5 HOMOLOGOUS INTERACTION BETWEEN δ-CELLS

5.1 INTRODUCTION

The complex structure of the pancreatic islets enables endocrine cells to be in direct contact with each other and to function as a micro-organ (Kim et al., 2009, Steiner et al., 2010). Islet cells can communicate *via* gap-junctions, which allow metabolic signals to flow from one cell to another. In the case of β-cells, gap-junctions (composed of connexin-36) regulate metabolic coupling between cells, which modulate electrical activity and insulin secretion (Ravier et al., 2005, Benninger et al., 2011). However, very little is known about the molecular identity of gap-junctions and their role in δ-cells. Two types of (potentially) metabolite-permeant channels can be found in pancreatic islets: connexins and pannexins (Cigliola et al., 2015).

5.1.1 Connexins

The human and mouse genome contain 20 and 21 genes encoding for connexins (Willecke et al., 2002, Bosco et al., 2011). All connexins share the same topology. They contain cytoplasmic N- and C-terminal regions and four membrane-spanning domains linked by two extracellular and one intracellular loop. Six connexins oligomerize to generate the pore-forming connexons (also known as hemichannels) (Goodenough, 1975). Gap-junctions are formed by two connexons in two adjacent cells (one from each of the coupled cells)

(Kumar and Gilula, 1996, Saez et al., 2005). Although transcripts for connexin-43 and connexin-45 are present, connexin-36 is the major isoform present in pancreatic islets (Serre-Beinier et al., 2000, Theis et al., 2004). Connexin-36 is expressed preferentially in the insulin-producing β-cells where it is responsible for β-cell coupling (Charpantier et al., 2007, Serre-Beinier et al., 2009). However, transcripts coding for connexin-36 have been found also in non-β cells (Serre-Beinier et al., 2000, Adriaenssens et al., 2016, Di Gruccio et al., 2016). To date, nothing is known about the functional role of these channels in α- and δ-cells.

5.1.2 Pannexins

Pannexins - from the Greek *pan* (“all”) and from the Latin *nexus* (“connection”) - are a family of vertebrate proteins identified by Panchin et al. (2000) as the homologues of the invertebrate innexins. The pannexin family comprises three members: Panx1, Panx2 and Panx3, each encoded by a different gene (Penuela et al., 2007, Penuela et al., 2013).

Pannexins and connexins do not share any sequence homology. However, all three members of the pannexin family feature similar membrane topology to the connexins. Each consists of four α-helical transmembrane domains, two extracellular loops and one intracellular loop, with both their N- and C-terminal domains exposed to the cytoplasm (Penuela et al., 2013). The term ‘pannexons’ has been used to indicate hexameric pannexin channels (Dahl

and Harris, 2009, Cheung et al., 2014). However, it is still debated whether pannexins are capable of forming gap-junctions (Dahl and Locovei, 2006, Sosinsky et al., 2011), because of the presence of N-linked glycosylation sites on their extracellular loops (Boassa et al., 2007).

Some studies have reported that pannexins are only large transmembrane channels, which connect the intracellular and extracellular regions of one cell to allow the passage of ions and small molecules like ATP (Bao et al., 2004). However, other studies have demonstrated that pannexins can generate functional gap-junctions (Bruzzone et al., 2003, Sahu et al., 2014). It seems likely that the ability of pannexins to form gap-junctions is cell-specific and depends on the post-translational glycosylation pattern, which varies greatly among different cells (Sahu et al., 2014).

Very little is known about the function of pannexins in the endocrine pancreas. However, transcripts coding for Panx1 and Panx2 are present in both mouse and human islet cells (Nica et al., 2013, Adriaenssens et al., 2016, Di Gruccio et al., 2016). Moreover, a putative role has been postulated for pannexins in β- to α-cell interactions (Meda, 2013).

Recently, Cigliola et al. (2015) compared islets isolated from connexin-36- and Panx1-null (knock out) mice. In connexin-36 null mice, increased basal and a loss of glucose-induced insulin release was observed. In Panx1 null mice no change in the basal secretion of insulin was detected but glucose-induced insulin secretion was impaired. They also observed a marked increase in the

basal glucagon secretion (unpublished data mentioned in (Cigliola et al., 2015)). These observations suggest that pannexins may play a pivotal role in cell-cell communication in islets.

Here, we have taken advantage of the possibility of imaging $[Ca^{2+}]_i$ dynamics in several δ-cells within SST-Cre-GCaMP3 islets, to investigate whether $[Ca^{2+}]_i$ oscillations are synchronized in different δ-cells across the pancreatic islet.

5.2 MATERIALS AND METHODS

5.2.1 Intracellular [Ca^{2+}] imaging

Ca^{2+} imaging recording and analysis were performed as reported in Section 2.10.

5.2.2 Correlation analysis of $[Ca^{2+}]_i$ imaging time series in δ-cells

In statistics, correlation describes how two variables are related. If two variables are positively related (i.e. correlate positively) it means that they move in the same direction. If they are inversely related (correlate negatively) they move in inverse directions. The degree of correlation can be estimated by several coefficients. The most common is Pearson's correlation coefficient, which assesses linear relationship between a paired set of data. The values of Pearson's correlation coefficient range from -1 to +1. A value of 0 indicates the absence of an association between variables. Values of +1 or -1 correspond to total positive or total negative linear correlation. By applying these principles to $[Ca^{2+}]_i$ imaging time series, it can be estimated whether Ca^{2+} signals of a pair of cells correlate positively, negatively or do not correlate. A detailed description of the method developed to assess the correlation between δ-cells is included in Appendix 3.

5.3 RESULTS

5.3.1 Assessment of electrical coupling in δ-cells

While performing $[Ca^{2+}]_i$ imaging experiments, it was observed that δ-cells demonstrate some degree of synchronization after exposure to 20 mM glucose (Figure 5-1B). Therefore, it was hypothesized that similar to β-cells, δ-cells might be electrically coupled. To test this hypothesis, the level of synchronization of δ-cells $[Ca^{2+}]_i$ signals was quantified using a previously described method (Stozer et al., 2013) (as outlined in Appendix 3, Section 8.3.1).

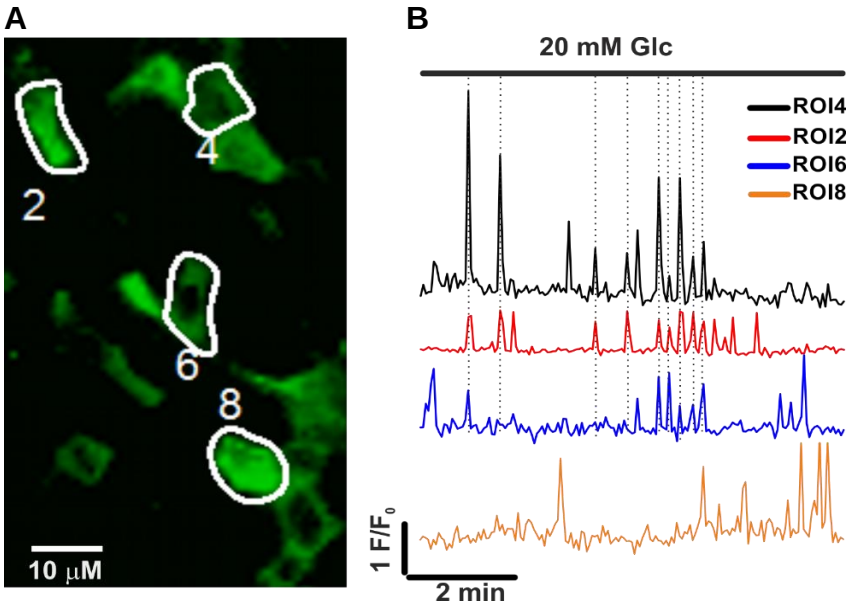

Figure 5-1 Synchronous $[Ca^{2+}]_i$ oscillations between δ-cells.

A Confocal image of a SST-Cre-GCaMP3 mouse islet. Four region of interest (ROI2, 4, 6, and 8) are indicated corresponding to individual δ-cells. **B**. $[Ca^{2+}]_i$ oscillations corresponding to the different ROIs. Dashed lines highlight synchronous $[Ca^{2+}]_i$ oscillations in ROIs 2, 4 and 6. ROI8 is asynchronous.

In brief, for each recording, the Pearson correlation coefficient of the $(i,j)^{th}$ pair of cells at the maximum lag (C_{ij}) was calculated during low (1 mM) and high (20 mM) glucose using a sliding window with duration $\Delta T = 150\ s$ (initially arbitrary chosen). Each correlation matrix could then be represented as a heatmap as shown in Figure 5-2. For example, in this recording (Figure 5-2) 12 ROIs (cells) were identified. Each heat-map represents the correlation between all pairs of cells in a distinct 150 s time window. In this recording, the baseline condition is 1 mM glucose. At T=300-450 s, 20 mM glucose is added. For each time-window, the average of C_{ij} for all pairs of cells (i,j) in that time window was calculated (R_{avg}). This represents the average correlation of all δ-cell pairs in that time window. In the presence of 1 mM glucose, the average correlations between cells is low (R_{avg}=0.07±0.08 in T=0-150 s), but increased in 20 mM glucose (R_{avg}=0.49±0.03 in T=900-1050 s; $p<0.005$, in the experiment displayed in Figure 5-2).

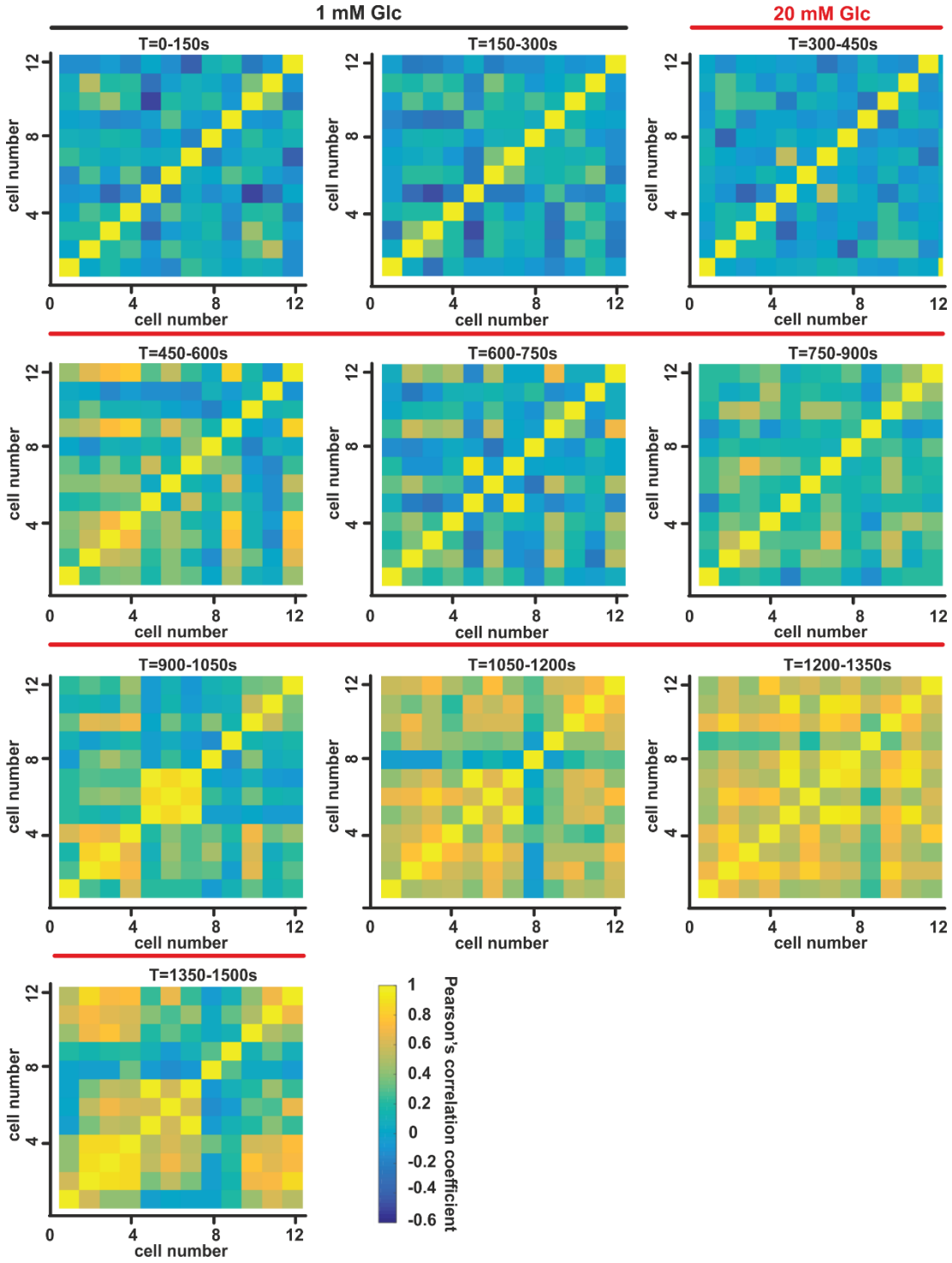
1 mM Glc
20 mM Glc
T=0-150s
T=150-300s
T=300-450s
T=450-600s
T=600-750s
T=750-900s
T=900-1050s
T=1050-1200s
T=1200-1350s
T=1350-1500s
cell number
0
4
8
12
1
0.8
0.6
0.4
0.2
0
-0.2
-0.4
-0.6
Pearson's correlation coefficient

Figure 5-2 Correlation matrices obtained for δ-cell pairs of one recording.

Heat-map representing the correlation matrix of the correlation coefficient between the cell pair (i, j), in 150 s time windows for a particular recording, which contained 12 δ-cells. In this recording, the glucose concentration was changed from 1 mM to 20 mM during time window T=300-450 s. The correlation between δ-cells subsequently increased. Yellow corresponds to positive Pearson's correlation coefficient (*i.e*. positive linear relation between *i* and *j*). Dark blue corresponds to negative Pearson's correlation coefficients (*i.e*. negative linear relation between *i* and *j*).

To ensure that the choice of a particular ΔT would not affect the calculated R_{avg}, the correlation analysis was repeated for four different ΔT=90 s, 120 s, 150 s and 180 s (*cf*. (Stozer et al., 2013)). Application of 20 mM glucose caused an increase in R_{avg} irrespective of the choice of ΔT (Figure 5-3). Thus, having ascertained that the results do not depend on the length of the chosen interval, for all subsequent analysis reported in this study, the duration ΔT=150 s was used.

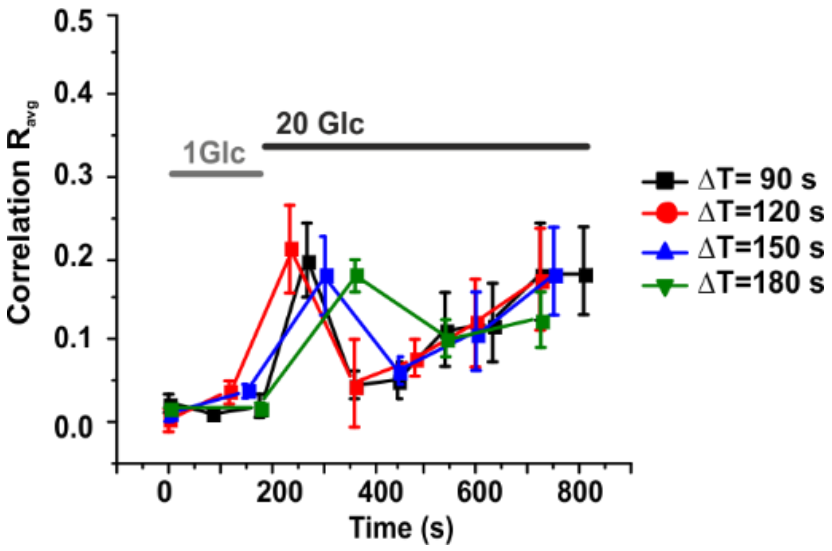

Figure 5-3 The increase in correlation at high glucose does not depend on the choice of the size of the time-window (ΔT).

The average correlation coefficient R_{avg} was calculated using different (ΔT=90, 120, 150, 180 s) to exclude the possibility that the results obtained were affected by the choice of the specific ΔT. The increase in R_{avg} upon glucose stimulation was independent of the chosen ΔT and followed the same pattern for all four ΔT. Data are the average of n=13 recordings.

The results of the correlation analysis of 16 $[Ca^{2+}]_i$ imaging recordings for ΔT=150 s are summarized in Figure 5-4. The average correlation between δ-cells significantly increased when glucose concentration was increased from 1 mM (R_{avg}=0.03±0.016 at 0 s and R_{avg}=0.06±0.013 at 150 s) to 20 mM (R_{avg}=0.19±0.04, at 300 s, and R_{avg}=0.18±0.04 at 750 s, Figure 5-4). Although the peak R_{avg} was only 0.19 in some recordings, R_{avg} increased to 0.5. (see Figure 5-4, dashed lines represent all individual recordings). Furthermore, when individual correlations between pairs of cells were investigated, it could be seen that some pairs of δ-cells displayed a high degree of correlation in 20 mM glucose ($C_{i,j}$>0.70, see two examples in Figure 5-5A-B). Thus, this analysis supported the existence of synchronous Ca^{2+} dynamics in δ-cells.

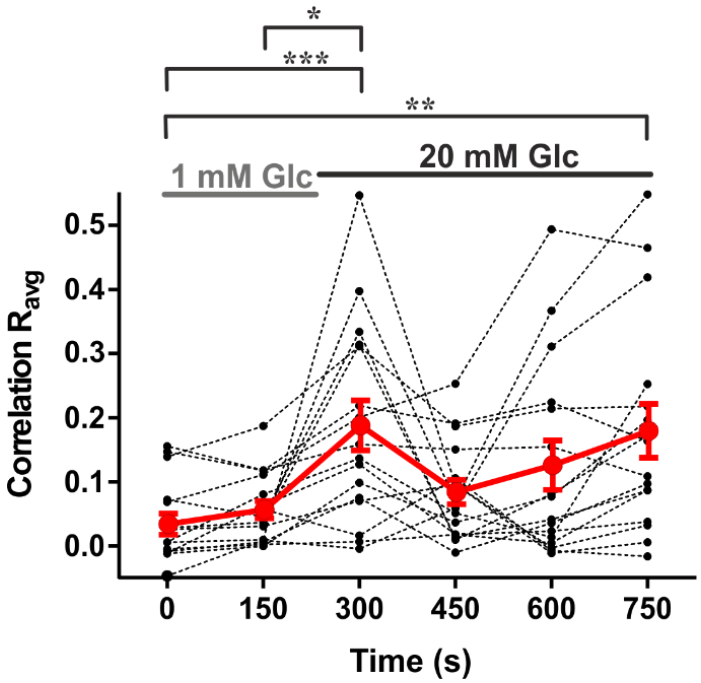

Figure 5-4 Correlation between δ-cells increases upon glucose stimulation.

Correlation analysis of δ-cells $[Ca^{2+}]_i$ imaging time series conducted using ΔT=150 s. Dashed lines represent the evolution of R_{avg} over each 150 s window for each of the n=16 recordings analysed. Red dots represent the mean R_{avg} over each 150 s windows. Glucose (Glc) was increased from 1 mM to 20 mM as indicated. Data were statistically analysed by one-way ANOVA (Friedman's test) followed by Dunn's *post hoc* test. *: p<0.05, **: p<0.005, ***: p<0.001 *vs* baseline values (1 mM glucose).

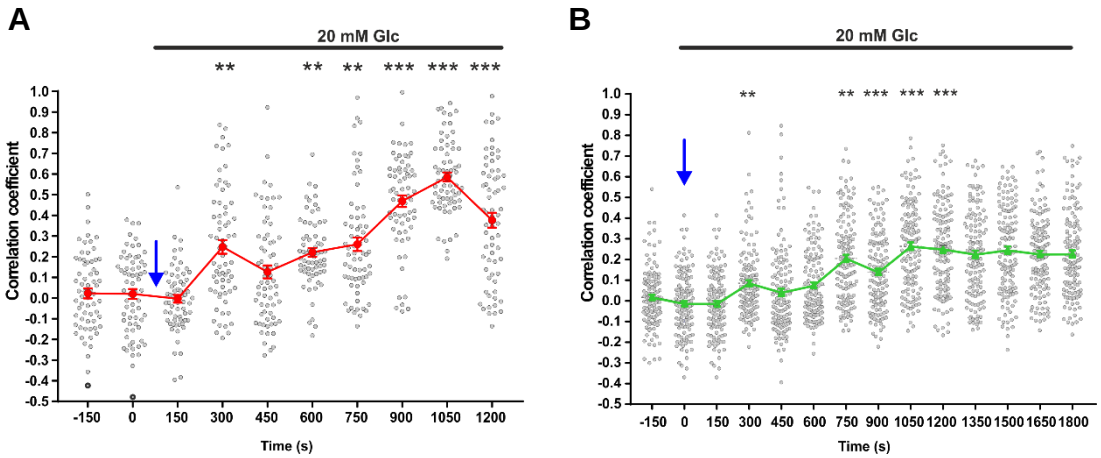

Figure 5-5 Example of average correlations in two distinct experiments.

A-B. Two different recordings showing (**A**) a high degree of correlation and (**B**) low degree of correlation following addition of 20 mM glucose. Blue arrows represent the time at which the extracellular solution was changed from 1 mM glucose to 20 mM glucose. Grey dots represent all the correlation coefficients of each distinct pair of cells in each of the 150 s time windows. Red and green dots represent the mean correlation coefficient R_{avg} in each time windows. Data were statistically analysed by one-way ANOVA (Friedman's test) followed by Dunn's *post hoc* test. **: $p<0.005$, ***: $p<0.001$ *vs* t=0.

5.3.2 Analysis of gap-junctions expression in δ-cells

After having ascertained that $[Ca^{2+}]_i$ oscillations in δ-cells oscillate synchronously, it was explored whether gap-junctions modulate somatostatin secretion. First, it was investigated which types of gap-junctions are expressed in δ- cells (Figure 5-6). Connexin-36 (encoded by the gene *Gjd2*), the major isoform expressed in pancreatic β-cells (Serre-Beinier et al., 2000), was expressed in both SST-negative and SST-positive cells. However, its levels were significantly lower in δ-cells (Figure 5-6, $p<0.05$). Connexin-43 (*Gja1*) expression was low in both δ-and non-δ-cells but no significant differences were observed (Figure 5-6, $p=0.1$). The expression levels of pannexin-1 (*Panx1*) were 7-fold higher in SST-positive compared to SST-negative cells (Figure 5-6, $p<0.05$). Pannexin-2, the other isoform expressed in pancreatic islets (as pannexin-3 is not expressed) was detected in δ- and non-δ cells with no significant differences (Figure 5-6, $p=0.4$). Pharmacological inhibitors were used to investigate whether gap-junctions composed of connexin-36 and pannexin-1 play a role on somatostatin secretion.

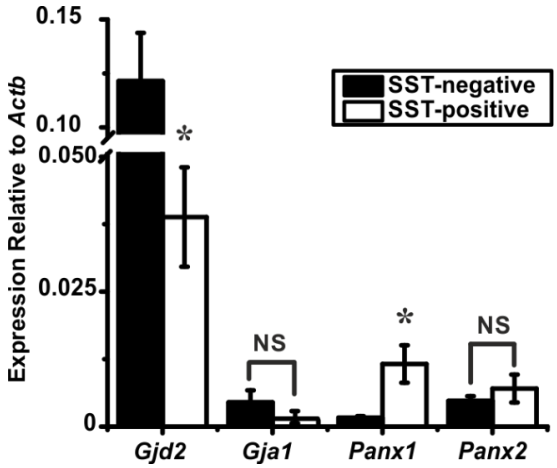

Figure 5-6 Gap-junctions expression in SST-negative and -positive cells.

Expression levels of gap-junction genes (*Gjd2, Gja1, Panx1* and *Panx2*) were assessed by qPCR. Each gene was compared for expression between SST-negative and SST-positive fractions (n=5 preparations). Statistical analysis was performed using unpaired Student's t-test. NS: not significant; *: $p<0.05$ *vs* SST-negative.

5.3.3 Role of connexin-36 in δ-cells

Addition of the specific connexin-36 blocker mefloquine (10 µM, Sigma) (Cruikshank et al., 2004) increased somatostatin secretion 3-fold in the presence of 20 mM glucose (Figure 5-7A, $p<0.05$). To test whether the blocker may affect the synchronization of $[Ca^{2+}]_i$ oscillations in δ-cells exposed to 20 mM glucose, the sliding window technique (as described previously) was used. As shown in Figure 5-7B, the R_{avg} was unaffected by the addition of 10µM mefloquine.

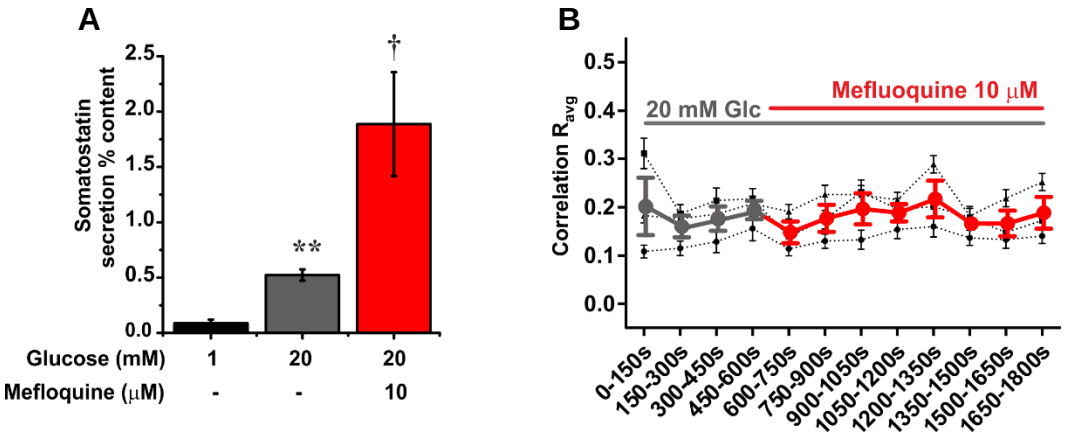

Figure 5-7 Effect of the connexin-36 inhibitor mefloquine on δ-cells.

A Effect of glucose and mefloquine on somatostatin secretion. Glucose and mefloquine were included as indicated. Somatostatin content did not change between groups. Data were obtained using 3 mice and n=5-6 replicates per condition. Data were analysed by one-way ANOVA followed by Tukey's *post hoc*. **: $p<0.005$ *vs* 1 mM glucose, †: $p<0.05$ *vs* 20 mM glucose. **B** Assessment of synchronization of δ-cells $[Ca^{2+}]_i$ oscillations before and upon addition of 10 µM mefloquine, in the presence of 20 mM glucose. Dashed lines represent the correlation coefficients of individual experiments. The grey and red dots represent mean correlation in each time window before and after mefloquine addition respectively (231 pairs of δ-cells; 3 islets from 3 mice). Data were statistically analysed by Friedman's test followed by Dunn's *post hoc*. No significant differences were observed across the conditions at any time-window.

5.3.4 Role of pannexins in δ-cells

To investigate whether pannexin channels play a role in regulating somatostatin secretion, the broad-spectrum gap-junction inhibitor carbenoxolone (CBX) was used. This blocker preferentially inhibits pannexin channels over connexin hemichannels (Bruzzone et al., 2005) and it has been shown to reduce cell synchronization in thalamocingulate slices (Chang et al., 2013).

In the presence of 20 mM glucose, CBX (50 µM, Sigma) did not have any effect on glucose-induced somatostatin secretion. However, a higher concentration of the drug (200 µM) strongly and significantly inhibited somatostatin release (Figure 5-8 A-B, $p<0.005$). Given that 200µM CBX had such a strong inhibitory effect on secretion, it was investigated whether this response was mediated by gap-junctions blockade. However, when applied at 20 mM glucose, CBX (200 µM) almost completely abolished $[Ca^{2+}]_i$ oscillations in δ-cells (Figure 5-8B-C).

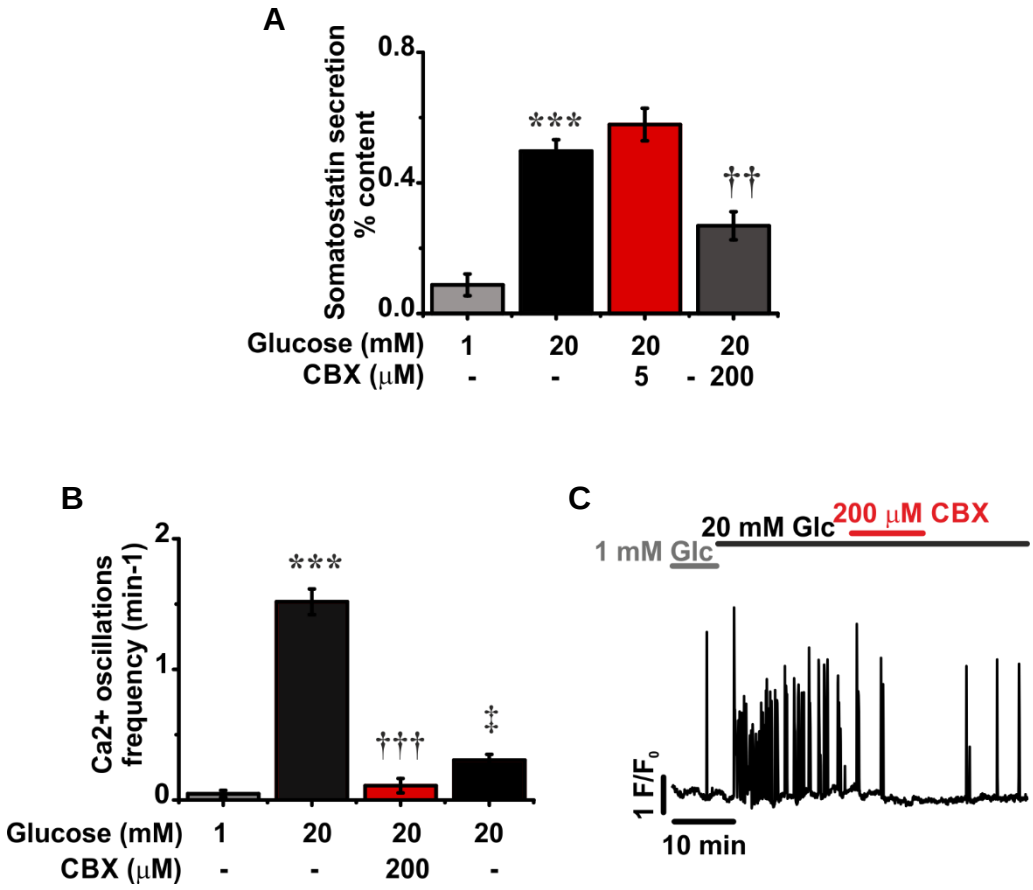

Figure 5-8 Effect of the gap-junctions inhibitor CBX on δ-cells.

A Somatostatin secretion measured in the presence of low (50 µM) or high (200 µM) CBX concentration. Somatostatin content did not change between groups. Data were obtained using 6 mice, n= 6-10 replicates. Data were analyzed by one-way ANOVA followed by Tukey's *post hoc* test. ***: p<0.001 vs 1 mM glucose, ††: p<0.005 *vs* 20 mM glucose. **B** Effect of 200 µM CBX in the presence of 20 mM glucose (Glc) on δ-cells Ca^{2+} oscillations. The inhibitory effect was partially reversed when CBX was washed out. **C** Representative recording of n=25 δ-cells from 3 islets from 3 mice. Data were analysed by one-way ANOVA followed by Tukey's *post hoc* test. ***: p<0.001 *vs* 1 mM glucose, †††: p<0.001 *vs* 20 mM glucose, ‡: p<0.05 *vs* 20 mM glucose in the presence of 200 µM CBX.

Due to the ambiguous results obtained with CBX, a more specific blocker of pannexin was used. For this purpose, 10Panx (Tocris), a 10 amino acids peptide that selectively blocks pannexin-1 (Pelegrin and Surprenant, 2006, Wang et al., 2007, Thompson et al., 2008) was tested in secretion experiments. As a control, scrambled 10Panx (Tocris), a peptide (10 amino acids as well), which does not inhibit pannexin currents (Wang et al., 2007), was used. In the presence of 20 mM glucose, somatostatin release was significantly inhibited (- 30%) when 10Panx (50 µM) was added (Figure 5-9A, $p<0.001$); no effect was obtained with the scrambled peptide (Figure 5-9A, $p>0.9$).

To test whether the inhibitory effect of 10Panx observed in secretion could be attributed to reduced synchronization of $[Ca^{2+}]_i$ oscillations in δ-cells, correlation analysis was performed. For these experiments islets were pre-incubated in 1 mM glucose in the presence of 10 Panx (50 µM) for 1 h and then exposed to 20 mM glucose (in the continued presence of 10 Panx). $[Ca^{2+}]_i$ recordings from these islets were compared to control recordings (obtained using islets preincubated in 1 mM glucose for 1 h and exposed 20 mM glucose alone during the experiment). Using the sliding window technique, it was observed that the correlation coefficients in the presence of 10 Panx were not different from the correlation coefficients in the absence of the drug (Figure 5-9B). Thus, the inhibitory effect exerted by the blocker could not be attributed to reduced synchronization of $[Ca^{2+}]_i$ oscillations.

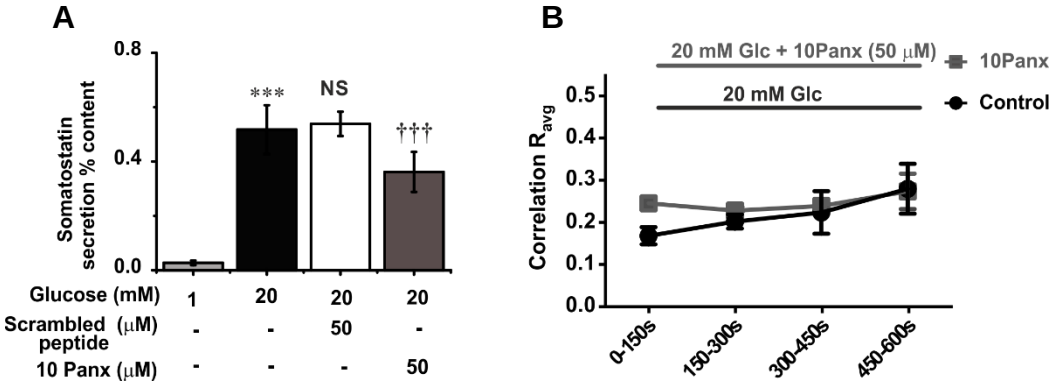

Figure 5-9 Effect of the specific pannexin-1 inhibitor 10Panx on δ-cells.

A Effect of glucose, 10 Panx and a scrambled control peptide on somatostain secretion.Glucose and the peptides were added as indicated. Somatostatin content did not change between groups. Data were generated using 9 mice (n=10-15 replicates). Data were analyzed by one-way ANOVA followed by Tukey's *post hoc* test. NS: not significant; ***: p<0.001 vs 1 mM glucose; †††: p<0.001 *vs* 20 mM glucose. **B** The average correlation between distinct pairs of cells (R_{avg}) calculated in 150 s windows in islets treated with 20 mM glucose alone (control; n=5 experiments, 1097 distinct cell-pairs) or exposed to the combination of 10Panx and 20 mM glucose (n=2 experiments, 319 distinct cell-pairs). Data were statistically analysed with Friedman's test followed by Dunn's *post hoc*. No significant differences were observed across the conditions at any time-window.

5.4 DISCUSSION

5.4.1 δ-cells crosstalk and its role on somatostatin secretion

In this Chapter, a correlation analysis approach based on the method proposed by Stozer et al. (2013) was employed to investigate the hypothesis that δ-cells are electrically coupled. The presence of a modest degree of coupling was supported by experimental evidence, as $[Ca^{2+}]_i$ oscillations appeared to be synchronous in δ-cells recorded within SST-Cre-GCaMP3 islets. Our analysis demonstrated that increasing glucose concentration from 1 mM to 20 mM leads to a significant increase of the average correlation coefficient (R_{avg}) of δ-cells $[Ca^{2+}]_i$ oscillations. It is noteworthy that these results were obtained taking into account not only neighbouring δ-cells, but all the δ-cells present in the field of view during the recordings. However, the correlation between δ-cells is weaker than the correlation observed between β-cells (Stozer et al., 2013); although the peak value R_{avg}=0.19 might not be considered as a strong correlation, it has to be taken into account that this is an average of the correlation between many cells pairs, some highly correlated, some not correlated or even negatively correlated (see examples reported in Figure 5-5). Thus, our analysis suggests that not all δ-cells within an islet are highly correlated but it highlights that many cell-pairs become more synchronized in the presence of stimulatory glucose concentration (Figure 5-4).

Interestingly, if secretion experiments and correlation analysis are compered, after 10 min exposure to 20 mM glucose, an increase in the correlation of δ-

cells $[Ca^{2+}]_i$ oscillations (Figure 5-4 – data point 750 s –) corresponds with an increase in somatostatin secretion (*cf*. Figure 4-5C – data point 30 min –). However, if for example, 20 min after glucose stimulation, the readily releasable pool of granules in δ-cells was depleted (Figure 4-5C – data point 40 min –), there may not be correlation between somatostatin secretion and δ-cells synchronisation (*cf.* Figure 5-2 – matrix 1200-1350 s –).

Moreover, the fact that a correlation was observed does not necessarily indicate that δ-cells are electrically connected. As synchronous $[Ca^{2+}]_i$ dynamics may be mediated by gap-junctions, exploring whether these channels modulate somatostatin secretion was a priority question.

The role of connexin-36 was addressed using the specific inhibitor mefloquine (Cruikshank et al., 2004). Regrettably, this compound has multiple sites of action and it blocks also the K_{ATP} channels (Gribble et al., 2000), which are important regulators of somatostatin secretion (see Chapter 4). However, it is unlikely that the stimulatory effect of the drug (Figure 5-7A) is due to closure of the K_{ATP} channels, as the blocker was tested at 20 mM glucose, *i.e*. when K_{ATP} channels can be expected to be completely closed. However, regardless of the exact mechanism, it seems that the effect of the drug is not mediated by inhibition of connexin-36. Because of the off-target effect of mefloquine, it is not possible to draw any firm conclusion from these experiments. Due to the lack of a more specific blocker, the question whether connexin-36 regulates somatostatin release cannot be addressed by using a simple pharmacological

approach and the final answer will have to await the genetic ablation of the connexin-36.

The finding that δ-cells expressed high levels of pannexin-1 channels is interesting. These data are in agreement with the transcriptomic data reported by Adriaenssens et al. (2016). By contrast Di Gruccio et al. (2016) found that Panx1 was expressed at similar levels in β- and δ-cells. This difference may be attributed to the different backgrounds of the mouse strains used in these two studies. In this context, it deserve reiterating that our experiments were performed using the same mouse model used by Adriaenssens et al. (2016) (Sst-Cre mice on a mixed C57Bl/6J and C57Bl/6N background), which is different from the one used in the study by Di Gruccio et al. (2016) (SST-ires-CRE (Taniguchi et al., 2011) on a C57BL/6NHsd background).

The possibility that pannexin-1 may or may not form gap-junctions was taken into account, as its role as hemichannel is still debated. The capacity of pannexins to form gap-junctions depends on the absence of post-translational modifications such as glycosylation. These modifications differ in different cell types (Sahu et al., 2014) and whether pannexin-1 is glycosylated in islet cells in general and δ-cells in particular, remains unknown. Elucidation of post-translational modification of pannexins in various tissues has been hindered by the limited specificity of the available antibodies (Cone et al., 2013). Nevertheless, data alluding to impaired insulin and glucagon secretion in pannexin-1 null mice (Cigliola et al., 2015) support the hypothesis that

pannexins exert a functional role in the regulation of pancreatic hormone secretion.

To address the role of pannexins, the broad gap-junction inhibitor CBX, which preferentially inhibits pannexin channels over connexins (Bruzzone et al., 2005) was initially selected. The evidence that CBX strongly abolished $[Ca^{2+}]_i$ oscillations could suggest a reduction of electrical coupling. However, CBX has been defined as a "dirty drug" because of its multiple sites of action (Connors, 2012). For example, if it blocks the voltage-gated Ca^{2+} channels (as reported by Vessey et al. (2004)), it would explain the suppression of $[Ca^{2+}]_i$ oscillations (*cf*. the effect of isradipine Figure 4-7B-C).

The availability of the more specific antagonist 10Panx allowed further investigation of the role of pannexin-1 on somatostatin secretion. The functional role of pannexin-1 in δ-cells was supported by the fact that 10Panx selectively reduced somatostatin secretion. However, the lack of effect of 10Panx on the correlation analysis suggested that inhibition of pannexin-1 does not reduce the synchronization of $[Ca^{2+}]_i$ oscillations. Thus, it remains to be determined how blockade of pannexin-1 by 10Panx can inhibit somatostatin secretion. Given the promiscuity of "specific" blockers, the best and most unequivocal approach will be to generate cell-specific knockout by crossing pannexin-1 floxed (Dvoriantchikova et al., 2012) or connexin-36 floxed (Wellershaus et al., 2008) mice with SST-Cre-GCaMP3 mice.

In conclusion, although these data suggest that δ-cells are synchronized, the underlying mechanism remains unestablished. It is possible that due to their neuron-like morphology δ-cells are coupled through gap junctions, located on their protrusions. The evidence that not only neighbouring δ-cells cells display a synchronous behaviour may support this hypothesis. Interestingly, also human δ-cells possess long cytoplasmic extensions (Grube and Bohn, 1983). It is therefore tempting to speculate that similar to their mouse counterpart human δ-cells might be electrically coupled.

However, it cannot be excluded that paracrine regulators released by the neighbouring α- or β-cells may modulate the synchronisation of δ-cells. The effects of insulin are addressed in the next Chapter.

6 PARACRINE REGULATION OF GLUCAGON SECRETION BY INSULIN-INDUCED STIMULATION OF SOMATOSTATIN RELEASE

6.1 INTRODUCTION

The paracrine mechanisms regulating hormone release in pancreatic islets are still poorly understood. Somatostatin is a powerful inhibitor of glucagon secretion (Koerker et al., 1974, Taborsky et al., 1978, Strowski et al., 2000). Insulin, serotonin and γ-amino-butyric acid (GABA), released from β-cells, are also regarded as strong inhibitors of glucagon release (Maruyama et al., 1984, Rorsman et al., 1989, Greenbaum et al., 1991, Xu et al., 2006, Almaca et al., 2016) (Figure 6-1).

Investigating the paracrine regulation of glucagon secretion is particularly relevant for the understanding of mechanisms underlying the systemic counter-regulatory response (Cryer, 1999). Impaired counter-regulation of insulin-induced hypoglycaemia is a major complication associated with the insulin therapy in diabetic patients (Gerich, 1988, Cryer, 2002). This is a potentially fatal condition but the causes remain unknown (Cryer, 2012).

It has been demonstrated that exogenous insulin inhibits Ca^{2+} oscillations in single α-cells (Ravier and Rutter, 2005) and that it lowers cAMP levels in α-cells within islets (Elliott et al., 2015). In support of a direct inhibitory effect of insulin on glucagon release, genetic ablation of insulin receptors in α-cells

stimulates glucagon secretion (Kawamori et al., 2009) but the effect was surprisingly weak. Thus, the current model of paracrine regulation of glucagon secretion assumes that insulin exerts a direct inhibitory effect on glucagon secreting α-cells (Figure 6-1). This model does not account of the fact that somatostatin can inhibit both insulin and glucagon release (Alberti et al., 1973, Koerker et al., 1974, Strowski et al., 2000, Hauge-Evans et al., 2009).

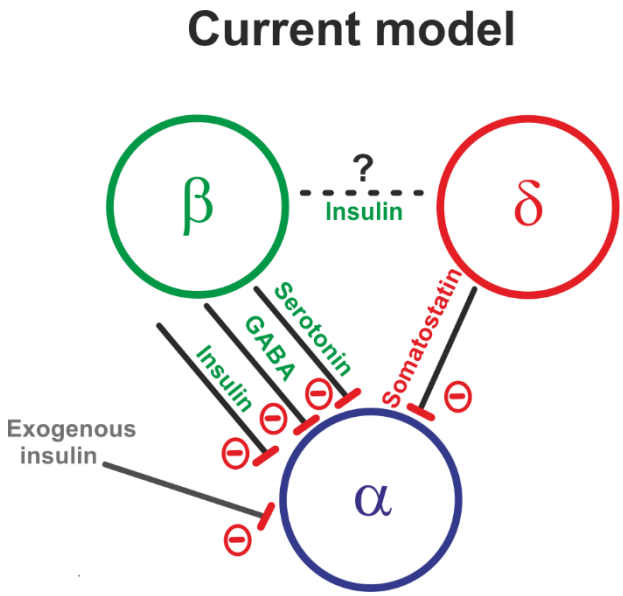

Figure 6-1 Current model of paracrine regulation of glucagon secretion.

To date, except for one study (Hauge-Evans et al., 2012), the effects of insulin on somatostatin secretion have not been investigated. During the past few years, an increasing number of reports have demonstrated that SSTR2 antagonism ameliorates the counter-regulatory response of glucagon during insulin-induced hypoglycaemia (Yue et al., 2012, Karimian et al., 2013, Yue et al., 2013, Leclair et al., 2016). This suggests an involvement of somatostatin in the impaired counterregulation of glucagon secretion. Further support for the role of somatostatin in hypoglycaemia comes from the evidence that patients with somatostatinomas, have an increased risk of hypoglycaemic events (He et al., 2009). Moreover, patients treated with long-lasting somatostatin analogues are also more prone to hypoglycaemia (Unek et al., 2009).

In this Chapter, the effects of insulin on somatostatin and glucagon secretion have been studied with a view to testing the hypothesis that insulin stimulates somatostatin release and that it in turn inhibits glucagon secretion.

6.2 MATERIALS AND METHODS

6.2.1 Generation of δ-cell specific insulin receptor knockout mice

To generate δ-cell-specific [4] insulin receptor knockout, SST-Cre-RFP-GCaMP3 mice were crossed with homozygous insulin receptor floxed mice ($IR^{fl/fl}$) (Jackson laboratory IR^{lox} Stock Number 006955, (Kulkarni et al., 1999)), which have loxP sites flanking exon 4 of the insulin receptor gene. In Cre-expressing tissues, exon 4 is excised from the insulin receptor gene. If translation were to occur, a truncated protein of 308 amino acids of the N-terminal residues of the insulin receptor α-subunit, lacking the high-affinity binding site, transmembrane domain, and kinase domain would putatively be produced (Kulkarni et al., 1999).

The first generation offspring of the SST-Cre-RFP-GCaMP3 and $IR^{fl/fl}$ mating produced SST-Cre mice heterozygous for the insulin receptor floxed allele (*i.e.*SST-Cre-$IR^{+/-}$). Heterozygous SST-Cre-RFP-$IR^{+/-}$ were back-crossed with $IR^{fl/fl}$ mice to generate mice that were homozygous for deletion of the insulin receptor specifically in somatostatin-expressing tissues, SIRKO mice (*i.e.* SST-Cre-RFP-$IR^{-/-}$, see Table 6-1 for the description of the alleles).

[4] It is acknowledged that there are also somatostatin-producing cells in the brain, in peripheral neurones and in the gastrointestinal tract and that insulin receptors will also be ablated in these tissues.

Genotype	Allele
$IR^{fl/fl}$	*Insr*^{tm1Khn}
SST-Cre-RFP-$IR^{-/-}$ (SIRKO)	*Sst-mCherry-2A-iCre* *Gt(ROSA)26Sor*^{tm1Hjf} *Insr*^{tm1Khn}

Table 6-1 Insulin receptor alleles.

To identify SIRKO mice, all pups (3-4 weeks old) were genotyped by performing PCR on genomic DNA isolated from earclips. The PCR protocol was the same as reported in Section 2.2 (Mouse genotyping). Like SST-Cre-RFP mice, SIRKO mice were tested for expression of β-catenin and Cre recombinase, mCherry, tdRFP and for insulin receptor floxed alleles (using primers reported in Table 6-2). SIRKO homozygous mice were identified by the presence of a single band of 330 bp, while heterozygous mice displayed two bands at 280 bp and 330 bp and wild-type a single band at 280 bp. Littermates which did not express SST-Cre were always used as controls, in order to exclude phenotypic differences between different genetic backgrounds. Male and female SIRKO mice were studied for some selected parameters (body weight, fed and fasting blood glucose levels, glucose and insulin tolerance).

Primer	Primer sequences
IRKO	Fwd: GGGGCAGTGAGTATTTTGGA Rev: TGGCCGTGAAAGTTAAGAGG

Table 6-2 IRKO mice sequencing primers.

6.2.2 Assessment of Cre recombination in pancreatic δ-cells from SIRKO mice

To confirm the knockout of insulin receptor in δ-cells, the deletion of exon 4 on RFP-positive fraction of δ-cells (obtained by FACS) was assessed by reverse transcription (RT)-PCR. To verify that no unspecific recombination occurred in other insulin receptor-expressing tissues, expression of the insulin receptor gene was assessed also in RFP-negative islets cells and in the liver (as negative controls). RNA from RFP-positive and RFP-negative islet cells was extracted as reported in Section 2.8. To extract RNA from the liver, 2 mg of tissue were homogenized (in RLT buffer from RNeasy Micro Kit, Qiagen) by passing through a syringe fitted with a 25-gauge needle. To generate cDNA, ~10 ng of total RNA (extracted from FAC-sorted RFP-positive islet cells, RFP-negative islet cells and from the liver of each SIRKO mouse) was reverse transcribed as described in Section 2.8. To assess by RT-PCR that Cre recombination had occurred, three sets of primers with the forward primer binding on exon 3 and the reverse primer binding on exon 5 were designed. After testing all the pairs of primers, the ones reported in Table 6-3 were chosen.

Primer	Sequence
IRex 3-5	Fwd: TGATGACCCCACCAAGTGTG Rev: TCCTCGAATCAGATGTAGCTTCC

Table 6-3 IRex3-5 primers sequences to assess Cre recombination in SIRKO mice.

RT-PCR should yield an amplicon of 514 bp in the wild-type tissues and an amplicon of 365 bp (lacking exon 4) in the SST-Cre expressing (RFP-postitive) cells of the SIRKO mice. The PCRs on cDNA from RFP-positive cells, RFP-negative islet cells and liver, were run using the same condition and the same protocol as described in Section 2.2. The PCR products were loaded onto 1.8% agarose gel containing ethidium bromide and visualized with ChemiDoc™ XRS + (Bio-Rad, Hercules, CA, USA). To verify that the 365 bp band obtained corresponded to the truncated transcript, while the 514 bp corresponded to the wild-type copy, the DNA was extracted from the gel fragments (using QIAquick Gel Extraction Kit, Qiagen). This DNA was cloned into a pGEM®-T Easy vector (Promega) and transformed using One Shot® OmniMAX 2 $T1^R$ E. coli strain (Life technologies) to amplify the amount of DNA available for sequencing. After culturing, the plasmids containing the PCR fragments were extracted from the bacterial cultures using Qiagen Miniprep kit (Qiagen). Sequencing of the fragments was performed using standard SP6 and T7 primers.

6.3 RESULTS

6.3.1 Effect of exogenous insulin on somatostatin release

To investigate whether insulin modulates somatostatin release under hypoglycaemic conditions, a series of secretion experiments, were performed at 4 mM glucose (a condition that mimics hypoglycaemia in mice *in vivo*). Increasing glucose concentration from 1 mM to 4 mM significantly inhibited glucagon secretion by 60% (Figure 6-2A), whilst stmulating somatostatin secretion by 50% (Figure 6-2B). Application of insulin (100 nM, Sigma) at 4 mM glucose, inhibited glucagon secretion by a further 50% (Figure 6-2A). This effect was paralleled by 3-fold stimulation in somatostatin release (Figure 6-2B). The inhibitory effect of insulin was observed already at 300 pM, a dose associated also with stimulation of somatostatin secretion (A Salehi and P Rorsman, personal communication). Notably, plasma insulin levels in insulin-treated diabetic patients may be as high as 500 µU/ml (3.5 nM) (Heding, 1972). Thus, insulin stimulates somatostatin release at physiologically relevant concentrations.

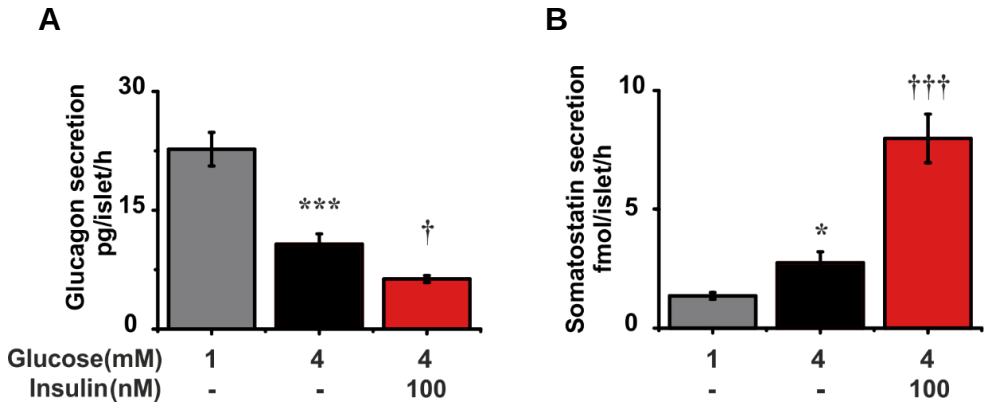

Figure 6-2 Effect of exogenous insulin on glucagon and somatostatin secretion.
A Effect of glucose and insulin on glucagon secretion. Glucose and insulin were added as indicated. **B** As in **A** but instead somatostatin secretion was assed. The results were obtained using 4 NMRI mice and n=10 replicates per condition. Data were analyzed by one-way ANOVA followed by Dunnett's *post hoc*. *: p<0.05, ***: p<0.001 *vs* 1 Mm glucose; †: p<0.05, †††: p<0.001 *vs* 4 mM glucose.

To explore how insulin exerts its effect on somatostatin release from pancreatic δ-cells, it was examined (by immunocytochemistry and by qPCR) whether pancreatic δ-cells from SST-Cre-RFP and SST-Cre-GCaMP3 mice express insulin receptor. Both methods showed that the insulin receptor is expressed in δ-cells at levels comparable to those found in non-δ-cells (Figure 6-3A-B)

Next, the effect of insulin was examined on isolated SST-Cre-GCaMP3 islets. Increasing glucose concentration from 1 mM to 4 mM increased the percentage of active cells from 28±4% to 52±7%. Subsequent application of insulin (100 nM) did not affect the proportion of already active δ-cells (Figure 6-3C). However, it significantly increased the frequency of Ca^{2+} oscillations in δ-cells by 30% (Figure 6-3D-E, $p<0.05$).

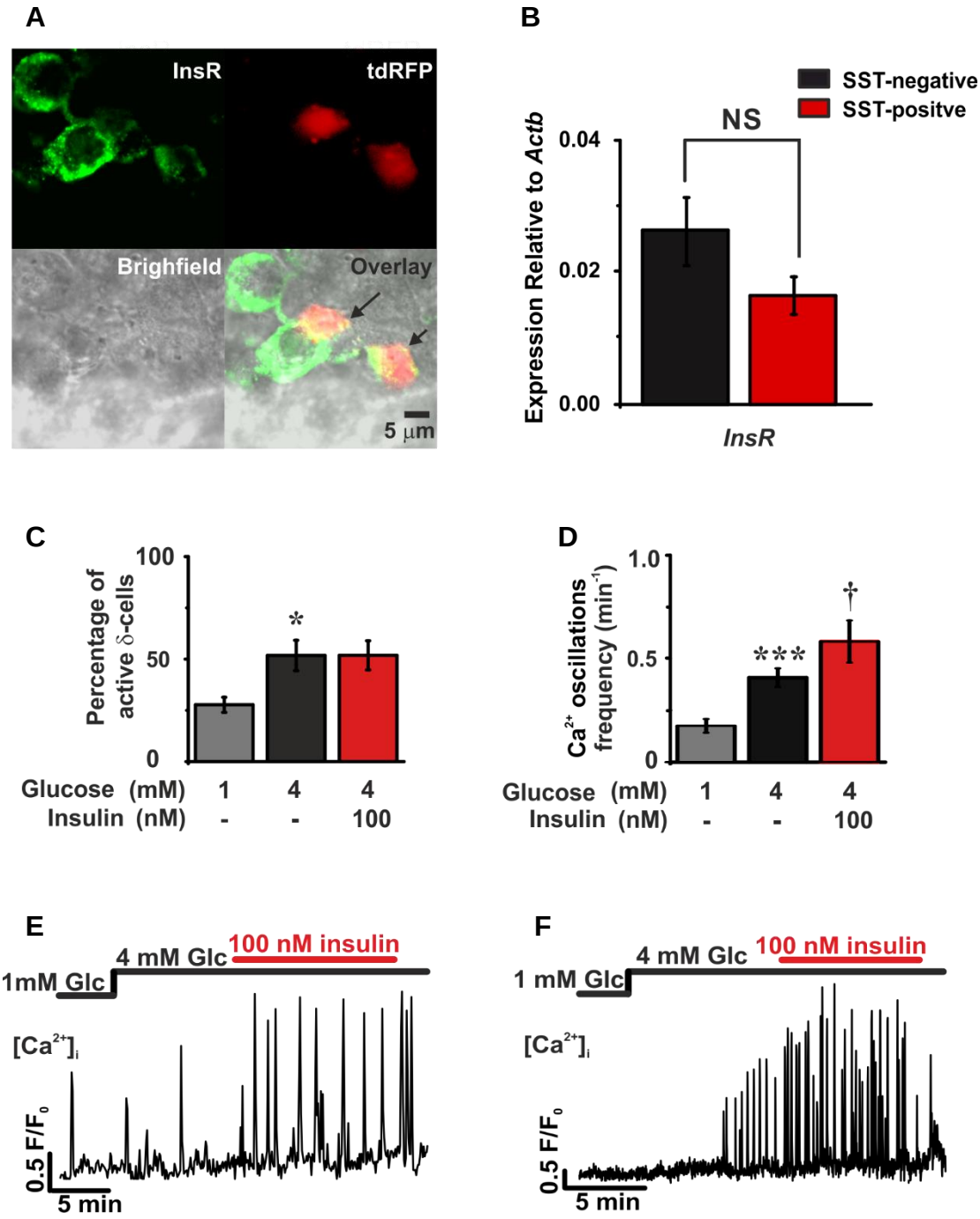
A
InsR
tdRFP
Brighfield
Overlay
5 μm
B
SST-negative
SST-positve
NS
Expression Relative to Actb
0.04
0.02
0.00
InsR
C
Percentage of active δ-cells
100
50
0
*
Glucose (mM) 1 4 4
Insulin (nM) - - 100
D
Ca2+ oscillations frequency (min-1)
1.0
0.5
0
***
†
Glucose (mM) 1 4 4
Insulin (nM) - - 100
E
1mM Glc
4 mM Glc
100 nM insulin
[Ca2+]i
0.5 F/F0
5 min
F
1 mM Glc
4 mM Glc
100 nM insulin
[Ca2+]i
0.5 F/F0
5 min

Figure 6-3 Insulin receptor expression and effect of insulin on $[Ca^{2+}]_i$ in SST-Cre-GCaMP3 islets

A Confocal image showing immunostaining for insulin receptor (green) and endogenously expressed tdRFP (red). Insulin receptor is expressed in δ-cells (yellow identifies colocalization of tdRFP and insulin receptor) but also in non δ-cells (i.e. tdRFP-negative cells). **B** Insulin receptor expression assessed by qPCR in SST-positive and SST-negative cells. Data were obtained from n=7 samples of cells fractions (obtained by FACS). Unpaired Student's t-test was used for statistical analysis. NS: not significant. **C** Percentage of active cells in response to 1 mM, 4 mM, 4 mM glucose (Glc) in the presence of 100 nM insulin. **D** $[Ca^{2+}]_i$ oscillations frequency calculated in the same conditions as in **C**. **E-F** Two representative recordings of n=54 cells from 11 islets, from 9 mice. Data were statistically analysed using one-way ANOVA followed by Dunnett's *post hoc*. *: p<0.05, ***: p<0.001 *vs* 1 mM glucose, †: p<0.05 *vs* 4 mM glucose.

6.3.2 Endogenous insulin regulates somatostatin release

As exogenous insulin stimulates somatostatin secretion, it was reasoned that in intact islets endogenous insulin released from neighbouring β-cells, may also potentiate somatostatin secretion from the neighbouring δ-cells. This hypothesis was tested by measuring somatostatin secretion at 1 mM and 20 mM glucose in the absence and presence of the insulin receptor antagonist S961 (Schäffer et al., 2008).

At basal glucose levels (1 mM), where very little insulin is released, S961 (5 µM, Sigma) had no effect on somatostatin secretion (Figure 6-4A). Likewise, at 1 mM glucose, the frequency of $[Ca^{2+}]_i$ oscillations in δ-cells was not affected in the presence of S961 (1 µM) (Figure 6-4B-D). However, at 20 mM glucose, where insulin secretion is strongly stimulated, the blocker reduced somatostatin secretion by 50% (Figure 6-4A) and the frequency of $[Ca^{2+}]_i$ oscillations in δ-cells by ~40% (Figure 6-4B-D).

In Chapter 5, it has been demonstrated that δ-cells display synchronous $[Ca^{2+}]_i$ oscillations. Using the sliding windows analysis (see Chapter 5 and Appendix 3), it was tested whether endogenous insulin regulates the synchronisation of those $[Ca^{2+}]_i$ oscillations. At T=300 s, when glucose concentration was increased from 1 mM to 20 mM, the average correlation coefficient was reduced in the presence of S961 (Figure 6-5, $p<0.001$).

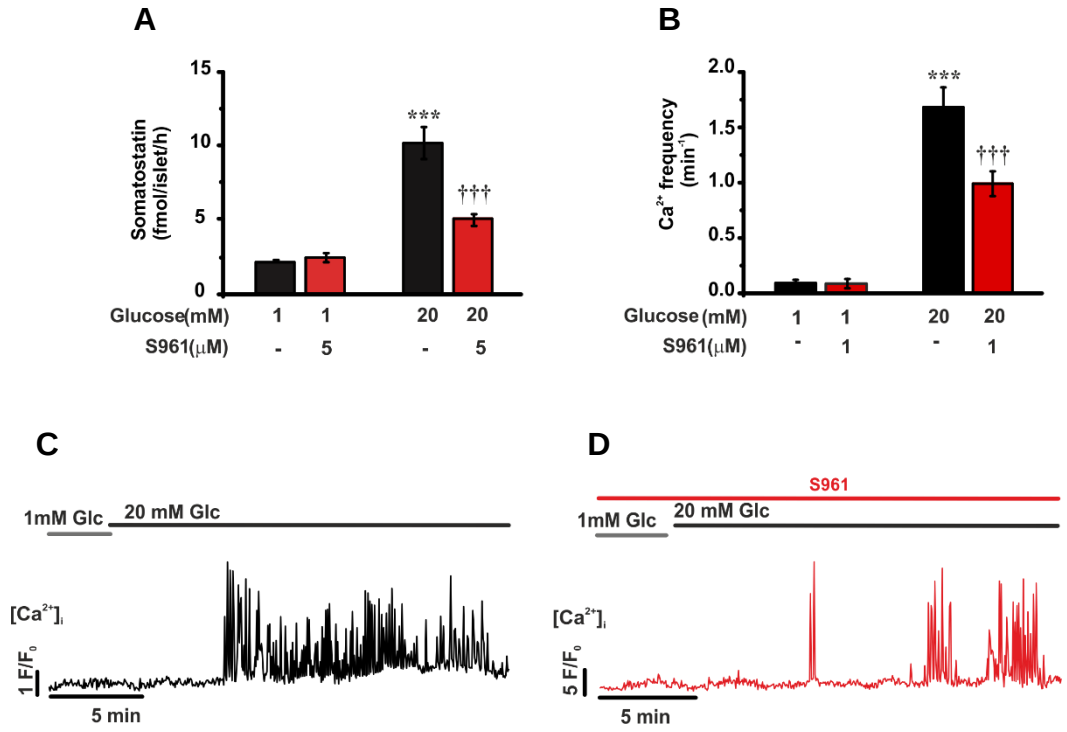

Figure 6-4 Effect of endogenous insulin on somatostatin release.

A Somatostatin secretion measured in islets incubated with or without the insulin receptor blocker S961 at 1 mM or 20 mM glucose. Data obtained using islets 3 mice (n=10 replicates) **B** Frequency of $[Ca^{2+}]_i$ oscillations in SST-Cre-GCaMP3 islets with or without the insulin receptor blocker S961. **C** A representative trace of n=46 cells from 5 islets from 4 mice, in the absence of S961. **D** A representative trace of n=46 cells from 6 islets from 4 mice in the presence of S961. Data were statically analysed using two-way ANOVA followed by Sidak's *post hoc* test. ***: p<0.001 *vs* 1 mM glucose; †††: p<0.001 *vs* 20 mM glucose in the absence of S961.

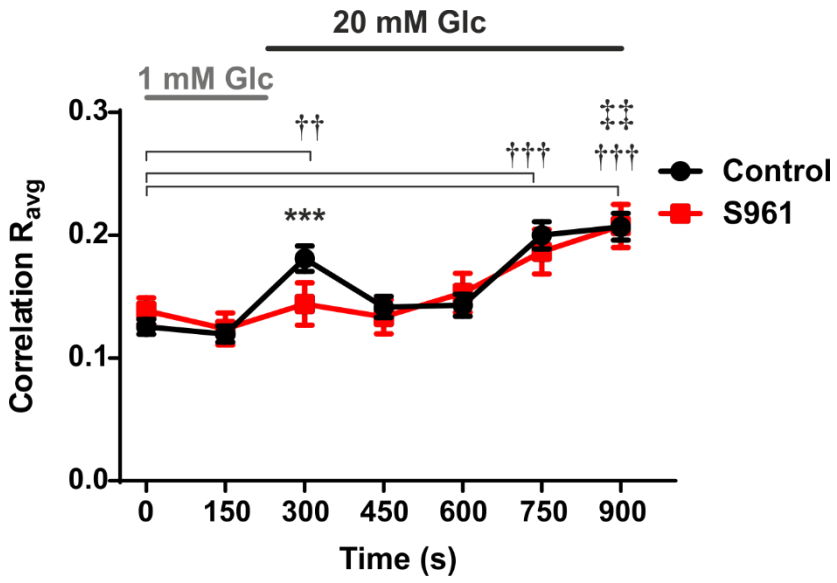

Figure 6-5 Correlation analysis in the presence of the insulin receptor blocker S961. Correlation analysis of $[Ca^{2+}]_i$ imaging time series of δ-cells in control islets or in islets treated with S961. Control n=256 cell pairs from 5 islets from 4 mice, S961 n=128 cell pairs from 6 islets from 4 mice. Differences between each data point were statistical analysed using Mann-Whitney test. ***: p<0.001. Control and S961 data were statistical analysed for differences *vs* t=0 (baseline) by one-way ANOVA followed by Tukey's *post hoc* test. ††: p<0.005, †††: p<0.001 *vs* t=0 Control; ‡‡: p<0.005 *vs* t=0 S961.

6.3.3 Validation of insulin receptor knockout in δ-cells from SIRKO mice

To further test the hypothesis that insulin potentiates somatostatin release *in vitro* and *in vivo*, δ-cell-specific insulin receptor knock-out mice were used. Mice lacking the insulin receptors in somatostatin-expressing tissues (including pancreatic δ-cells) were generated as described in Section 6.2.1. These mice are referred to as SIRKO mice. For each SIRKO mouse, it was ascertained by qPCR that the RFP-positive cells, isolated from SIRKO islets, expressed mainly somatostatin (i.e. SST-positive cells and therefore δ-cells). In contrast, RFP-negative cells expressed primarily insulin and glucagon and were assumed therefore to be comprised of α- and β- cells (Figure 6-6 A-B).

To confirm that recombination had occurred, and that the insulin receptor was knocked-out exclusively in δ-cells of pancreatic islets, RT-PCR was carried out using total RNA extracted from FACS-enriched RFP-positive and RFP-negative cells, isolated from islets from SIRKO mice. In addition to the RFP-negative fraction, the liver was also used as a negative control, to exclude any unspecific recombination in other insulin-responsive tissues. The 514-bp PCR product detected in the liver and in the non δ-cells indicated the presence of wild-type copy of the insulin receptor. The smaller product of 365 bp observed in δ-cells, suggested that recombination had occurred and that exon 4 (149 bp) had been removed (Figure 6-6C). These results were confirmed by sequencing the 514 bp and the 365 bp PCR products detected in the non-δ- and in the δ-cells, respectively (Figure 6-7).

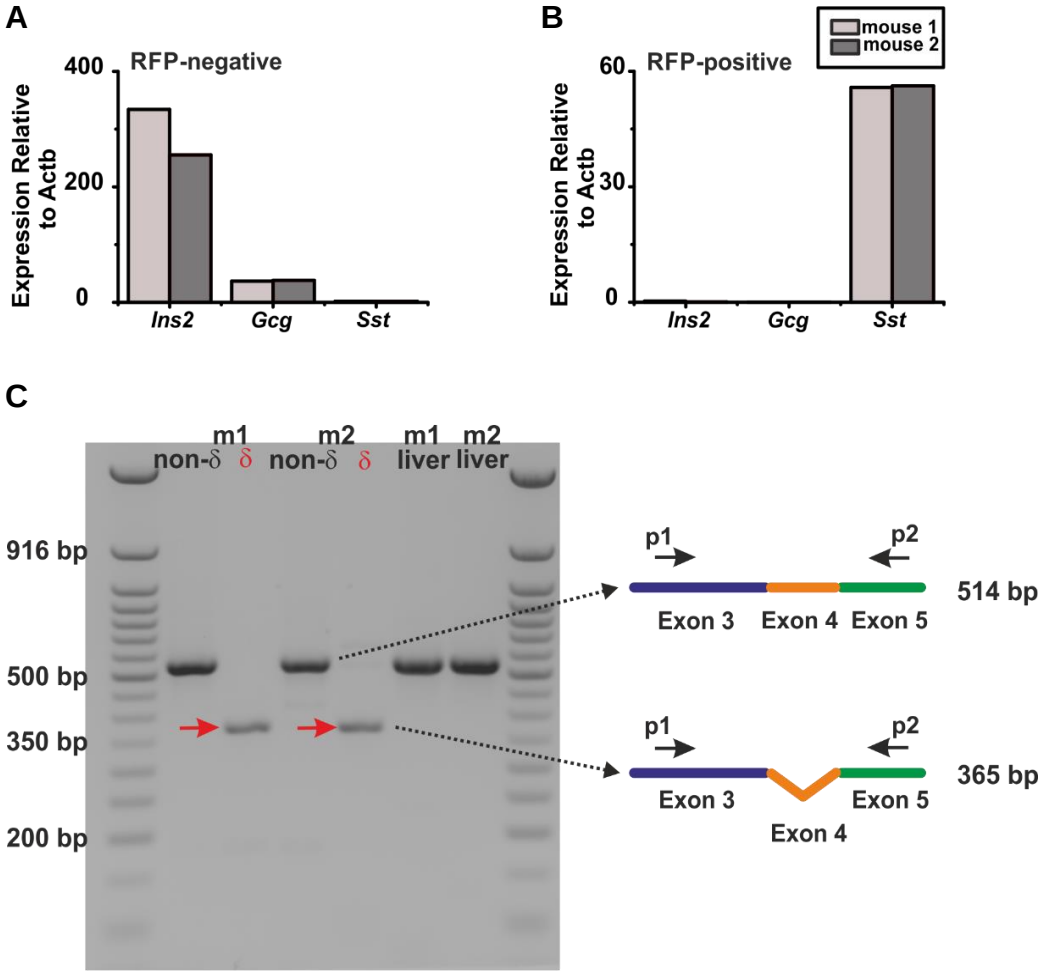

Figure 6-6 Assessment of insulin receptor recombination in SIRKO mice.

A-B Islet cells from each SIRKO mouse were FAC-sorted into RFP-negative (**A**) and RFP-positive fractions (**B**). It was ascertained that the RFP-negative cells showed enriched expression of insulin (*Ins2*) and glucagon (*Gcg*) and that the RFP-positive cells expressed mainly somatostatin (*Sst*). **C** Agarose gel showing a low molecular weight band ~365 bp exclusively in δ-cells from both mice (mouse 1 and mouse 2). The presence of a higher molecular weight band ~514 bp in non-δ-cells and in the liver indicates the presence of wild-type insulin receptor gene.

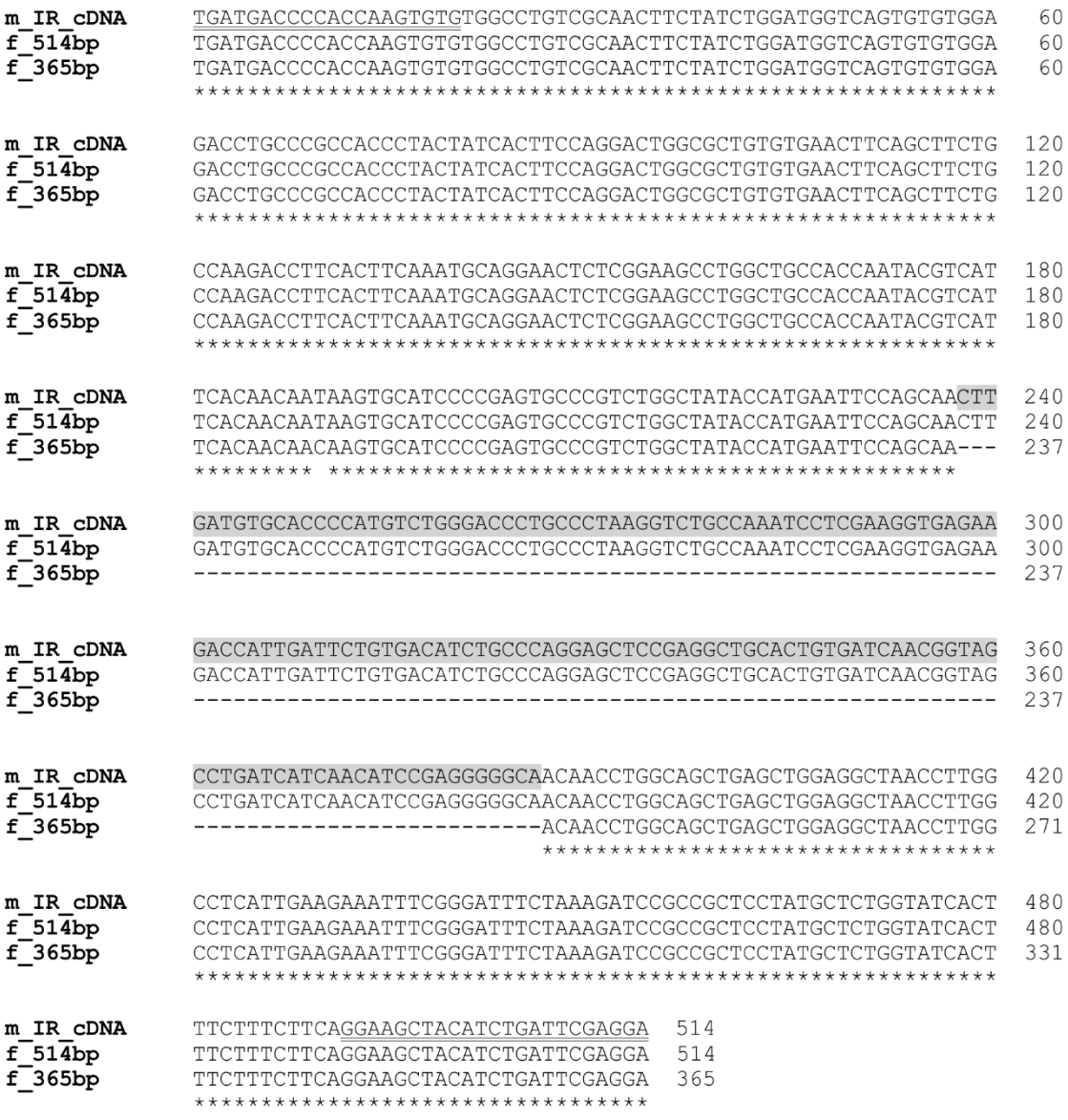

Figure 6-7 Sequence alignment demonstrating removal of exon 4 in δ-cells.

Nucleotide alignment performed using Kalign (McWilliam et al., 2013).

Top line (m_IR_cDNA) is the sequence of the cDNA of the mouse insulin receptor (NM_010568.3) from nucleotide 1227 to 1740 (designated numbering 1-514 for ease of presentation). Middle line (f_514bp) corresponds to the sequence of the cDNA obtained from non-δ-cells. Bottom line (f_365bp) is the sequence of the cDNA obtained from δ-cells.

Sequences of the primers used for PCR are underlined. Highlighted sequence corresponds to the sequence of the exon 4 (149 bp). Exon 4 was removed exclusively in the cDNA obtained from δ-cells.

6.3.4 Physiological characterization of SIRKO mice

To ascertain that knock out of insulin receptor in somatostatin-expressing tissues did not have any harmful effect, several parameters were tested in control and SIRKO mice. In male mice (12-20 weeks old), body weights were not different between SIRKO and control littermates (Figure 6-8A). Fed and 3 h fasting blood glucose levels did not show any significant difference between control and SIRKO mice (Figure 6-8B-C). To test glucose tolerance an ipGTT was carried out on SIRKO mice and control littermates. Although SIRKO mice displayed slightly higher blood glucose levels after fasting, no statistically significant differences were observed between the two groups (Figure 6-8D).

In female mice (12-20 weeks old), similar to what observed in males, no differences in body weight were observed between SIRKO and control littermates (Figure 6-9 A). Fed and 3 h fasting blood glucose levels did not show any statistically significant difference between control and SIRKO mice (Figure 6-9B-C). Similarly, the glucose tolerance test did not disclose any difference between control and SIRKO mice (Figure 6-9D). Blood glucose levels had returned to the initial levels in female but not in male mice (150 min after the ip glucose injection, Figure 6-8D and Figure 6-9D).

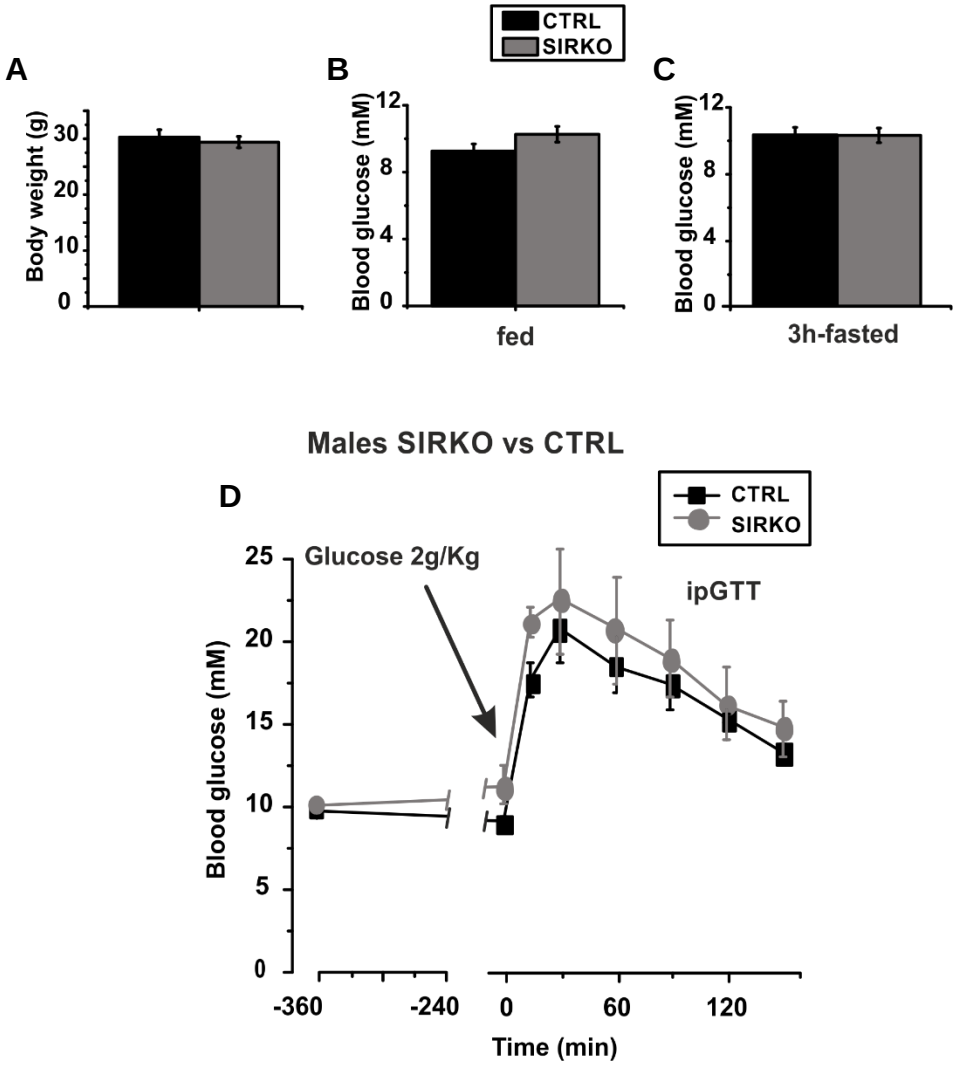

Figure 6-8 Physiological characterization of SIRKO male mice.

A Body weight measured in n=12 mice for each genotype. **B** Fed blood glucose levels (n=9 mice for each genotype). **C** Blood glucose levels after 3 h fasting (n=6 mice). **A-C** Data were statistically analyzed by unpaired Student's t-test. No significant differences were observed. **D** Glucose tolerance test measured in n=6 male mice for each genotype. Mice were fasted for 6 h prior to the test. Data were statistically analyzed by two-way ANOVA followed by Sidak's *post hoc* test. No significant differences were detected.

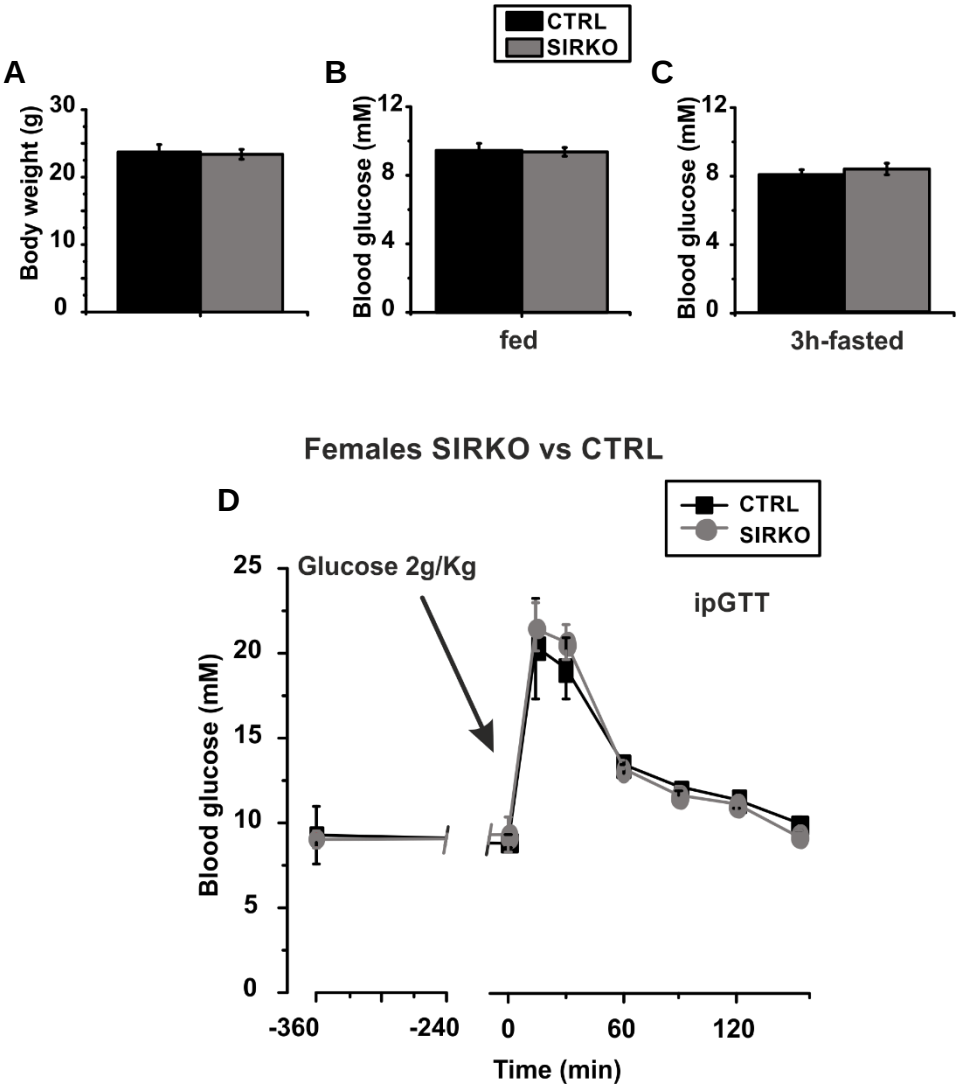

Figure 6-9 Physiological characterization of SIRKO female mice.

A Body weight measured in n=12 mice for each genotype. **B** Fed blood glucose levels (n=12 mice for each genotype). **C** Blood glucose levels after 3h fasting (n=9-10 mice). **A-C** Data were statistically analyzed by unpaired Student's t-test. No significant differences were observed. **D** Glucose tolerance test measured in n=6 female mice for each genotype. Mice were fasted for 6 h prior to the test. Data were statistically analyzed by two-way ANOVA followed by Sidak's *post hoc* test. No significant differences were detected.

6.3.5 Reduced hypoglycaemic effect in female SIRKO mice

To test the role of insulin-stimulated somatostatin secretion *in vivo*, ipITT in SIRKO mice and control littermates was performed. Experiments were conducted separately for each sex. In males, no differences were observed between SIRKO mice and control littermates. Although insulin injection lowered blood glucose levels, they remained around 5.5-6 mM in both groups (Figure 6-10A). Whereas, blood glucose levels fell to ~2 mM in control female mice, they remained around 5 mM 60 min after insulin injection in SIRKO females (Figure 6-10B).

To assess the impact of handling (and fasting) the mice, the experiments were repeated without injecting any insulin. In both control and SIRKO mice, the mere handling of the mice increased blood glucose by 2 mM. This effect was detectable at all time point after t=0 (Figure 6-10C). This may explain why no hypoglycaemic effect is observed at t=15 min in the ipITT experiments.

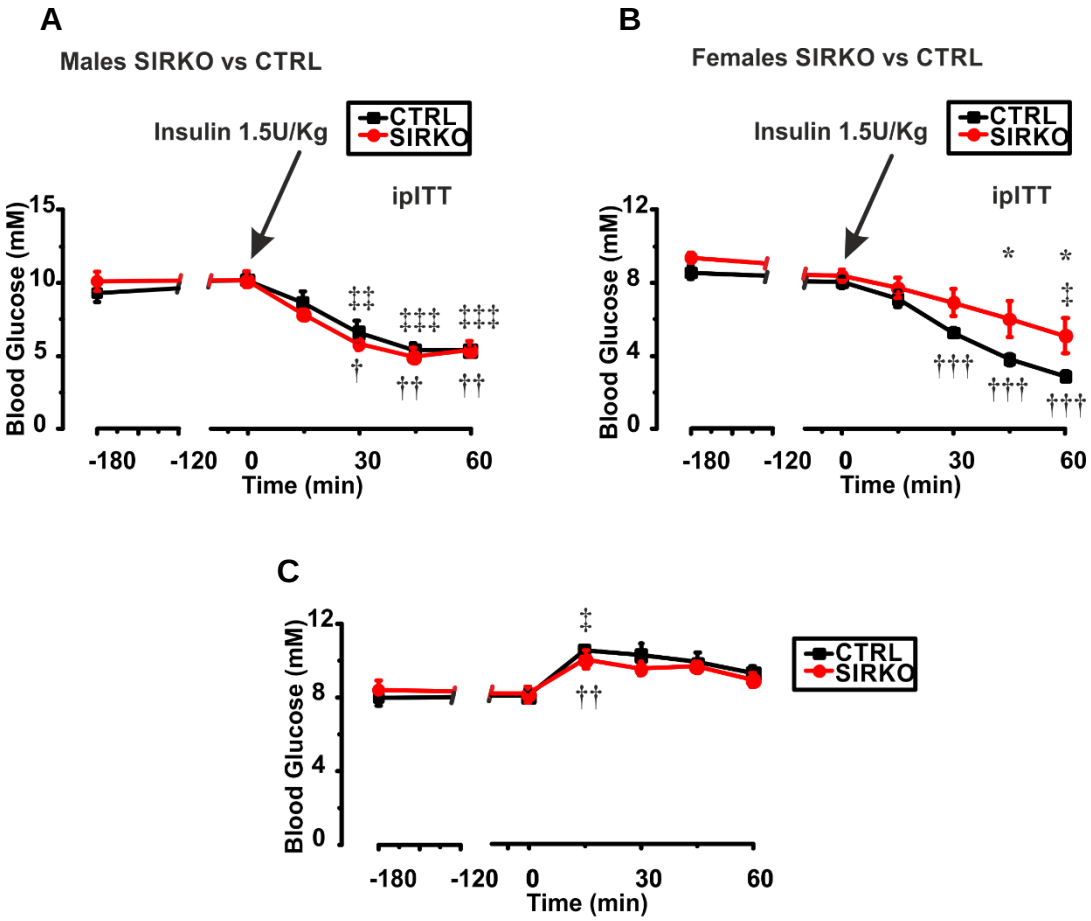

Figure 6-10 Insulin effect *in vivo* in SIRKO mice.

A Insulin tolerance test measured in n=6 male mice for each genotype. **B** Insulin tolerance test measured in n=10 control littermates (CTRL) and n=9 SIRKO females. **C** Effect of handling the mice on blood glucose in n=6 mice female mice for each genotype. Data were statistically analysed by two-way ANOVA followed by Sidak's *post hoc* test. *: p<0.05 *vs* control mice. CTRL and SIRKO mice were also analysed by one-way ANOVA followed by Tukey's *post hoc*. †: p<0.05, ††: p<0.005, †††: p<0.001 *vs* t=0 CTRL; ‡: p<0.05, ‡‡: p<0.005, ‡‡‡: p<0.001 *vs* t=0 SIRKO.

6.3.6 Insulin effect *in vitro* in SIRKO mice

Insulin tolerance test is a simple method to measure insulin sensitivity *in vivo.* However, injected insulin will have an effect not only in the pancreas but in many other tissues, including liver, muscle and kidney. Thus, to elucidate whether the insulin effects observed in SIRKO mice *in vivo* could be attributed primarily to the action of pancreatic hormones, a series of secretion experiments were performed *in vitro.* Pancreatic islets were isolated from SIRKO and control mice from both males and females and were analysed separately. The effect of insulin was compared at 1 mM glucose, a condition which mimics severe (fatal) hypoglycaemia and at 4 mM glucose, a condition that resembles the hypoglycaemic levels observed in *in vivo* experiments (see Figure 6-10B).

At 1 mM glucose, no differences in glucagon secretion were observed between control and knockout mice. Addition of 100 nM insulin in the presence of 1 mM glucose, marginally inhibited glucagon secretion in both control and SIRKO mice (males and females) but this effect was no statistically significant (Figure 6-11A-B). Somatostatin secretion was comparable in both mouse models and not affected by insulin at this glucose concentration, regardless of sex (Figure 6-11C-D).

Application of 100 nM insulin in the presence of 4 mM glucose, inhibited glucagon secretion by ~35% in male control mice but was ineffective in SIRKO mice (Figure 6-12A). This correlated with >2-fold stimulation of somatostatin secretion in control mice, an effect lost in islets from SIRKO male mice (Figure

6-12C). In female control mice, addition of 100 nM insulin in the presence of 4 mM glucose strongly inhibited glucagon release by ~35% (i.e. similar to males) (Figure 6-12B), while somatostatin, measured in parallel, was stimulated by 2-fold. In female SIRKO mice, the effects of insulin on both glucagon and somatostatin were lost (Figure 6-12B, D).

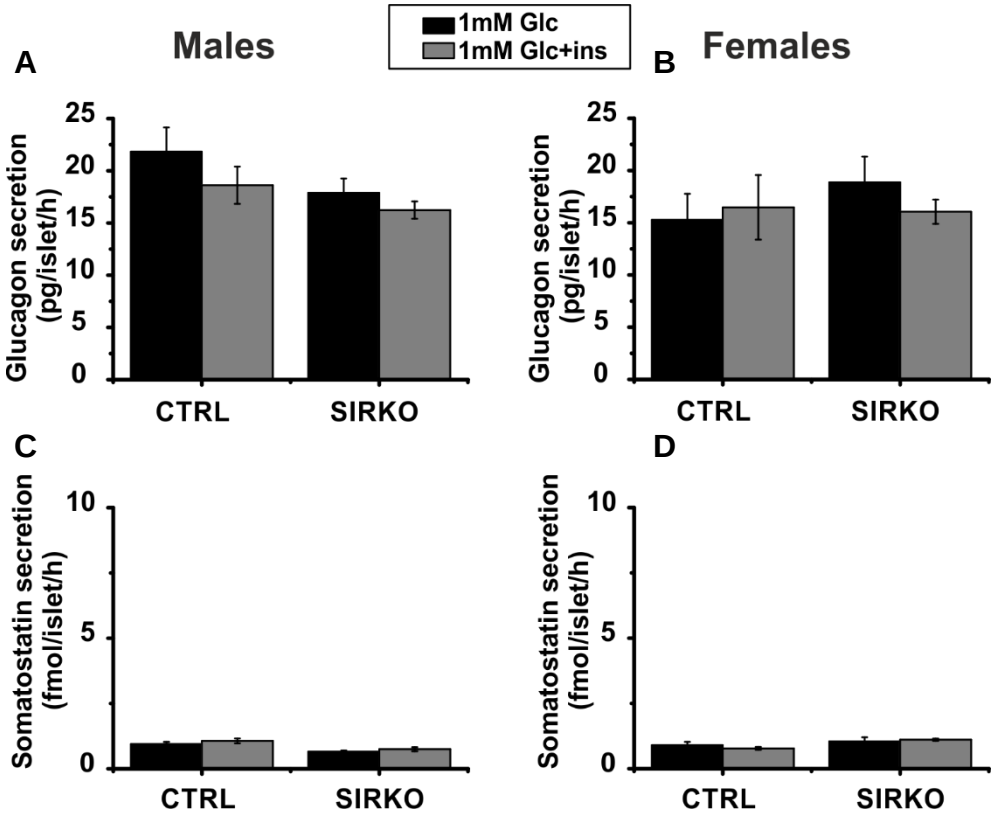

Figure 6-11 Effect of insulin at 1 mM glucose in control and SIRKO mice.

A, C Glucagon and somatostatin secretion measured in control and SIRKO males at 1 mM glucose in absence or presence of 100 nM insulin. **B, D** As in **A, C** but female control and SIRKO mice were used. Results obtained using 4 control and 4 knockout males, 4 control and 4 knockout females, n= 8-10 replicates per each condition. Females and males were analyzed separately using one-way ANOVA followed by Dunnett's *post hoc* test. No significant differences were detected.

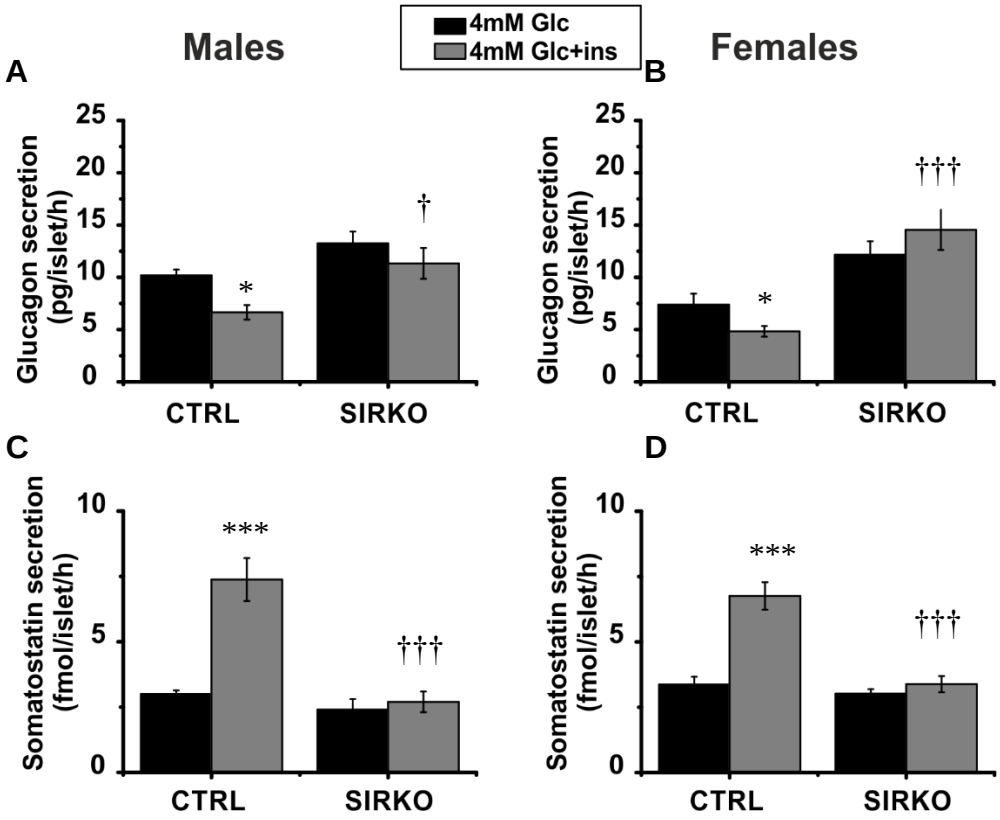

Figure 6-12 Effect of insulin at 4 mM glucose in control and SIRKO mice.

A, C Glucagon and somatostatin secretion measured in control and SIRKO males at 4 mM glucose in absence or presence of 100 nM insulin. **B, D** As in **A, C** but female control and SIRKO mice were used. Results obtained using 4 control and 4 knockout males, 4 control and 4 knockout females, n= 8-10 replicates per each condition. Females and males were analyzed separately using one-way ANOVA followed by Dunnett's *post hoc* test. *: $p<0.05$, ***: $p<0.001$ *vs* 4 mM glucose; †: $p<0.05$, †††: $p<0.001$ *vs* 4 mM glucose in the presence of insulin in the control mice.

6.3.7 Use of somatostatin receptor blocker 2

To investigate the hypothesis that insulin-induced inhibition of glucagon secretion is mediated by somatostatin, the effects of the SSTR2 [5] blocker, CYN154806 (Feniuk et al., 2000) were tested on glucagon and somatostatin secretion. Addition of insulin in the presence of 4 mM glucose inhibited glucagon release by 40% and increased somatostatin secretion of ~3 fold. The effects on glucagon secretion were abolished in the presence of CYN154806 (100 nM, Tocris). Application of CYN154806 increased glucagon secretion at 4 mM glucose, suggesting that somatostatin release at this glucose concentration is sufficient to tonically inhibit glucagon secretion. No effects of the antagonist on somatostatin release were observed (Figure 6-13A-B). These results suggest that insulin-induced inhibition of glucagon secretion may be indeed mediated by insulin-induced stimulation of somatostatin secretion.

[5] Believed to be the principal SSTR in α-cells (Strowski et al., 2000) when these studies were initiated.

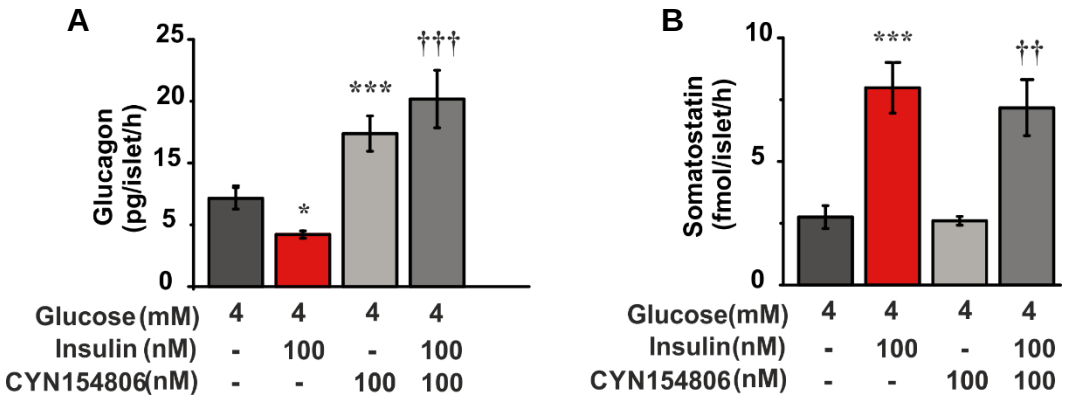

Figure 6-13 *In vitro* effect of CYN154806 and insulin on hormone secretion.

A Glucagon secretion from NMRI islets measured at 4 mM glucose and in the presence of insulin or CYN154806 or both. **B** Somatostatin secretion measured on the same islets used in **A**. For these experiments 4 NMRI mice and n=10 replicates were used. Data were analized using one-way ANOVA followed by Dunnett's *post hoc* test. *: $p<0.05$, ***: $p<0.001$ vs 4 mM glucose in the absence of insulin; ††: $p<0.005$, †††: $p<0.001$ *vs* 4mM in the presence of insulin.

6.4 DISCUSSION

6.4.1 Insulin potentiates somatostatin release

Glucagon secretion is finely regulated by the complex interplay of several paracrine factors including insulin (Maruyama et al., 1984, Ravier and Rutter, 2005, Elliott et al., 2015), GABA (Rorsman et al., 1989), serotonin (Almaca et al., 2016) and somatostatin (Koerker et al., 1974, Strowski et al., 2000, Hauge-Evans et al., 2009). Understanding the paracrine regulation of glucagon secretion is particularly important to identify the causes of impaired counter-regulation of glucagon secretion in insulin-induced hypoglycaemia, one of the major complication arising from the insulin therapy in diabetic patient (Cryer, 1999). Impaired counter-regulation in insulin-induced hypoglycaemia has been attributed to a direct inhibitory effect exerted by insulin on α-cells (Figure 6-1).

In this study the interrelationship between insulin, glucagon and somatostatin has been investigated. It was demonstrated that insulin inhibits glucagon secretion whilst stimulating somatostatin release. These findings suggest that the glucagonostatic effect of insulin might be mediated by somatostatin secretion. These results might seem to be in disagreement with the study done by Hauge-Evans et al (2012). However, these investigators tested insulin at 1 mM, 7 mM and 20 Mm glucose. An important difference is that our experiments were conducted at 4 mM glucose (a concentration that does not stimulate endogenous insulin release). Thus, these data agree with those of Hauge-Evans et al. (2012) in showing weak effects of insulin on somatostatin release

at both 1 (Figure 6-11C-D) and 10 mM glucose (Salehi A and Rorsman P personal communication).

Direct effects of insulin at 1 mM glucose on glucagon-secreting α-cells, either by inhibition of $[Ca^{2+}]_i$ (Ravier and Rutter, 2005) or by lowering cAMP (Elliott et al., 2015), have been reported. Indeed, α-cells, like β- and δ-, express insulin receptors (Adriaenssens et al., 2016, Di Gruccio et al., 2016) but it seems unlikely that insulin directly modulates α-cells function by their activation.

The observation that insulin-induced inhibition of glucagon secretion may be mediated by stimulation of somatostatin is supported by evidence reported by Le Marchand and Piston (2010). In this latter study, the authors demonstrated that insulin inhibited glucagon release in intact islets but was unable to reduce glucagon secretion in pure fractions of α-cells (obtained by FACS). This strongly suggests that the inhibitory effect of insulin on glucagon secretion may be mediated by paracrine signalling.

Pancreatic δ-cells express insulin receptor (Figure 6-3A-B), and many of its downstream signalling components such as insulin receptor substrate 1 and 2 (*Irs1* and *Irs2*), phosphatidylinositol 3-Kinase regulatory subunits (*Pik3r1, Pik3r2, Pik3r3, Pik3r4*) and catalytic subunits (*Pik3ca, Pik3cb, Pik3cd)* and protein kinase B (*Akt1, Akt2, Akt3*) (Adriaenssens et al., 2016, Di Gruccio et al., 2016). Importantly, insulin receptor is encoded by a single gene (*Insr*) but can exist in two isoform A and B, which differ only by the absence or presence of exon 11. In β-cells it has been reported that insulin signalling through

receptor A activates transcription of insulin gene, while receptor B mediates transcription of glucokinase (Leibiger et al., 2001). In the present study, the qPCR data were generated using primers unable to distinguish between the two isoforms, as they recognized a sequence between exon 8 and 9 of the insulin receptor gene. Thus, it remains to be determined if both isoforms are expressed in δ-cells.

Nevertheless, it was demonstrated that insulin directly stimulates somatostatin release by increasing the frequency of $[Ca^{2+}]_i$ oscillations. Secretion data suggest that this pathway is mediated by CICR, as the stimulatory effect of insulin on somatostatin secretion was lost in the presence of thapsigargin (Salehi A and Rorsman P, personal communication). However, further experiments are required to establish whether this pathway involves activation of IRS1 and PI3-kinase, as suggested in the case of β-cells (Aspinwall et al., 2000).

6.4.2 Glucagonostatic effect of insulin is mediated by somatostatin

Support for the role of somatostatin in insulin-induced hypoglycaemia comes from experiments using mice where the insulin receptor has been genetically ablated in somatostatin-expressing tissue, including pancreatic δ-cells (called SIRKO mice). While no differences were observed between SIRKO and control males during ipITT, female SIRKO mice were much less insulin-sensitive than control littermates. Elevated plasma glucagon levels, which

increase hepatic glucose production, may have contributed to the reduced hypoglycaemic effect of insulin in female SIRKO mice. This hypothesis is supported also by *in vitro* data: in the presence of hypoglycaemic condition (4 mM) islets from female SIRKO mice secreted more glucagon compared to control littermates (Figure 6-12B).

Why SIRKO females exhibit a more dramatic *in vivo* phenotype than SIRKO males (Figure 6-10A-B) is not yet known but it may be relevant that the same dose of insulin (1.5U/Kg) induced different responses in male and female control mice. While the blood glucose levels dropped below 5 mM after 30 min from insulin injection in females (Figure 6-10B), blood glucose levels never dropped below 5.5 mM in males (Figure 6-10A). Differences in insulin sensitivity between sexes have been reported and they might be attributed to reduced insulin action and lipogenesis observed in male adipocytes compared to female adipocytes (Macotela et al., 2009).

During the ipGTT, glucose levels returned to basal levels within 150 min in females while they remained elevated in males (Figure 6-9D and Figure 6-8D). This observation emphasizes that both control and SIRKO males are more glucose-intolerant than females. To understand why SIRKO male mice respond differently from SIRKO females, it would have been helpful to measure the blood glucagon and somatostatin levels after the ipITT. However, due to the limitations of the project licence (restriction about the amount of blood) it has not been possible to generate this set of data.

Importantly, the SIRKO mice, were generated using SST-Cre-RFP, which targets not only pancreatic δ-cells but any other somatostatin-expressing tissue such as D-cells in the stomach (Adriaenssens et al., 2015). Thus, it cannot be excluded that the effect exerted by insulin *in vivo,* during the ipITT, is in part mediated by other somatostatin expressing-cells. In man, stimulation of somatostatin release from the gastrointestinal tract or from the hypothalamus during hypoglycaemia, has been suggested by several studies (Wass et al., 1980, Webb et al., 1984, Francis and Ensinck, 1987). Therefore, from the *in vivo* SIRKO data alone, it was not possible to conclude that the improved insulin tolerance of female SIRKO mice reflects effects mediated locally by somatostatin released from the pancreatic δ-cells.

This underlines the importance of the *in vitro* data. Using isolated islets, it was demonstrated that insulin's glucagonostatic effect is indeed mediated by stimulation of somatostatin release. In islets from SIRKO mice, insulin failed to inhibit glucagon release and this effect was paralleled by loss of stimulation of somatostatin secretion. The effects of insulin on glucagon and somatostatin secretion were similar using islets from both male and female, control and SIRKO mice (Figure 6-12A-D). Notably, these effects were observed at 4 mM glucose but not at 1 mM. This echoes the observation in the $[Ca^{2+}]_i$ imaging experiments (Figure 6-3C-F).

It could be argued that the data from SIRKO mice are at variance with observation in αIRKO mice, in which insulin receptor was specifically ablated in glucagon secreting α-cells (Kawamori et al., 2009). The latter study

suggested that insulin directly inhibits glucagon release from α-cells because plasma glucagon levels were increased in αIRKO mice compared to controls. However, in that study no *in vitro* evidence demonstrating a loss of the inhibitory effect of insulin on glucagon secretion in islets isolated from αIRKO mice was provided. The effects of α-cell ablation of the insulin receptor were surprisingly weak (Kawamori et al., 2009). In fact, the observation that insulin-induced hypoglycaemia triggered a strong stimulation of glucagon secretion in both wildtype (with insulin receptor) and αIRKO mice suggest that insulin is without a major direct effect the α-cells.

Our work provides also evidence that endogenous insulin modulates somatostatin secretion (Figure 6-4A-D). The intergranular concentration of insulin is 100 mM (Huang et al., 1995, Rorsman and Renstrom, 2003). Thus, the granular insulin content can be diluted 1,000,000 times and yet elevate interstitial insulin to 100 nM. In support of a modulatory effect of endogenous insulin, it was observed synchronization of δ-cell $[Ca^{2+}]_i$ oscillations during the first few minutes after exposure to high glucose, which correspond to the first phase of insulin secretion (Henquin et al., 2006); an effect that was abolished in the presence of the insulin receptor antagonist S961.

6.4.3 Role of SSTR2 receptor antagonist

The hypothesis that insulin-induced hypoglycaemia is mediated by stimulation of somatostatin, which in turn inhibits glucagon release, was tested further

using a somatostatin receptor blocker. *In vitro* experiments, clearly showed that the inhibitory effect exerted by insulin on glucagon secretion was completely lost in the presence of the SSTR2 antagonist CYN154806. Notably, the blocker did not affect somatostatin secretion. This strongly suggests that somatostatin is an important paracrine regulator which mediates the glucagonostatic effect of insulin. Several previous studies report an amelioration of hypoglycaemia in the presence of a SSTR2 blocker in both control and diabetic rats (Yue et al., 2012, Karimian et al., 2013, Yue et al., 2013). Our data suggest that these effects may be mediated by antagonising the glucagonostatic effect of insulin-induced endogenous (intraislet) somatostatin release.

Taken together, these findings generated by this study suggest that insulin (exogenous or endogenous) stimulates somatostatin release and that this in turn inhibits glucagon release. Based on these data, a revised model of paracrine regulation of glucagon secretion may be proposed (Figure 6-14).

These findings underscore the importance of understanding insulin-induced stimulation of somatostatin secretion from a therapeutic viewpoint. However, it could be argued that a SSTR antagonist may erroneously stimulate glucagon release, when used along with the insulin therapy during hyperglycaemic conditions. In fact, in this scenario insulin stimulates somatostatin, which is unable to inhibit glucagon release, due to the presence of the blocker. However undesired elevated glucagon levels will still be prevented by glucose, which

exerts its inhibitory effect on α-cells (MacDonald et al., 2007, Zhang et al., 2013b).

. Therefore , it could be argued (based on these findings) that a somatostatin receptors antagonist should be used as an adjunct to the insulin therapy to prevent life-threatening hypoglycaemic event in insulin-treated diabetic patients.

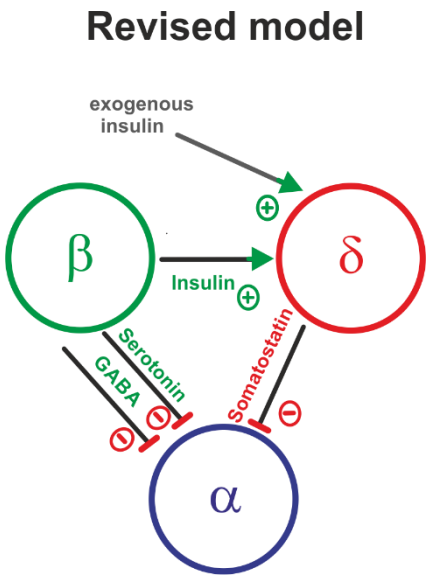

Figure 6-14 Revised model of regulation of glucagon secretion.

According to the data presented in this study insulin (exogenous or endogenous) can stimulate somatostatin release from δ-cells which in turn inhibit glucagon secretion from α-cell.

7 CONCLUSIONS

In this study, the SST-Cre-GCaMP3 mouse model (Adriaenssens et al., 2016) has been characterized physiologically and demonstrated to be an extremely valuable tool to investigate the regulation of somatostain secretion from δ-cells (Chapter 3).

Using these mice, the model of glucose-stimulated somatostatin has been refined. It has been clarified that closure of K_{ATP} is required for somatostatin secretion (as no secretion occurs in the presence of diazoxide) but this event is “permissive” (Chapter 4).

The key role of the CICR mechanism, in the control of somatostatin secretion described previously (Zhang et al., 2007) was confirmed. Interestingly, electrical activity and changes in intracellular [Ca^{2+}] did not correlate in δ-cells. $[Ca^{2+}]_i$ oscillations were superimposed on a plateau of elevated $[Ca^{2+}]_i$ (Figure 3-6A) but they were abolished in the presence of high-$[K^+]_o$ (condition which allow to investigate exclusively CICR) and thapsigargin (Figure 4-13E), independently of changes in membrane potential. Based on these observations, it is tempting to speculate that membrane depolarization and entry of extracellular Ca^{2+} through voltage-gated Ca^{2+} channels lead to elevated $[Ca^{2+}]_i$ plateau, which in turn trigger $[Ca^{2+}]_i$ oscillations that represent Ca^{2+} release from intracellular stores.

The poor correlation between electrical activity and $[Ca^{2+}]_i$ oscillations in δ-cells and the persistence of $[Ca^{2+}]_i$ oscillations under voltage-clamp conditions (Figure 4-10A-B) indicate that in addition to being regulated by an intrinsic CICR mechanism, somatostatin release from δ-cells may be modulated *via* extrinsic processes mediated by gap-junctions or paracrine signalling. The findings that the synchronisation of the $[Ca^{2+}]_i$ oscillations in δ-cells and glucose-induced somatostatin secretion were reduced in the presence of the insulin receptor blocker S961, are suggestive of an important role of insulin released from the β-cells in the regulation of glucose-stimulated somatostatin secretion.

To date, it is accepted that insulin-induced hypoglycaemia in part is mediated by insulin-induced inhibition of glucagon release directly from α-cells (Maruyama et al., 1984, Greenbaum et al., 1991, Ravier and Rutter, 2005, Kawamori et al., 2009). Using mice where insulin receptor has been ablated specifically in somatostatin-expressing cells, (SIRKO), it has been possible to demonstrate that insulin-induced inhibition of glucagon secretion is mediated by insulin-stimulated somatostatin release (Figure 6-12A-D). The evidence that SSTR2 blocker abolishes the glucagonostatic effect of insulin *in vitro* (Figure 6-13A-B), emphasizes the pivotal role of somatostatin in the inhibition of glucagon release.

To conclude, the findings presented in this study suggest the novel idea that somatostatin secretion may be regulated by at least four different mechanisms: 1) by electrical activity; 2) by CICR mechanism; 3) by homologous cross-talk with other δ-cells, most probably *via* gap-junctions, which facilitates synchronous Ca^{2+} oscillations; and 4) by paracrine signalling mediated by insulin, a powerful stimulator of somatostatin release, secreted by the neighbouring β-cells.

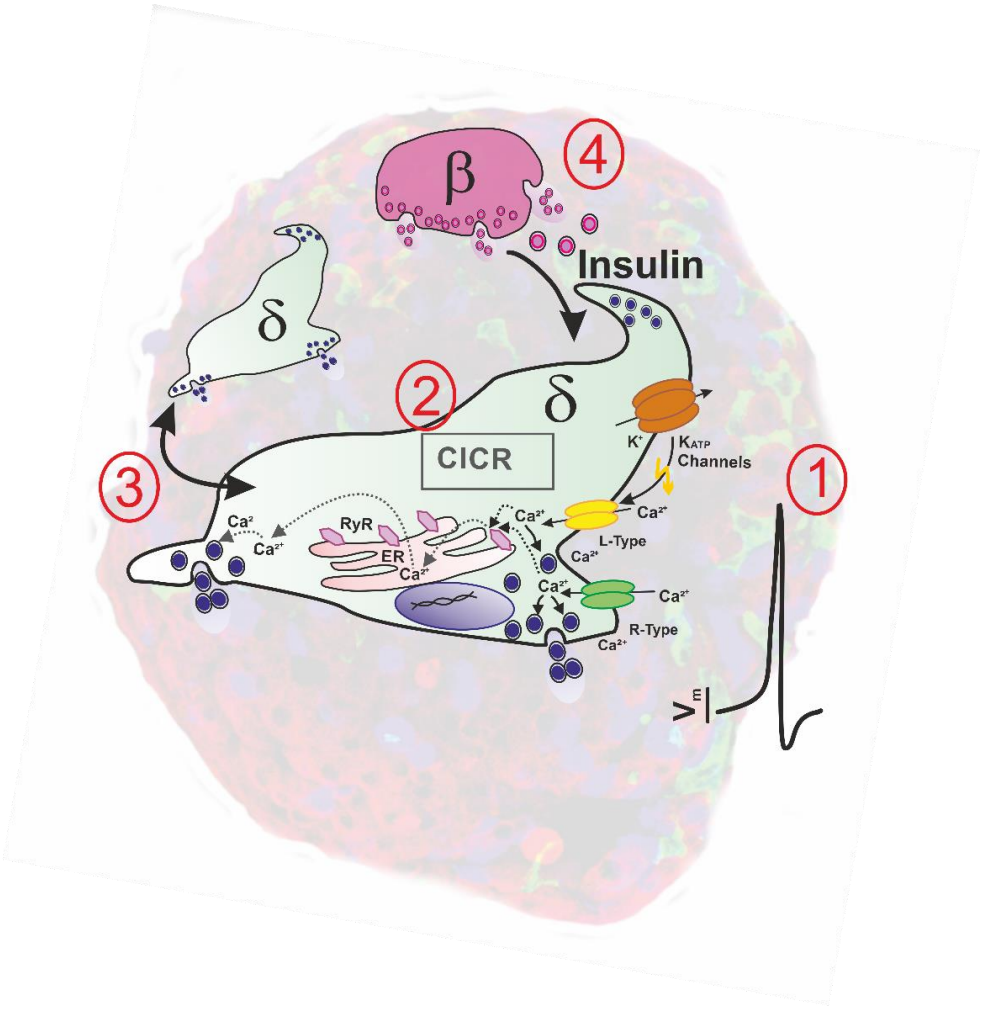

Figure 7-1 Revised model of regulation of somatostatin release.

Somatostatin secretion can be regulated at the intracellular level by action potential firing (1) by CICR (2), by homologous interaction with other δ-cells (3) and by paracrine signalling mediated by the neighbouring β-cells (4).

8 APPENDICES

8.1 APPENDIX 1: GENERATION OF SST-Cre-GCAMP3 MICE

SST-Cre mice were created by Dr. Reimann (University of Cambridge) by cloning the somatostatin promoter from Bacterial artificial chromosome BAC bQ73b10 with NOD background. A rpsLneo sequence (Genebridges, Heidelberg, Germany) was inserted after the stop codon in SST-exon 2. This sequence, which gives kanamycin resistance and streptomycin sensitivity was used for selection. The sequence between the start codon in exon-1 and rpsLneo was then removed and substituted with mCherry-2A-iCre sequence. Therefore, these mice express an iCRE transgene under the SST- promoter (*Sst*-mCherry-2A-iCre). Unfortunately, mCherry did not emit any fluorescence. Therefore, in order to express a fluorescent marker in δ-cells, the mice were crossed with ROSA26tdRFP or ROSA26GCaMP3 (Chera et al., 2014). The ROSA26 locus is located on mouse chromosome 6 and is ubiquitously expressed. The ROSA26 locus has a high rate of homologous recombination which has made it a preferred site for knocking in a transgene to achieve a conditional transgenic overexpression (Friedrich and Soriano, 1991). This strategy takes advantage of the Cre-Loxp technology, a site-specific recombinase technology, which is used to insert or delete a DNA sequence at specific sites in the genome of a host cell. The Cre recombinase recognizes and recombines the LoxP sequences. In the ROSA26-transgene construct, a LoxP-flanked STOP cassette (which includes stop codons in all three reading frames followed by one to several SV40 polyadenylation sequences) prevents

transcription of the downstream gene (Luche et al., 2007). The reporter gene is under the control of CAG (CMV early enhancer/chicken β-actin) promoter, which is inserted in the ROSA26 locus upstream of the STOP cassette. The STOP cassette is excised only in tissues which express Cre recombinase. This event allows CAG-driven expression of the reporter gene. Therefore, when bred with the ROSA26tdRFP, Sst-mCherry-2A-iCre mice enable the expression of tdRFP in SST-expressing tissues, including pancreatic δ-cells. These mice are called SST-Cre-RFP. To investigate Ca^{2+} signalling in δ-cells, these mice were subsequently crossed with ROSA26GCaMP3 to generate SST-Cre-RFP-GCaMP3. Initially, it was thought that the presence of the two fluorescent markers (RFP and GCaMP3) was necessary because the Ca^{2+} sensor GCaMP3 in the absence of Ca^{2+} fluoresces very dimly. However, after demonstrating that the fluorescence of GCaMP3 alone was enough to identify and to image δ-cells within intact islets, it was decided to start crossing the original mouse Sst-mCherry-2A-iCre only with the ROSA26GCaMP3 to create the SST-Cre-GCaMP3 mouse model.

8.2 APPENDIX 2: CHARACTERIZATION OF THE HUMAN SOMATOSTATINOMA CELL LINE QGP-1

8.2.1 Introduction

Due to the limitations in identifying living human δ-cells in pancreatic islets, a tool to investigate somatostatin release *in vitro* was essential. In this study, the possibility of using the somatostatin-secreting human cell line QGP-1 was evaluated. This cell line was established more than 20 years ago by Iguchi et al. (1990) but, since its generation, QGP-1 cells have not been widely used in the efforts to understand the regulation of somatostatin secretion. Thus, this study explored and explained how QGP-1 cell line might be used as a model to investigate somatostatin secretion *in vitro.*

8.2.2 Materials and methods

8.2.2.1 Immunocytochemistry

QGP-1 cells were fixed in 4% paraformaldehyde, permeabilized with 0.1% Triton X-100 in PBS containing 5% goat serum for 10-15 min, followed by blocking of non-specific binding with 5% goat serum for 30 min. The cells were incubated with primary antibodies (guinea pig anti-insulin (1:1000 Sigma), mouse anti-glucagon (1:2000; Sigma) and rabbit anti-somatostatin (1: 500; Sigma) for 1 h at room temperature. They were then incubated with secondary antibodies: goat anti-guinea pig-Alexa-555 and anti-mouse Alexa-488 or goat anti-rabbit Alexa-568 and anti-mouse Alexa-488 (all from Invitrogen and used

at 1:500), for 1h at room temperature. Samples were visualised with a Zeiss LSM 510 META confocal microscope using appropriate lasers and filters.

8.2.2.2 Cell culture and secretion assay

QGP1 were cultured in RPMI (21875-034) containing 11.1 mM glucose and supplemented with 10% FBS (10099-141), 1% penicillin-streptomycin (15140-122), 1% glutamax (35050-087). All the reagents were from Gibco. The cells were plated onto 24-well plates and cultured for 3-4 days. The day before the assay, the above culture medium was replaced with RPMI containing 5.5 mM glucose (instead of 11.1), to rest the cells. On the day of the experiment, QGP-1 cells were preincubated with Hanks Balanced Salt Solution (HBSS) containing (mM) 114 NaCl, 4.7 KCl, 25.5 $NaHCO_3$, 1.2 KH_2PO_4, 1.16 $MgSO_4$, 2 HEPES, 2.5 $CaCl_2$ and 0.07% BSA but no glucose for 2 h at 37 ºC and 5% CO_2. They were then stimulated with glucose and other stimuli as indicated for 1 h. The collected supernatants were centrifuged and stored at -20 ºC. The cell pellet from each well was lysed with acid-ethanol and stored at -20 ºC. Somatostatin concentration, in both pellet and supernatant fractions, was determined using a RIA kit (Eurodiagnostica).

8.2.2.3 Membrane potential recordings

Membrane potential recordings were performed using the perforated-patch technique. The pipette solution contained (in mM): 128 K-gluconate,10 KCl, 10 NaCl, 1 $MgCl_2$, 10 HEPES (pH 7.35 with KOH) and 20 µg/ml of the pore-forming antibiotic amphotericin B. In these experiments, the extracellular

(KRB) solution consisted of (mM) 140 NaCl, 3.6 KCl, 0.5 $MgSO_4$, 0.5 NaH_2PO4, 2 $NaHCO_3$, 5 HEPES, 1.5 $CaCl_2$ and glucose and/or tolbutamide or diazoxide as indicated. All electrophysiological experiments were performed at 34 ºC.

8.2.2.4 Real-time quantitative RT-PCR

The levels of gene expression in QGP-1, EndoC-βH1 and human islets were determined using real-time quantitative RT-PCR. Total RNA was extracted using TRIzol Reagent (Invitrogen) PureLink RNA Mini Kit (Life Technologies) and PureLink® DNase Set (Life Technologies) following manufacturer's instructions. cDNA was then synthesised by reverse transcription carried out using High Capacity RNA-to-cDNA™ Kit (Life Technologies). Real-time quantitative RT–PCR was performed using SYBR Green kit (QuantiFast SYBR Green PCR Kit, Qiagen) and ABI PRISM 7900HT Sequence Detection System (Applied Biosystems). Primers used were QuantiTect Primer Assays (β-actin: cat #QT00095431 and glucokinase cat #QT00000812, Qiagen). Each sample was run and analysed in triplicate.

8.2.2.5 Statistical analysis

Statistical analyses were performed using Sigma plot 13.0 and GraphPad Prism software 6.0. Unless otherwise stated data are represented as the mean ± standard error (S.E.) of at least three independent experiments. For normally distributed data, differences between two groups were assessed by two-tailed

unpaired Student's t-test, while for differences between more groups one-way ANOVA-followed by a *post hoc* test was used.

8.2.3 Results

8.2.3.1 Glucose-induced stimulation of somatostatin secretion

The human cell line QGP-1 was evaluated to determine whether it would be a suitable model to investigate how somatostatin release is regulated. It was confirmed by immunocytochemistry that QGP-1 cells exclusively express somatostatin, as insulin and glucagon were not detected (Figure A2-1A-C).

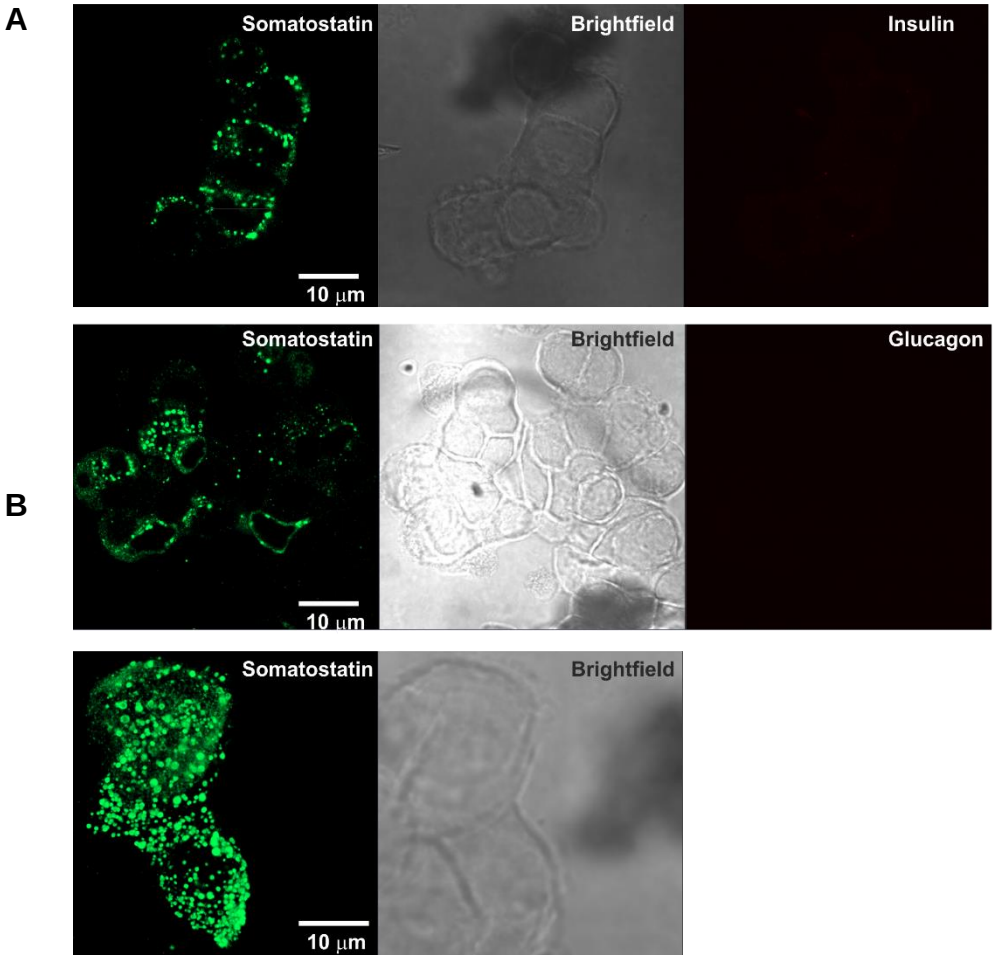

Figure A2-1 Immunostaining of QGP-1 cells.

A Cells were stained for somatostatin and insulin, **B** and somatostatin and glucagon. **C** 3D reconstruction of Z-stack confocal images of a single QGP-1 cell containing exclusively somatostatin granules.

As somatostatin is released in a glucose-dependent manner, it was tested whether QGP-1 cells preserve such glucose-dependent mechanism of secretion. Unlike primary human δ-cells, somatostatin secretion did not change significantly when cells were exposed to 0.5 mM, 6 mM or 20 mM glucose (Figure A2-2).

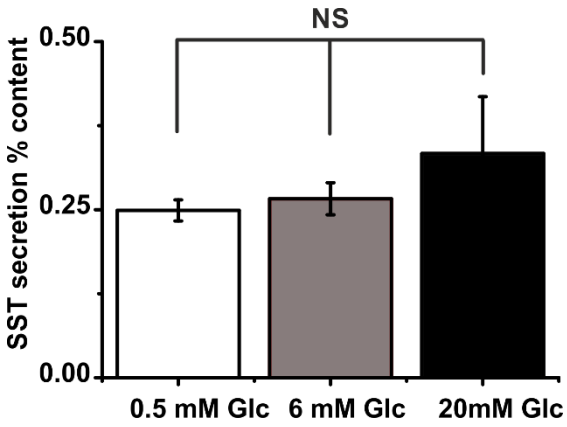

Figure A2-2 Somatostatin secretion from QGP-1 cells in response to glucose.

Glucose-stimulated somatostatin secretion in cells were incubated with 0.5, 6 and 20 mM glucose (Glc). Data obtained from n=3 independent experiment, 6 replicates per condition. Data were assessed by one-way ANOVA followed by Tukey's *post hoc*. NS: not significant.

Electrophysiological measurements of membrane potential showed that increasing glucose concentration from 1 mM to 20 mM failed to stimulate action potentials in QGP-1 cells. This is in agreement with the earlier secretion experiments, where glucose failed to stimulate somatostatin release. However, application of the K_{ATP} channels blocker, tolbutamide (200µM) strongly stimulated electrical activity. This effect was reversibly antagonised by the K_{ATP} channel opener diazoxide (100 µM) which hyperpolarized the cell (Figure A2-3). These observations suggested that the cause of impaired glucose-induce somatostatin release in QGP-1 cells lies downstream of the K_{ATP} channels.

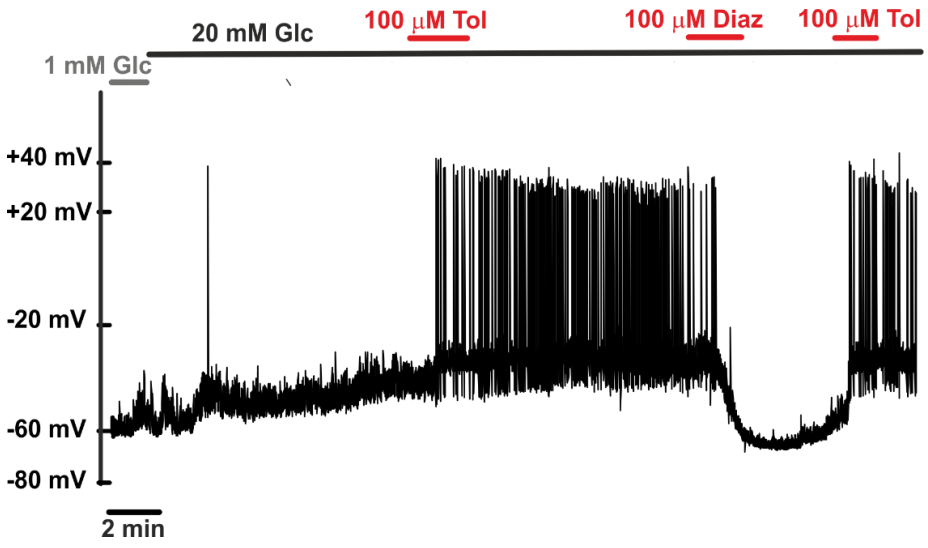

Figure A2-3 Membrane potential recording of a QGP-1 cell.

Effect of glucose, tolbutamide and diazoxide on membrane potentials in a QGP-1 cell. Glucose (20 mM) was unable to stimulate electrical activity in QGP-1 cells. However, the K_{ATP} channels blocker, tolbutamide (100 µM), stimulated action potentials in QGP-1 cells and this effect was reversed by the K_{ATP} channels opener diazoxide (100 µM).

It was reasoned that defects in glucose metabolism might account for impaired somatostatin secretion in QGP-1 cells. Quantitative real-time PCR (qPCR) analysis of mRNA levels showed that the expression of the glucose sensor, glucokinase (GCK), was significantly reduced in QGP-1 cells compared to human islets (Figure A2-4A). To avoid cross-contamination from non-β-cells in the islets, the expression levels of glucokinase in QGP-1 cell line and in the human β-cell line EndoC-βH1 (Ravassard et al., 2011) were also compared. Similar to what was observed in human islets, the expression levels of glucokinase in the EndoC-βH1 cells were significantly higher than in QGP-1 (Figure A2-4B).

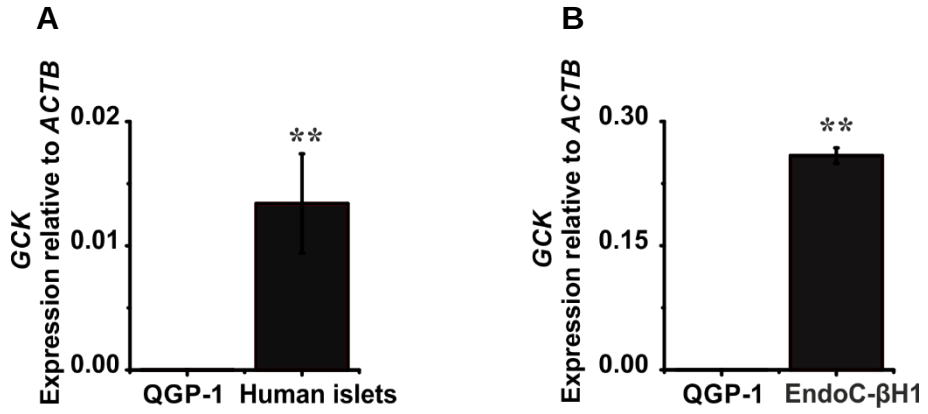

Figure A2-4 Glucokinase expression in QGP-1, human islets and EndoC-βH1 cells.
A Glucokinase (*GCK*) expression assessed by qPCR in QGP-1 cells and Human islets. **B** As in **A** but instead QGP-1 and EndoC-βH1 cells were used. Data were assessed by unpaired Student's t-test versus *GCK* expression in QGP1 cells. **: $p<0.005$.

8.2.3.2 Amplification of glucose-induced somatostatin release

Although glucose-induced somatostatin release is impaired in QGP-1 cells, studies were extended to investigate whether pathways downstream of glucose metabolism may still be functional in the QGP-1 cell line. In the case of β-cells, insulin secretion is stimulated upon glucose uptake which increases cytosolic Ca^{2+} concentration and can be further amplified by cAMP (Brisson et al., 1972). Hence, it was decided to determine whether cAMP-elevating agents could increase somatostatin secretion in QGP-1 cells. Indeed, forskolin, which stimulates adenylate cyclase activity and increases intracellular cAMP levels, strongly stimulated somatostatin release in QGP-1 cell line at 3 mM glucose (Figure A2-5A). In addition, theophylline, a phosphodiesterase inhibitor that prevent the intracellular break-down of cAMP, slightly but significantly enhanced somatostatin release at 6 mM glucose (Figure A2-5B). Human primary δ-cells express the muscarinic receptor M1 activation of which strongly stimulates somatostatin secretion (Molina et al., 2014). M1 is a G-coupled receptor, which can bind to G proteins of class Gq (Thomas et al., 2008). Gq-protein-coupled receptors activate phospholipase C which produces inositol trisphosphate and increases intracellular Ca^{2+}. Similar to cAMP-elevating agents, the cholinergic drug acetylcholine strongly stimulated somatostatin release from QGP-1 cells (Figure A2-5C).

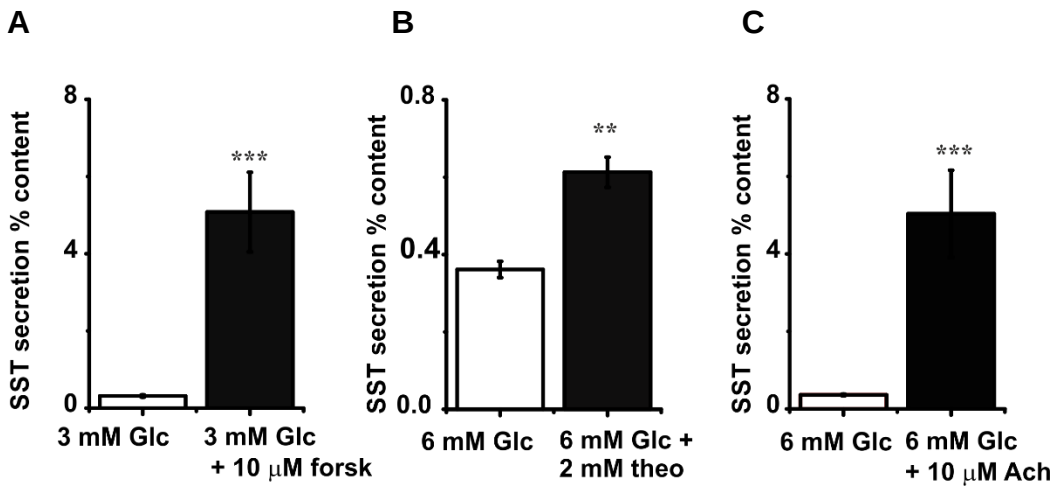

Figure A2-5 Effect of cAMP-elevating agent and Ca^{2+}-elevating agent on somatostatin secretion from QGP-1.

A Somatostatin secretion in the presence of 3 mM glucose (Glc). Forskolin (forsk, 10 µM) was added as indicated. **B** Effect of the phosphodiesterase inhibitor, theophylline (theo) on somatostatin secretion. **C** Somatostatin secretion with or without the Ca^{2+}-elevating agent acetylcholine (Ach). n=3 for each experiment. Data were assessed using unpaired Student's t-test *vs* **A** 3mM glucose and **B-C** 6 mM glucose. **: p<0.005,***: p<0.001.

8.2.4 Discussion

In this study, the merits of the somatostatin-secreting human cell line QGP-1, as a useful tool to investigate somatostatin secretion in vitro, were evaluated. The results confirmed that QGP-1 cells lack glucose sensitivity, as previously reported (Iguchi et al., 1990). However, the findings did demonstrate that the loss of glucose sensitivity in these cells is not due to impairment of the K_{ATP} channels, because the K_{ATP} channels blocker tolbutamide strongly stimulated electrical activity in QGP-1 cells. Moreover, the stimulatory effect of tolbutamide was perfectly reversed by the K_{ATP} channel opener diazoxide.

Therefore, according to this data, impaired glucose-induced somatostatin secretion in QGP-1 cells might be attributed to defects in glucose metabolism.

In particular, it was observed that glucokinase is an important glucose sensor in somatostatin-secreting cells. These data suggest that impaired glucose response in QGP-1 cells has to be attributed to the low expression of the glucokinase enzyme. This finding is similar to that reported by Sakura et al. (Sakura et al., 1998) for β-cells: in glucokinase knockout mice the sulphonylurea tolbutamide was still able to trigger electrical activity while 20 mM glucose failed to induce membrane depolarization.

In summary, this study evaluated whether the QGP-1 cell line can be used to investigate pathways that regulate somatostatin release, downstream of glucose metabolism. cAMP is an intracellular metabolic signal which regulates insulin release in pancreatic β-cells (Seino et al., 2009). Therefore, it was reasoned that bypassing glucose metabolism with cAMP-elevating agents could stimulate somatostatin release in the QGP-1 cells. In fact, stimulation of adenylate cyclase with forskolin, or inhibition of phosphodiesterase with theophylline significantly stimulated somatostatin release. Similarly, activation of muscarinic acetylcholine receptors, which induces elevation of intracellular $[Ca^{2+}]_i$ strongly stimulated somatostatin release.

These data emphasise that the QGP-1 cell line is not a useful tool to explore the regulation of glucose-induced somatostatin secretion, *per se*.

8.3 APPENDIX 3: CORRELATION ANALYSIS OF TIMES SERIES

8.3.1 Correlation analysis of times series

To assess the degree of coupling between δ-cells in different experimental conditions, the analysis of $[Ca^{2+}]_i$ imaging data followed that of Stozer et al. (2013).For each experiment, an n-tuple of time-series were obtained for the n δ-cells (ROIs):

$$x_1(t), x_2(t), \dots, x_i(t), \dots, x_n(t).$$

For each pair of δ-cells (i, j) with time-series $x_i(t), x_j(t)$ the correlation C_{ij} between the cells was calculated as follows. First, a cross-correlation between $x_i(t)$ and $x_j(t)$ was conducted using the $xcorr$ function in MATLAB 6.1 (2000; The MathWorks, Natick, MA). This analysis yielded the lag at which the correlation between $x_i(t)$ and $x_j(t)$ was maximum. (If $i = j$ then this lag would be 0.) This lag was restricted to be at most 3s (one sampling interval). This choice was supported by the evidence that $[Ca^{2+}]_i$ oscillations recorded from β-cells located in two different regions of the islets can be delayed by 1-2s (Santos et al., 1991).

Suppose the lag at which correlation between $x_i(t)$ and $x_j(t)$ is maximum, is $\Delta\tau$. The second step was to calculate the Pearson's correlation coefficient between $x_i(t)$ and $x_j(t - \Delta\tau)$

$$C_{ij} = \frac{cov(x_i(t), x_j(t - \Delta\tau))}{\sigma_i \sigma_j}$$

Where cov is the covariance and σ_i and σ_j is the standard deviation of $x_i(t)$ and $x_j(t - \Delta\tau)$, respectively. This gives the correlation between the Ca^{2+} signals of δ-cells i and j (C_{ij}) and the associated p-value (for testing the hypothesis that there is no relationship between $x_i(t)$ and $x_j(t - \Delta\tau)$). This analysis was conducted using MATLABs $corrcoef$ function. If the p-value was >0.05, then the time-series were considered not significantly correlated and C_{ij}=0. These data would yield an n-by-n correlation matrix, where the (i, j)th entry was C_{ij}. This matrix is symmetric with diagonal elements C_{ii}=1.

The data for this matrix was represented as a heatmap, to track the correlations between particular cell-pairs through time and across experimental conditions. This correlation was calculated before and during an experimental condition (*e.g.* 1→20mM glucose), to assess how the experimental condition influenced the correlation between $[Ca^{2+}]_i$ oscillations in δ-cells. To determine how the correlation between two cells changes over time with a better temporal resolution, a "sliding window" technique was employed. Time-series data was partitioned into m equal sized distinct time-windows of size ΔT, to assess how the correlation between δ-cells i and j changed over time. This would yield correlations

$$C_{ij;1}, \dots, C_{ij;k}, \dots, C_{ij;M}$$

Where $C_{ij;k}$ is the correlation between cells i and j during the kth time-window (of duration ΔT). To ensure that the subsequent results were not due to the choice of partition of the time-series (ΔT), the analysis was repeated for a number of different ΔT, namely ΔT=90, 120, 150, 180 s. An example MATLAB script for conducting this analysis is included below.

8.3.2 Example script for correlation analysis

```
% Created 13/7/16 by Linford Briant and Elisa Vergari.
% Note that this script will not work unless you address the following required
% inputs:
% DataLocation
% File.xlsx
% sampling_interval
% cor_seq_dummy - alter appropriately

clear all
close all
clc

cd('DataLocation') %% point to where the excell file is, e.g. C:\Documents

N=xlsread('File.xlsx'); %% Data file of ROIs in columns; first column is time

sampling_interval=3; % replace with sampling interval of file (in seconds)

for i=2:6; % there are 5 cells in File.xlsx from column 2 to 6; change as
appropriate if datafile contains more ROIs/cells
```

```
for j=2:6; % there are 5 cells in File.xlsx from column 2 to 6; change as appropriate if datafile contains more ROIs/cells
    X=[];
    Y=[];
    cor_seq=[];
    lags=[];
    cor_seq_positive=[];
    second_max_value=[];
    X_hat=[];
    Y_hat=[];

    X=N(:,i); % change this if you want to split the analysis into different time-windows
    Y=N(:,j); % change this if you want to split the analysis into different time-windows
    X=X-mean(X);
    Y=Y-mean(Y);

    [cor_seq,lags]=xcorr(X,Y); % calculates cross-correlation

    cor_seq_dummy=cor_seq(lags<1 & lags>-1); % restricts correlation to 1 lag; change according to sampling interval.

    max_value = max(cor_seq_dummy);

    maxa=lags(cor_seq==max_value); % gives lag that gives maximum xcorr

    lag_of_max(i-1,j-1) = maxa(1); % gives lag that gives maximum xcorr

    if lag_of_max(i-1,j-1)>0 %% following if command shifts time-series appropriately, depending on whether lag_of_max is positive of negative.
        X_hat = X(lag_of_max+1:end);
```

```
            Y_hat = Y(1:end-lag_of_max);
        else
            X_hat = X(-lag_of_max+1:end);
            Y_hat = Y(1:end+lag_of_max);
        end
        [Correlation(i-1,j-1),Significance(i-1,j-1)]=corrcoef(X_hat,Y_hat);          %
calculates correlation and p-value
    end
end
```

9 REFERENCES

Adriaenssens, A., Lam, B. Y., Billing, L., Skeffington, K., Sewing, S., Reimann, F. & Gribble, F. 2015. A transcriptome-led exploration of molecular mechanisms regulating somatostatin-producing D-Cells in the gastric epithelium. *Endocrinology,* 156**,** 3924-36.

Adriaenssens, A. E., Svendsen, B., Lam, B. Y., Yeo, G. S., Holst, J. J., Reimann, F. & Gribble, F. M. 2016. Transcriptomic profiling of pancreatic alpha, beta and delta cell populations identifies delta cells as a principal target for ghrelin in mouse islets. *Diabetologia,* 59**,** 2156-65.

Aguilar-Parada, E., Eisentraut, A. M. & Unger, R. H. 1969. Pancreatic glucagon secretion in normal and diabetic subjects. *Am J Med Sci,* 257**,** 415-9.

Ahren, B. 2000. Autonomic regulation of islet hormone secretion - Implications for health and disease. *Diabetologia,* 43**,** 393-410.

Akerboom, J., Chen, T. W., Wardill, T. J., Tian, L., Marvin, J. S., Mutlu, S., Calderon, N. C., Esposti, F., Borghuis, B. G., Sun, X. R., Gordus, A., Orger, M. B., Portugues, R., Engert, F., Macklin, J. J., Filosa, A., Aggarwal, A., Kerr, R. A., Takagi, R., Kracun, S., Shigetomi, E., Khakh, B. S., Baier, H., Lagnado, L., Wang, S. S., Bargmann, C. I., Kimmel, B. E., Jayaraman, V., Svoboda, K., Kim, D. S., Schreiter, E. R. & Looger, L. L. 2012. Optimization of a GCaMP calcium indicator for neural activity imaging. *J Neurosci,* 32**,** 13819-40.

Alberti, K. G., Christensen, N. J., Christensen, S. E., Hansen, A. P., Iversen, J., Lundbaek, K., Seyer-Hansen, K. & Orskov, H. 1973. Inhibition of insulin secretion by somatostatin. *Lancet,* 2**,** 1299-301.

Alberts, B., Johnson, A. & Lewis, J., Et Al. 2002. Molecular Biology of the Cell. 4th edition. Cell Junctions. New York: Garland Science; Available from: http://www.ncbi.nlm.nih.gov/books/NBK26857/.

Almaca, J., Molina, J., Menegaz, D., Pronin, A. N., Tamayo, A., Slepak, V., Berggren, P. O. & Caicedo, A. 2016. Human Beta Cells Produce and Release Serotonin to Inhibit Glucagon Secretion from Alpha Cells. *Cell Rep,* 17**,** 3281-3291.

American Diabetes Association 2010. Diagnosis and classification of diabetes mellitus. *Diabetes Care,* 33**,** S62-S69.

Amherdt, M., Patel, Y. C. & Orci, L. 1987. Selective binding of somatostatin-14 and somatostatin-28 to islet cells revealed by quantitative electron microscopic autoradiography. *J Clin Invest,* 80**,** 1455-8.

Arimura, A., Sato, H., Dupont, A., Nishi, N. & Schally, A. V. 1975. Somatostatin: abundance of immunoreactive hormone in rat stomach and pancreas. *Science,* 189**,** 1007-9.

Arredouani, A., Ruas, M., Collins, S. C., Parkesh, R., Clough, F., Pillinger, T., Coltart, G., Rietdorf, K., Royle, A., Johnson, P., Braun, M., Zhang, Q., Sones, W.,

Shimomura, K., Morgan, A. J., Lewis, A. M., Chuang, K. T., Tunn, R., Gadea, J., Teboul, L., Heister, P. M., Tynan, P. W., Bellomo, E. A., Rutter, G. A., Rorsman, P., Churchill, G. C., Parrington, J. & Galione, A. 2015. Nicotinic acid adenine dinucleotide phosphate (NAADP) and endolysosomal two-pore channels modulate membrane excitability and stimulus-secretion coupling in mouse pancreatic beta cells. *J Biol Chem,* 290**,** 21376-92.

Asada, N., Shibuya, I., Iwanaga, T., Niwa, K. & Kanno, T. 1998. Identification of alpha- and beta-cells in intact isolated islets of Langerhans by their characteristic cytoplasmic Ca2+ concentration dynamics and immunocytochemical staining. *Diabetes,* 47**,** 751-7.

Ashcroft, F. M., Proks, P., Smith, P. A., Ammala, C., Bokvist, K. & Rorsman, P. 1994. Stimulus-secretion coupling in pancreatic beta cells. *J Cell Biochem,* 55 Suppl**,** 54-65.

Ashcroft, F. M. & Rorsman, P. 1989. Electrophysiology of the pancreatic beta-cell. *Prog Biophys Mol Biol,* 54**,** 87-143.

Aspinwall, C. A., Qian, W.-J., Roper, M. G., Kulkarni, R. N., Kahn, C. R. & Kennedy, R. T. 2000. Roles of insulin receptor substrate-1, phosphatidylinositol 3-kinase, and release of intracellular Ca^{2+} stores in insulin-stimulated insulin secretion in β-cells. *Journal of Biological Chemistry,* 275**,** 22331-22338.

Ayala, J. E., Samuel, V. T., Morton, G. J., Obici, S., Croniger, C. M., Shulman, G. I., Wasserman, D. H., Mcguinness, O. P. & Consortium, N. I. H. M. M. P. C. 2010. Standard operating procedures for describing and performing metabolic tests of glucose homeostasis in mice. *Dis Model Mech,* 3**,** 525-34.

Bao, L., Locovei, S. & Dahl, G. 2004. Pannexin membrane channels are mechanosensitive conduits for ATP. *Febs Letters,* 572**,** 65-68.

Baskin, D. G., Gorray, K. C. & Fujimoto, W. Y. 1984. Immunocytochemical identification of cells containing insulin, glucagon, somatostatin, and pancreatic polypeptide in the islets of Langerhans of the guinea pig pancreas with light and electron microscopy. *Anat Rec,* 208**,** 567-78.

Bates, C. M., Kegg, H., Petrevski, C. & Grady, S. 2003. Expression of somatostatin receptors 3, 4, and 5 in mouse kidney proximal tubules. *Kidney Int,* 63**,** 53-63.

Benninger, R. K., Head, W. S., Zhang, M., Satin, L. S. & Piston, D. W. 2011. Gap junctions and other mechanisms of cell-cell communication regulate basal insulin secretion in the pancreatic islet. *J Physiol,* 589**,** 5453-66.

Bergsten, P., Grapengiesser, E., Gylfe, E., Tengholm, A. & Hellman, B. 1994. Synchronous oscillations of cytoplasmic Ca^{2+} and insulin release in glucose-stimulated pancreatic islets. *J Biol Chem,* 269**,** 8749-53.

Berts, A., Ball, A., Dryselius, G., Gylfe, E. & Hellman, B. 1996. Glucose stimulation of somatostatin-producing islet cells involves oscillatory Ca^{2+} signaling. *Endocrinology,* 137**,** 693-7.

Blodgett, D. M., Nowosielska, A., Afik, S., Pechhold, S., Cura, A. J., Kennedy, N. J., Kim, S., Kucukural, A., Davis, R. J., Kent, S. C., Greiner, D. L., Garber, M. G., Harlan, D. M. & Diiorio, P. 2015. Novel observations from next-generation RNA sequencing of highly purified human adult and fetal islet cell subsets. *Diabetes,* 64**,** 3172-81.

Bloom, W. 1931. A new type of granular cell in the islets of Langerhans of man. *The Anatomical Record,* 49**,** 363-371.

Boassa, D., Ambrosi, C., Qiu, F., Dahl, G., Gaietta, G. & Sosinsky, G. 2007. Pannexin1 channels contain a glycosylation site that targets the hexamer to the plasma membrane. *Journal of Biological Chemistry,* 282**,** 31733-31743.

Bootman, M. D., Berridge, M. J. & Roderick, H. L. 2002. Calcium signalling: more messengers, more channels, more complexity. *Curr Biol,* 12**,** R563-5.

Bosco, D., Haefliger, J. A. & Meda, P. 2011. Connexins: key mediators of endocrine function. *Physiol Rev,* 91**,** 1393-445.

Bosco, D., Orci, L. & Meda, P. 1989. Homologous but not heterologous contact increases the insulin-secretion of individual pancreatic beta-cells. *Experimental Cell Research,* 184**,** 72-80.

Braun, M., Ramracheya, R., Amisten, S., Bengtsson, M., Moritoh, Y., Zhang, Q., Johnson, P. R. & Rorsman, P. 2009. Somatostatin release, electrical activity, membrane currents and exocytosis in human pancreatic delta cells. *Diabetologia,* 52**,** 1566-78.

Braun, M., Ramracheya, R., Bengtsson, M., Zhang, Q., Karanauskaite, J., Partridge, C., Johnson, P. R. & Rorsman, P. 2008. Voltage-gated ion channels in human pancreatic beta-cells: electrophysiological characterization and role in insulin secretion. *Diabetes,* 57**,** 1618-28.

Brazeau, P., Rivier, J., Vale, W. & Guillemin, R. 1974. Inhibition of growth hormone secretion in the rat by synthetic somatostatin. *Endocrinology,* 94**,** 184-7.

Brazeau, P., Vale, W., Burgus, R., Ling, N., Butcher, M., Rivier, J. & Guillemin, R. 1973. Hypothalamic polypeptide that inhibits the secretion of immunoreactive pituitary growth hormone. *Science,* 179**,** 77-9.

Breder, C. D., Yamada, Y., Yasuda, K., Seino, S., Saper, C. B. & Bell, G. I. 1992. Differential expression of somatostatin receptor subtypes in brain. *J Neurosci,* 12**,** 3920-34.

Brereton, M. F., Vergari, E., Zhang, Q. & Clark, A. 2015. Alpha-, Delta- and PP-cells: Are they the architectural cornerstones of islet structure and co-ordination? *J Histochem Cytochem,* 63**,** 575-91.

Brisson, G. R., Malaisse-Lagae, F. & Malaisse, W. J. 1972. The stimulus-secretion coupling of glucose-induced insulin release. VII. A proposed site of action for adenosine-3',5'-cyclic monophosphate. *J Clin Invest,* 51**,** 232-41.

Bruzzone, R., Barbe, M. T., Jakob, N. J. & Monyer, H. 2005. Pharmacological properties of homomeric and heteromeric pannexin hemichannels expressed in Xenopus oocytes. *J Neurochem,* 92**,** 1033-43.

Cabrera, O., Berman, D. M., Kenyon, N. S., Ricordi, C., Berggren, P. O. & Caicedo, A. 2006. The unique cytoarchitecture of human pancreatic islets has implications for islet cell function. *Proc Natl Acad Sci U S A,* 103**,** 2334-9.

Caicedo, A. 2013. Paracrine and autocrine interactions in the human islet: more than meets the eye. *Seminars in Cell & Developmental Biology,* 24**,** 11-21.

Calcraft, P. J., Ruas, M., Pan, Z., Cheng, X., Arredouani, A., Hao, X., Tang, J., Rietdorf, K., Teboul, L., Chuang, K. T., Lin, P., Xiao, R., Wang, C., Zhu, Y., Lin, Y., Wyatt, C. N., Parrington, J., Ma, J., Evans, A. M., Galione, A. & Zhu, M. X. 2009. NAADP mobilizes calcium from acidic organelles through two-pore channels. *Nature,* 459**,** 596-600.

Chang, W. P., Wu, J. J. & Shyu, B. C. 2013. Thalamic modulation of cingulate seizure activity via the regulation of gap junctions in mice thalamocingulate slice. *PLoS One,* 8**,** e62952.

Charpantier, E., Cancela, J. & Meda, P. 2007. Beta cells preferentially exchange cationic molecules via connexin 36 gap junction channels. *Diabetologia,* 50**,** 2332-41.

Cheng-Xue, R., Gomez-Ruiz, A., Antoine, N., Noel, L. A., Chae, H. Y., Ravier, M. A., Chimienti, F., Schuit, F. C. & Gilon, P. 2013. Tolbutamide controls glucagon release from mouse islets differently than glucose: involvement of K_{ATP} channels from both alpha-cells and delta-cells. *Diabetes,* 62**,** 1612-22.

Chera, S., Baronnier, D., Ghila, L., Cigliola, V., Jensen, J. N., Gu, G., Furuyama, K., Thorel, F., Gribble, F. M., Reimann, F. & Herrera, P. L. 2014. Diabetes recovery by age-dependent conversion of pancreatic delta-cells into insulin producers. *Nature,* 514**,** 503-7.

Cheung, G., Chever, O. & Rouach, N. 2014. Connexons and pannexons: newcomers in neurophysiology. *Front Cell Neurosci,* 8**,** 348.

Churchill, G. C., Okada, Y., Thomas, J. M., Genazzani, A. A., Patel, S. & Galione, A. 2002. NAADP mobilizes Ca^{2+} from reserve granules, lysosome-related organelles, in sea urchin eggs. *Cell,* 111**,** 703-8.

Cigliola, V., Allagnat, F., Berchtold, L. A., Lamprianou, S., Haefliger, J. A. & Meda, P. 2015. Role of connexins and pannexins in the pancreas. *Pancreas,* 44**,** 1234-44.

Cone, A. C., Ambrosi, C., Scemes, E., Martone, M. E. & Sosinsky, G. E. 2013. A comparative antibody analysis of pannexin1 expression in four rat brain regions reveals varying subcellular localizations. *Front Pharmacol,* 4**,** 6.

Connors, B. W. 2012. Tales of a dirty drug: carbenoxolone, gap junctions and seizures. *Epilepsy Curr,* 12**,** 66-8.

Cruikshank, S. J., Hopperstad, M., Younger, M., Connors, B. W., Spray, D. C. & Srinivas, M. 2004. Potent block of Cx36 and Cx50 gap junction channels by mefloquine. *Proc Natl Acad Sci U S A,* 101**,** 12364-9.

Cryer, P. E. 1999. Hypoglycemia is the limiting factor in the management of diabetes. *Diabetes Metab Res Rev,* 15**,** 42-6.

Cryer, P. E. 2002. Hypoglycaemia: the limiting factor in the glycaemic management of Type I and Type II diabetes. *Diabetologia,* 45**,** 937-48.

Cryer, P. E. 2012. Minireview: Glucagon in the pathogenesis of hypoglycemia and hyperglycemia in diabetes. *Endocrinology,* 153**,** 1039-48.

Dahl, G. & Harris, A. L. 2009. Pannexins or connexins? *In Connexins: A Guide.* Totowa, NJ: Humana Press pp 287-301.

Dahl, G. & Locovei, S. 2006. Pannexin: to gap or not to gap, is that a question? *IUBMB Life,* 58**,** 409-19.

De Smedt, H., Missiaen, L., Parys, J. B., Bootman, M. D., Mertens, L., Van Den Bosch, L. & Casteels, R. 1994. Determination of relative amounts of inositol trisphosphate receptor mRNA isoforms by ratio polymerase chain reaction. *Journal of Biological Chemistry,* 269**,** 21691-21698.

De Vos, A., Heimberg, H., Quartier, E., Huypens, P., Bouwens, L., Pipeleers, D. & Schuit, F. 1995. Human and rat beta cells differ in glucose transporter but not in glucokinase gene expression. *J Clin Invest,* 96**,** 2489-95.

Di Gruccio, M., Mawla, A., Donaldson, C., Noguchi, G., Vaughan, J., Cowing-Zitron, C., Van Der Meulen, T. & Huising, M. 2016. Comprehensive alpha, beta and delta cell transcriptomes reveal that ghrelin selectively activates delta cells and promotes somatostatin release from pancreatic islets. *Molecular Metabolism,* Volume 5, **,** 449–458.

Dvoriantchikova, G., Ivanov, D., Barakat, D., Grinberg, A., Wen, R., Slepak, V. Z. & Shestopalov, V. I. 2012. Genetic ablation of pannexin1 protects retinal neurons from ischemic injury. *PLoS One,* 7**,** e31991.

Elliott, A. D., Ustione, A. & Piston, D. W. 2015. Somatostatin and insulin mediate glucose-inhibited glucagon secretion in the pancreatic alpha-cell by lowering cAMP. *Am J Physiol Endocrinol Metab,* 308**,** E130-43.

Endo, M. 1977. Calcium release from the sarcoplasmic reticulum. *Physiological Reviews,* 57**,** 71-108.

Fabiato, A. & Fabiato, F. 1975. Contractions induced by a calcium-triggered release of calcium from the sarcoplasmic reticulum of single skinned cardiac cells. *J Physiol,* 249**,** 469-95.

Feniuk, W., Jarvie, E., Luo, J. & Humphrey, P. P. A. 2000. Selective somatostatin sst(2) receptor blockade with the novel cyclic octapeptide, CYN-154806. *Neuropharmacology,* 39**,** 1443-1450.

Ferone, D., Pivonello, R., Kwekkeboom, D. J., Gatto, F., Ameri, P., Colao, A., De Krijger, R. R., Minuto, F., Lamberts, S. W. J., Van Hagen, P. M. & Hofland, L. J. 2012. Immunohistochemical localization and quantitative expression of somatostatin receptors in normal human spleen and thymus: Implications for the in vivo visualization during somatostatin receptor scintigraphy. *Journal of Endocrinological Investigation,* 35**,** 528-534.

Francis, B. H. & Ensinck, J. W. 1987. Differential alterations of the circulating prosomatostatin-derived peptides during insulin-induced hypoglycemia in man. *J Clin Endocrinol Metab,* 65**,** 880-4.

Friedrich, G. & Soriano, P. 1991. Promoter traps in embryonic stem-cells - a genetic screen to identify and mutate developmental genes in mice. *Genes & Development,* 5**,** 1513-1523.

Fujii, Y., Gonoi, T., Yamada, Y., Chihara, K., Inagaki, N. & Seino, S. 1994. Somatostatin receptor subtype SSTR2 mediates the inhibition of high-voltage-activated calcium channels by somatostatin and its analogue SMS 201-995. *FEBS Letters,* 355**,** 117-120.

Fujita, T. 1968. D cell, the third endocrine element of the pancreatic islet. *Arch Histol Jpn,* 29**,** 1-40.

Furshpan, E. J. & Potter, D. D. 1957. Mechanism of nerve-impulse transmission at a crayfish synapse. *Nature,* 180**,** 342-343.

Gafni, J., Munsch, J. A., Lam, T. H., Catlin, M. C., Costa, L. G., Molinski, T. F. & Pessah, I. N. 1997. Xestospongins: potent membrane permeable blockers of the inositol 1,4,5-trisphosphate receptor. *Neuron,* 19**,** 723-33.

Gerich, J. E. 1981. Somatostatin and diabetes. *Am J Med,* 70**,** 619-26.

Gerich, J. E. 1988. Lilly lecture 1988. Glucose counterregulation and its impact on diabetes mellitus. *Diabetes,* 37**,** 1608-17.

Ghezzi, C. & Wright, E. M. 2012. Regulation of the human Na^+-dependent glucose cotransporter hSGLT2. *American Journal of Physiology-Cell Physiology,* 303**,** C348-C354.

Goodenough, D. A. 1975. The structure of cell membranes involved in intercellular communication. *Am J Clin Pathol,* 63**,** 636-45.

Göpel, S. O., Kanno, T., Barg, S. & Rorsman, P. 2000. Patch-clamp characterisation of somatostatin-secreting -cells in intact mouse pancreatic islets. *J Physiol,* 528**,** 497-507.

Gould, G. W. & Holman, G. D. 1993. The glucose transporter family: structure, function and tissue-specific expression. *Biochem J,* 295 (Pt 2)**,** 329-41.

Greenbaum, C. J., Havel, P. J., Taborsky, G. J., Jr. & Klaff, L. J. 1991. Intra-islet insulin permits glucose to directly suppress pancreatic α–cell function. *J Clin Invest,* 88**,** 767-73.

Gribble, F. M., Davis, T. M., Higham, C. E., Clark, A. & Ashcroft, F. M. 2000. The antimalarial agent mefloquine inhibits ATP-sensitive K-channels. *Br J Pharmacol,* 131**,** 756-60.

Grill, V. & Efendić, S. 1984. Stimulation by calcium and barium of somatostatin release. Evidence for lower sensitivity of D- vis-à-vis B- and A-cells. *Acta Physiol Scand,* 122**,** 401-7.

Gromada, J., Høy, M., Buschard, K., Salehi, A. & Rorsman, P. 2001. Somatostatin inhibits exocytosis in rat pancreatic alpha-cells by G(i2)-dependent activation of calcineurin and depriming of secretory granules. *J Physiol,* 535**,** 519-32.

Grube, D. & Bohn, R. 1983. The microanatomy of human islets of Langerhans, with special reference to somatostatin D-cells. *Arch Histol Jpn,* 46**,** 327-53.

Halban, P. A., Wollheim, C. B., Blondel, B., Meda, P., Niesor, E. N. & Mintz, D. H. 1982. The possible importance of contact between pancreatic-islet cells for the control of insulin release. *Endocrinology,* 111**,** 86-94.

Hauge-Evans, A. C., Anderson, R. L., Persaud, S. J. & Jones, P. M. 2012. Delta cell secretory responses to insulin secretagogues are not mediated indirectly by insulin. *Diabetologia,* 55**,** 1995-2004.

Hauge-Evans, A. C., King, A. J., Carmignac, D., Richardson, C. C., Robinson, I. C., Low, M. J., Christie, M. R., Persaud, S. J. & Jones, P. M. 2009. Somatostatin secreted by islet δ-cells fulfills multiple roles as a paracrine regulator of islet function. *Diabetes,* 58**,** 403-11.

He, X., Wang, J., Wu, X., Kang, L. & Lan, P. 2009. Pancreatic somatostatinoma manifested as severe hypoglycemia. *J Gastrointestin Liver Dis,* 18**,** 221-4.

Heding, L. G. 1972. Determination of total serum insulin (IRI) in insulin-treated diabetic patients. *Diabetologia,* 8**,** 260-6.

Heimberg, H., De Vos, A., Moens, K., Quartier, E., Bouwens, L., Pipeleers, D., Van Schaftingen, E., Madsen, O. & Schuit, F. 1996. The glucose sensor protein glucokinase is expressed in glucagon-producing alpha-cells. *Proc Natl Acad Sci U S A,* 93**,** 7036-41.

Hellerstroem, C. & Hellman, B. 1960. Some aspects of silver impregnation of the islets of Langerhans in the rat. *Acta Endocrinol (Copenh),* 35**,** 518-32.

Hellman, B. 2009. Pulsatility of insulin release-a clinically important phenomenon. *Ups J Med Sci,* 114**,** 193-205.

Hellman, B., Salehi, A., Gylfe, E., Dansk, H. & Grapengiesser, E. 2009. Glucose generates coincident insulin and somatostatin pulses and antisynchronous glucagon pulses from human pancreatic islets. *Endocrinology,* 150**,** 5334-40.

Henquin, J.-C., Nenquin, M., Stiernet, P. & Ahren, B. 2006. *In vivo* and *in vitro* glucose-induced biphasic insulin secretion in the mouse. *Diabetes,* 55**,** 441.

Henquin, J. C. 2000. Triggering and amplifying pathways of regulation of insulin secretion by glucose. *Diabetes,* 49**,** 1751-60.

Henquin, J. C. 2004. Pathways in β-cell stimulus-secretion coupling as targets for therapeutic insulin secretagogues. *Diabetes,* 53 Suppl 3**,** S48-58.

Hobart, P., Crawford, R., Shen, L., Pictet, R. & Rutter, W. J. 1980. Cloning and sequence analysis of cDNAs encoding two distinct somatostatin precursors found in the endocrine pancreas of anglerfish. *Nature,* 288**,** 137-41.

Hökfelt, T., Efendić, S., Hellerström, C., Johansson, O., Luft, R. & Arimura, A. 1975. Cellular localization of somatostatin in endocrine-like cells and neurons of the rat with special references to the A1-cells of the pancreatic islets and to the hypothalamus. *Acta Endocrinol Suppl (Copenh),* 200**,** 5-41.

Huang, L., Shen, H., Atkinson, M. A. & Kennedy, R. T. 1995. Detection of exocytosis at individual pancreatic beta-cells by amperometry at a chemically-modified microelectrode. *Proceedings of the National Academy of Sciences of the United States of America,* 92**,** 9608-9612.

Iguchi, H., Hayashi, I. & Kono, A. 1990. A somatostatin-secreting cell line established from a human pancreatic islet cell carcinoma (somatostatinoma): release experiment and immunohistochemical study. *Cancer Res,* 50**,** 3691-3.

Ipp, E., Rivier, J., Dobbs, R. E., Brown, M., Vale, W. & Unger, R. H. 1979. Somatostatin analogs inhibit somatostatin release. *Endocrinology,* 104**,** 1270-3.

Johnson, J. H., Newgard, C. B., Milburn, J. L., Lodish, H. F. & Thorens, B. 1990. The high Km glucose transporter of islets of Langerhans is functionally similar to the low affinity transporter of liver and has an identical primary sequence. *J Biol Chem,* 265**,** 6548-51.

Kailey, B., Van De Bunt, M., Cheley, S., Johnson, P. R., Macdonald, P. E., Gloyn, A. L., Rorsman, P. & Braun, M. 2012. SSTR2 is the functionally dominant somatostatin receptor in human pancreatic β- and α-cells. *Am J Physiol Endocrinol Metab,* 303**,** E1107-16.

Karimian, N., Qin, T., Liang, T., Osundiji, M., Huang, Y., Teich, T., Riddell, M. C., Cattral, M. S., Coy, D. H., Vranic, M. & Gaisano, H. Y. 2013. Somatostatin receptor type 2 antagonism improves glucagon counterregulation in biobreeding diabetic rats. *Diabetes,* 62**,** 2968-77.

Kawamori, D., Kurpad, A. J., Hu, J., Liew, C. W., Shih, J. L., Ford, E. L., Herrera, P. L., Polonsky, K. S., Mcguinness, O. P. & Kulkarni, R. N. 2009. Insulin signaling in alpha cells modulates glucagon secretion in vivo. *Cell Metab,* 9**,** 350-61.

Kim, A., Miller, K., Jo, J., Kilimnik, G., Wojcik, P. & Hara, M. 2009. Islet architecture: A comparative study. *Islets,* 1**,** 129-36.

Koerker, D. J., Ruch, W., Chideckel, E., Palmer, J., Goodner, C. J., Ensinck, J. & Gale, C. C. 1974. Somatostatin: hypothalamic inhibitor of the endocrine pancreas. *Science,* 184**,** 482-4.

Kreienkamp, H. J., Hönck, H. H. & Richter, D. 1997. Coupling of rat somatostatin receptor subtypes to a G-protein gated inwardly rectifying potassium channel (GIRK1). *FEBS Lett,* 419**,** 92-4.

Kulkarni, R. N., Bruning, J. C., Winnay, J. N., Postic, C., Magnuson, M. A. & Kahn, C. R. 1999. Tissue-specific knockout of the insulin receptor in pancreatic beta cells creates an insulin secretory defect similar to that in type 2 diabetes. *Cell,* 96**,** 329-39.

Kumar, N. M. & Gilula, N. B. 1996. The gap junction communication channel. *Cell,* 84**,** 381-8.

Kumar, U., Sasi, R., Suresh, S., Patel, A., Thangaraju, M., Metrakos, P., Patel, S. C. & Patel, Y. C. 1999. Subtype-selective expression of the five somatostatin receptors (hSSTR1-5) in human pancreatic islet cells: a quantitative double-label immunohistochemical analysis. *Diabetes,* 48**,** 77-85.

Langerhans, P. 1869 Eiträge zur mikroskopischen Anatomie der Bauspeicheldrüse. Inaugeral-Dissertation. Friedrich-Wilhelms-Universität. pp 1±39. *(translation by Morrison H (1937) B Berlin, pp 1±32 as Contributions to the microscopic anatomy of the pancreas. John Hopkins Press, Baltimore)*.

Le Marchand, S. J. & Piston, D. W. 2010. Glucose suppression of glucagon secretion: metabolic and calcium responses from alpha-cells in intact mouse pancreatic islets. *J Biol Chem,* 285**,** 14389-98.

Leclair, E., Liggins, R. T., Peckett, A. J., Teich, T., Coy, D. H., Vranic, M. & Riddell, M. C. 2016. Glucagon responses to exercise-induced hypoglycaemia are improved by somatostatin receptor type 2 antagonism in a rat model of diabetes. *Diabetologia,* 59**,** 1724-31.

Lee, B. & Laychock, S. G. 2001. Inositol 1,4,5-trisphosphate receptor isoform expression in mouse pancreatic islets: effects of carbachol. *Biochemical Pharmacology,* 61**,** 327-336.

Lefebvre, P. J. & Luyckx, A. S. 1979. Glucagon and diabetes: a reappraisal. *Diabetologia,* 16**,** 347-54.

Leibiger, B., Leibiger, I. B., Moede, T., Kemper, S., Kulkarni, R. N., Kahn, C. R., De Vargas, L. M. & Berggren, P. O. 2001. Selective insulin signaling through A and B insulin receptors regulates transcription of insulin and glucokinase genes in pancreatic beta cells. *Mol Cell,* 7**,** 559-70.

Lohr, C. 2003. Monitoring neuronal calcium signalling using a new method for ratiometric confocal calcium imaging. *Cell Calcium,* 34**,** 295-303.

Low, M. J., Otero-Corchon, V., Parlow, A. F., Ramirez, J. L., Kumar, U., Patel, Y. C. & Rubinstein, M. 2001. Somatostatin is required for masculinization of growth hormone-regulated hepatic gene expression but not of somatic growth. *J Clin Invest,* 107**,** 1571-80.

Luche, H., Weber, O., Nageswara Rao, T., Blum, C. & Fehling, H. J. 2007. Faithful activation of an extra-bright red fluorescent protein in "knock-in" Cre-reporter mice ideally suited for lineage tracing studies. *Eur J Immunol,* 37**,** 43-53.

Ludvigsen, E., Olsson, R., Stridsberg, M., Janson, E. T. & Sandler, S. 2004. Expression and distribution of somatostatin receptor subtypes in the pancreatic islets of mice and rats. *Journal of Histochemistry & Cytochemistry,* 52**,** 391-400.

Macdonald, P. E., De Marinis, Y. Z., Ramracheya, R., Salehi, A., Ma, X., Johnson, P. R., Cox, R., Eliasson, L. & Rorsman, P. 2007. A K ATP channel-dependent pathway within alpha cells regulates glucagon release from both rodent and human islets of Langerhans. *PLoS Biol,* 5**,** e143.

Macotela, Y., Boucher, J., Tran, T. T. & Kahn, C. R. 2009. Sex and depot differences in adipocyte insulin sensitivity and glucose metabolism. *Diabetes,* 58**,** 803-12.

Maechler, P. & Wollheim, C. B. 1999. Mitochondrial glutamate acts as a messenger in glucose-induced insulin exocytosis. *Nature,* 402**,** 685-9.

Marcinkiewicz, M., Ramla, D., Seidah, N. G. & Chrétien, M. 1994. Developmental expression of the prohormone convertases PC1 and PC2 in mouse pancreatic islets. *Endocrinology,* 135**,** 1651-60.

Maruyama, H., Hisatomi, A., Orci, L., Grodsky, G. M. & Unger, R. H. 1984. Insulin within islets is a physiologic glucagon release inhibitor. *J Clin Invest,* 74**,** 2296-9.

Matschinsky, F. M. 1990. Glucokinase as glucose sensor and metabolic signal generator in pancreatic beta-cells and hepatocytes. *Diabetes,* 39**,** 647-52.

Mcwilliam, H., Li, W., Uludag, M., Squizzato, S., Park, Y. M., Buso, N., Cowley, A. P. & Lopez, R. 2013. Analysis tool web services from the EMBL-EBI. *Nucleic Acids Research,* 41**,** W597-W600.

Meda, P. 2013. Protein-mediated interactions of pancreatic islet cells. *Scientifica (Cairo),* 2013**,** 621249.

Meda, P., Kohen, E., Kohen, C., Rabinovitch, A. & Orci, L. 1982. Direct communication of homologous and heterologous endocrine islet cells in culture. *Journal of Cell Biology,* 92**,** 221-226.

Menge, B. A., Grüber, L., Jørgensen, S. M., Deacon, C. F., Schmidt, W. E., Veldhuis, J. D., Holst, J. J. & Meier, J. J. 2011. Loss of inverse relationship between pulsatile insulin and glucagon secretion in patients with type 2 diabetes. *Diabetes,* 60**,** 2160-8.

Michaels, R. L. & Sheridan, J. D. 1981. Islets of Langerhans: dye coupling among immunocytochemically distinct cell types. *Science,* 214**,** 801-3.

Molina, J., Rodriguez-Diaz, R., Fachado, A., Jacques-Silva, M. C., Berggren, P. O. & Caicedo, A. 2014. Control of insulin secretion by cholinergic signaling in the human pancreatic islet. *Diabetes,* 63**,** 2714-2726.

Muniyappa, R., Lee, S., Chen, H. & Quon, M. J. 2008. Current approaches for assessing insulin sensitivity and resistance in vivo: advantages, limitations, and appropriate usage. *American Journal of Physiology - Endocrinology And Metabolism,* 294**,** E15-E26.

Nadal, A., Quesada, I. & Soria, B. 1999. Homologous and heterologous asynchronicity between identified alpha-, beta- and delta-cells within intact islets of Langerhans in the mouse. *J Physiol,* 517 (Pt 1)**,** 85-93.

Nagasaki, K. & Fleischer, S. 1988. Ryanodine sensitivity of the calcium release channel of sarcoplasmic reticulum. *Cell Calcium,* 9**,** 1-7.

Nakai, J., Ohkura, M. & Imoto, K. 2001. A high signal-to-noise Ca^{2+} probe composed of a single green fluorescent protein. *Nat Biotechnol,* 19**,** 137-41.

Naylor, E., Arredouani, A., Vasudevan, S. R., Lewis, A. M., Parkesh, R., Mizote, A., Rosen, D., Thomas, J. M., Izumi, M., Ganesan, A., Galione, A. & Churchill, G. C. 2009. Identification of a chemical probe for NAADP by virtual screening. *Nat Chem Biol,* 5**,** 220-6.

Nica, A. C., Ongen, H., Irminger, J. C., Bosco, D., Berney, T., Antonarakis, S. E., Halban, P. A. & Dermitzakis, E. T. 2013. Cell-type, allelic, and genetic signatures in the human pancreatic beta cell transcriptome. *Genome Research,* 23**,** 1554-1562.

Nita, Ii, Hershfinkel, M., Fishman, D., Ozeri, E., Rutter, G. A., Sensi, S. L., Khananshvili, D., Lewis, E. C. & Sekler, I. 2012. The mitochondrial Na^{+}/Ca^{2+} exchanger upregulates glucose dependent Ca^{2+} signalling linked to insulin secretion. *PLoS One,* 7**,** e46649.

O'rahilly, S., Turner, R. C. & Matthews, D. R. 1988. Impaired pulsatile secretion of insulin in relatives of patients with non-insulin-dependent diabetes. *N Engl J Med,* 318**,** 1225-30.

Oheim, M., Van 'T Hoff, M., Feltz, A., Zamaleeva, A., Mallet, J. M. & Collot, M. 2014. New red-fluorescent calcium indicators for optogenetics, photoactivation and multi-color imaging. *Biochim Biophys Acta,* 1843**,** 2284-306.

Oka, T., Sato, K., Hori, M., Ozaki, H. & Karaki, H. 2002. Xestospongin C, a novel blocker of IP(3) receptor, attenuates the increase in cytosolic calcium level and degranulation that is induced by antigen in RBL-2H3 mast cells. *Br J Pharmacol,* 135**,** 1959-66.

Orci, L., Baetens, D., Rufener, C., Amherdt, M., Ravazzola, M., Studer, P., Malaisse-Lagae, F. & Unger, R. H. 1976. Hypertrophy and hyperplasia of somatostatin-containing D-cells in diabetes. *Proc Natl Acad Sci U S A,* 73**,** 1338-42.

Orci, L., Malaisse-Lagae, F., Ravazzola, M., Rouiller, D., Renold, A. E., Perrelet, A. & Unger, R. 1975. A morphological basis for intercellular communication between alpha- and beta-cells in the endocrine pancreas. *J Clin Invest,* 56**,** 1066-70.

Orci, L. & Unger, R. H. 1975. Functional subdivision of islets of Langerhans and possible role of D cells. *Lancet,* 2**,** 1243-4.

Orci, L., Unger, R. H. & Renold, A. E. 1973. Structural coupling between pancreatic-islet cells. *Experientia,* 29**,** 1015-1018.

Panchin, Y., Kelmanson, I., Matz, M., Lukyanov, K., Usman, N. & Lukyanov, S. 2000. A ubiquitous family of putative gap junction molecules. *Curr Biol,* 10**,** R473-4.

Paredes, R. M., Etzler, J. C., Watts, L. T. & Lechleiter, J. D. 2008. Chemical Calcium Indicators. *Methods (San Diego, Calif.),* 46**,** 143-151.

Patel, Y. C. 1992. General aspects of the biology and function of somatostatin. *Somatostatin.* Berlin, Heidelberg: Springer Berlin Heidelberg pp 1-16.

Patel, Y. C., Liu, J.-L., Galanopoulou, A. & Papachristou, D. N. 2010. Production, action, and degradation of somatostatin. *Comprehensive Physiology.* John Wiley & Sons, Inc.

Patel, Y. C. & Srikant, C. B. 1997. Somatostatin receptors. *Trends Endocrinol Metab,* 8**,** 398-405.

Patel, Y. C., Wheatley, T. & Ning, C. 1981. Multiple forms of immunoreactive somatostatin: comparison of distribution in neural and nonneural tissues and portal plasma of the rat. *Endocrinology,* 109**,** 1943-9.

Patel, Y. C., Wheatley, T. & Zingg, H. H. 1980. Increased blood somatostatin concentration in streptozotocin diabetic rats. *Life Sci,* 27**,** 1563-70.

Pelegrin, P. & Surprenant, A. 2006. Pannexin-1 mediates large pore formation and interleukin-1beta release by the ATP-gated P2X7 receptor. *EMBO J,* 25**,** 5071-82.

Penuela, S., Bhalla, R., Gong, X. Q., Cowan, K. N., Celetti, S. J., Cowan, B. J., Bai, D., Shao, Q. & Laird, D. W. 2007. Pannexin 1 and pannexin 3 are glycoproteins that exhibit many distinct characteristics from the connexin family of gap junction proteins. *Journal of Cell Science,* 120**,** 3772-3783.

Penuela, S., Gehi, R. & Laird, D. W. 2013. The biochemistry and function of pannexin channels. *Biochimica Et Biophysica Acta-Biomembranes,* 1828**,** 15-22.

Polak, J. M., Pearse, A. G., Grimelius, L. & Bloom, S. R. 1975. Growth-hormone release-inhibiting hormone in gastrointestinal and pancreatic D cells. *Lancet,* 1**,** 1220-2.

Quesada, I., Fuentes, E., Andreau, E., Meda, P., Nadal, A. & Soria, B. 2003. On-line analysis of gap junctions reveals more efficient electrical than dye coupling between islet cells. *American Journal of Physiology-Endocrinology and Metabolism,* 284**,** E980-E987.

Quesada, I., Nadal, A. & Soria, B. 1999. Different effects of tolbutamide and diazoxide in alpha, beta-, and delta-cells within intact islets of Langerhans. *Diabetes,* 48**,** 2390-7.

Rasband, W. S. 1997-2016. ImageJ, U.S. National Institutes of Health, Bethesda, Maryland, USA, http://imagej.nih.gov/ij/,.

Ravassard, P., Hazhouz, Y., Pechberty, S., Bricout-Neveu, E., Armanet, M., Czernichow, P. & Scharfmann, R. 2011. A genetically engineered human pancreatic β cell line exhibiting glucose-inducible insulin secretion. *J Clin Invest,* 121**,** 3589-97.

Ravier, M. A., Güldenagel, M., Charollais, A., Gjinovci, A., Caille, D., Söhl, G., Wollheim, C. B., Willecke, K., Henquin, J. C. & Meda, P. 2005. Loss of connexin36 channels alters beta-cell coupling, islet synchronization of glucose-induced Ca^{2+} and insulin oscillations, and basal insulin release. *Diabetes,* 54**,** 1798-807.

Ravier, M. A. & Rutter, G. A. 2005. Glucose or insulin, but not zinc ions, inhibit glucagon secretion from mouse pancreatic alpha-cells. *Diabetes,* 54**,** 1789-97.

Renström, E., Ding, W. G., Bokvist, K. & Rorsman, P. 1996. Neurotransmitter-induced inhibition of exocytosis in insulin-secreting beta cells by activation of calcineurin. *Neuron,* 17**,** 513-22.

Rodriguez-Diaz, R., Abdulreda, M. H., Formoso, A. L., Gans, I., Ricordi, C., Berggren, P. O. & Caicedo, A. 2011. Innervation patterns of autonomic axons in the human endocrine pancreas. *Cell Metab,* 14**,** 45-54.

Rodriguez-Diaz, R., Speier, S., Molano, R. D., Formoso, A., Gans, I., Abdulreda, M. H., Cabrera, O., Molina, J., Fachado, A., Ricordi, C., Leibiger, I., Pileggi, A., Berggren, P. O. & Caicedo, A. 2012. Noninvasive in vivo model demonstrating the effects of autonomic innervation on pancreatic islet function. *Proc Natl Acad Sci U S A,* 109**,** 21456-61.

Rorsman, P., Berggren, P. O., Bokvist, K., Ericson, H., Mohler, H., Ostenson, C. G. & Smith, P. A. 1989. Glucose-inhibition of glucagon secretion involves activation of GABAA-receptor chloride channels. *Nature,* 341**,** 233-6.

Rorsman, P. & Renstrom, E. 2003. Insulin granule dynamics in pancreatic beta cells. *Diabetologia,* 46**,** 1029-45.

Saez, J. C., Retamal, M. A., Basilio, D., Bukauskas, F. F. & Bennett, M. V. 2005. Connexin-based gap junction hemichannels: gating mechanisms. *Biochim Biophys Acta,* 1711**,** 215-24.

Sahu, G., Sukumaran, S. & Bera, A. K. 2014. Pannexins form gap junctions with electrophysiological and pharmacological properties distinct from connexins. *Scientific Reports,* 4.

Sakura, H., Ashcroft, S. J., Terauchi, Y., Kadowaki, T. & Ashcroft, F. M. 1998. Glucose modulation of ATP-sensitive K-currents in wild-type, homozygous and heterozygous glucokinase knock-out mice. *Diabetologia,* 41**,** 654-9.

Salehi, A., Qader, S. S., Grapengiesser, E. & Hellman, B. 2007. Pulses of somatostatin release are slightly delayed compared with insulin and antisynchronous to glucagon. *Regul Pept,* 144**,** 43-9.

Samols, E. & Harrison, J. 1976. Intraislet negative insulin-glucagon feedback. *Metabolism,* 25**,** 1443-7.

Samols, E., Tyler, J. M. & Marks, V. 1972. Glucagon-Insulin interrelationships, in Lefebvre P, Unger R (ed): Glucagon, New York, Pergamon,. pp 151-173.

Santos, R. M., Rosario, L. M., Nadal, A., Garcia-Sancho, J., Soria, B. & Valdeolmillos, M. 1991. Widespread synchronous $[Ca^{2+}]_i$ oscillations due to bursting electrical activity in single pancreatic islets. *Pflugers Arch,* 418**,** 417-22.

Schafer, J., Baumeister, H., Lorenz, A. & Meyerhof, W. 1998. Localization of somatostatin receptor subtype mRNA in the rat gastrointestinal tract and regulation of SSTR1 gene expression. *Z Ernahrungswiss,* 37 Suppl 1**,** 75-9.

Schäffer, L., Brand, C. L., Hansen, B. F., Ribel, U., Shaw, A. C., Slaaby, R. & Sturis, J. 2008. A novel high-affinity peptide antagonist to the insulin receptor. *Biochemical and Biophysical Research Communications,* 376**,** 380-383.

Schmidt-Supprian, M. & Rajewsky, K. 2007. Vagaries of conditional gene targeting. *Nature Immunology,* 8**,** 665-668.

Schmittgen, T. D. & Livak, K. J. 2008. Analyzing real-time PCR data by the comparative C(T) method. *Nat Protoc,* 3**,** 1101-8.

Schuit, F., Moens, K., Heimberg, H. & Pipeleers, D. 1999. Cellular origin of hexokinase in pancreatic islets. *Journal of Biological Chemistry,* 274**,** 32803-32809.

Seino, S., Takahashi, H., Fujimoto, W. & Shibasaki, T. 2009. Roles of cAMP signalling in insulin granule exocytosis. *Diabetes Obes Metab,* 11 Suppl 4**,** 180-8.

Serre-Beinier, V., Bosco, D., Zulianello, L., Charollais, A., Caille, D., Charpantier, E., Gauthier, B. R., Diaferia, G. R., Giepmans, B. N., Lupi, R., Marchetti, P., Deng, S., Buhler, L., Berney, T., Cirulli, V. & Meda, P. 2009. Cx36 makes channels coupling human pancreatic beta-cells, and correlates with insulin expression. *Hum Mol Genet,* 18**,** 428-39.

Serre-Beinier, V., Le Gurun, S., Belluardo, N., Trovato-Salinaro, A., Charollais, A., Haefliger, J. A., Condorelli, D. F. & Meda, P. 2000. Cx36 preferentially connects beta-cells within pancreatic islets. *Diabetes,* 49**,** 727-34.

Sheppard, M., Shapiro, B., Pimstone, B., Kronheim, S., Berelowitz, M. & Gregory, M. 1979. Metabolic clearance and plasma half-disappearance time of exogenous somatostatin in man. *J Clin Endocrinol Metab,* 48**,** 50-3.

Short, K. W., Head, W. S. & Piston, D. W. 2014. Connexin 36 mediates blood cell flow in mouse pancreatic islets. *Am J Physiol Endocrinol Metab,* 306**,** E324-31.

Smith, W. H., Nair, R. U., Adamson, D., Kearney, M. T., Ball, S. G. & Balmforth, A. J. 2005. Somatostatin receptor subtype expression in the human heart: differential expression by myocytes and fibroblasts. *J Endocrinol,* 187**,** 379-86.

Snutch, T. P., Peloquin, J., Mathews, E. & Mcrory, J. E. 2000-2013. Molecular properties of voltage-gated Ca^{2+} channels. In: Madame Curie Bioscience Database [Internet]. Austin (TX). Landes Bioscience;. https://www.ncbi.nlm.nih.gov/books/NBK6181/.

Sosinsky, G. E., Boassa, D., Dermietzel, R., Duffy, H. S., Laird, D. W., Macvicar, B., Naus, C. C., Penuela, S., Scemes, E., Spray, D. C., Thompson, R. J., Zhao, H. B. & Dahl, G. 2011. Pannexin channels are not gap junction hemichannels. *Channels (Austin),* 5**,** 193-7.

Speier, S., Nyqvist, D., Cabrera, O., Yu, J., Molano, R. D., Pileggi, A., Moede, T., Kohler, M., Wilbertz, J., Leibiger, B., Ricordi, C., Leibiger, I. B., Caicedo, A. & Berggren, P. O. 2008. Noninvasive in vivo imaging of pancreatic islet cell biology. *Nat Med,* 14**,** 574-8.

Srikant, C. B. & Patel, Y. C. 1986. Somatostatin receptors on rat pancreatic acinar cells. Pharmacological and structural characterization and demonstration of down-regulation in streptozotocin diabetes. *J Biol Chem,* 261**,** 7690-6.

Steiner, D. J., Kim, A., Miller, K. & Hara, M. 2010. Pancreatic islet plasticity: interspecies comparison of islet architecture and composition. *Islets,* 2**,** 135-45.

Stozer, A., Gosak, M., Dolensek, J., Perc, M., Marhl, M., Rupnik, M. S. & Korosak, D. 2013. Functional connectivity in islets of Langerhans from mouse pancreas tissue slices. *PLoS Comput Biol,* 9**,** e1002923.

Strowski, M. Z., Kohler, M., Chen, H. Y., Trumbauer, M. E., Li, Z., Szalkowski, D., Gopal-Truter, S., Fisher, J. K., Schaeffer, J. M., Blake, A. D., Zhang, B. B. & Wilkinson, H. A. 2003. Somatostatin receptor subtype 5 regulates insulin secretion and glucose homeostasis. *Mol Endocrinol,* 17**,** 93-106.

Strowski, M. Z., Parmar, R. M., Blake, A. D. & Schaeffer, J. M. 2000. Somatostatin inhibits insulin and glucagon secretion via two receptors subtypes: an in vitro study of pancreatic islets from somatostatin receptor 2 knockout mice. *Endocrinology,* 141**,** 111-7.

Taborsky, G. J., Jr., Smith, P. H. & Porte, D., Jr. 1978. Interaction of somatostatin with the A and B cells of the endocrine pancreas. *Metabolism,* 27**,** 1299-302.

Takahashi, A., Camacho, P., Lechleiter, J. D. & Herman, B. 1999. Measurement of intracellular calcium. *Physiological Reviews,* 79**,** 1089-1125.

Taniguchi, H., He, M., Wu, P., Kim, S., Paik, R., Sugino, K., Kvitsiani, D., Fu, Y., Lu, J., Lin, Y., Miyoshi, G., Shima, Y., Fishell, G., Nelson, S. B. & Huang, Z. J. 2011. A resource of Cre driver lines for genetic targeting of GABAergic neurons in cerebral cortex. *Neuron,* 71**,** 995-1013.

Thastrup, O., Cullen, P. J., Drøbak, B. K., Hanley, M. R. & Dawson, A. P. 1990. Thapsigargin, a tumor promoter, discharges intracellular Ca^{2+} stores by specific inhibition of the endoplasmic reticulum Ca^{2+}-ATPase. *Proceedings of the National Academy of Sciences of the United States of America,* 87**,** 2466-2470.

Theis, M., Mas, C., Doring, B., Degen, J., Brink, C., Caille, D., Charollais, A., Kruger, O., Plum, A., Nepote, V., Herrera, P., Meda, P. & Willecke, K. 2004. Replacement by a lacZ reporter gene assigns mouse connexin36, 45 and 43 to distinct cell types in pancreatic islets. *Exp Cell Res,* 294**,** 18-29.

Thomas, R. L., Mistry, R., Langmead, C. J., Wood, M. D. & Challiss, R. A. 2008. G protein coupling and signaling pathway activation by m1 muscarinic acetylcholine receptor orthosteric and allosteric agonists. *J Pharmacol Exp Ther,* 327**,** 365-74.

Thompson, R. J., Jackson, M. F., Olah, M. E., Rungta, R. L., Hines, D. J., Beazely, M. A., Macdonald, J. F. & Macvicar, B. A. 2008. Activation of pannexin-1 hemichannels augments aberrant bursting in the hippocampus. *Science,* 322**,** 1555-9.

Thorens, B. 2014. Neural regulation of pancreatic islet cell mass and function. *Diabetes Obes Metab,* 16 Suppl 1**,** 87-95.

Thorens, B., Sarkar, H. K., Kaback, H. R. & Lodish, H. F. 1988. Cloning and functional expression in bacteria of a novel glucose transporter present in liver, intestine, kidney, and beta-pancreatic islet cells. *Cell,* 55**,** 281-90.

Thoss, V. S., Pérez, J., Probst, A. & Hoyer, D. 1996. Expression of five somatostatin receptor mRNAs in the human brain and pituitary. *Naunyn-Schmiedeberg's Archives of Pharmacology,* 354**,** 411-419.

Tian, L., Hires, S. A., Mao, T., Huber, D., Chiappe, M. E., Chalasani, S. H., Petreanu, L., Akerboom, J., Mckinney, S. A., Schreiter, E. R., Bargmann, C. I., Jayaraman, V., Svoboda, K. & Looger, L. L. 2009. Imaging neural activity in worms, flies and mice with improved GCaMP calcium indicators. *Nat Methods,* 6**,** 875-81.

Ueberberg, B., Tourne, H., Redman, A., Walz, M. K., Schmid, K. W., Mann, K. & Petersenn, S. 2005. Differential expression of the human somatostatin receptor subtypes sst1 to sst5 in various adrenal tumors and normal adrenal gland. *Hormone and Metabolic Research,* 37**,** 722-728.

Unek, I. T., Celtik, A., Yener, S., Yavuzsen, T., Alacacioglu, A., Cokmert, S., Oztop, I., Demirkan, B., Dicle, O., Sagol, O., Bekis, R. & Yilmaz, U. 2009. Hypoglycemia induced by long-acting somatostatin analogues in a patient with nonfunctional neuroendocrine tumor. *J BUON,* 14**,** 135-8.

Unger, R. H. & Orci, L. 1977. Possible roles of the pancreatic D-cell in the normal and diabetic states. *Diabetes,* 26**,** 241-4.

Unger, R. H. & Orci, L. 1982. The role of glucagon in diabetes. *Compr Ther,* 8**,** 53-9.

Van Der Meulen, T., Donaldson, C. J., Caceres, E., Hunter, A. E., Cowing-Zitron, C., Pound, L. D., Adams, M. W., Zembrzycki, A., Grove, K. L. & Huising, M. O. 2015. Urocortin3 mediates somatostatin-dependent negative feedback control of insulin secretion. *Nat Med,* 21**,** 769-76.

Varecza, Z., Elekes, K., László, T., Perkecz, A., Pintér, E., Sándor, Z., Szolcsányi, J., Keszthelyi, D., Szabó, Á., Sándor, K., Molnár Tá, F., Szántó, Z., Pongrácz, J. E. & Helyes, Z. 2009. Expression of the Somatostatin Receptor Subtype 4 in Intact and Inflamed Pulmonary Tissues. *J Histochem Cytochem,* 57**,** 1127-37.

Vessey, J. P., Lalonde, M. R., Mizan, H. A., Welch, N. C., Kelly, M. E. & Barnes, S. 2004. Carbenoxolone inhibition of voltage-gated Ca^{2+} channels and synaptic transmission in the retina. *J Neurophysiol,* 92**,** 1252-6.

Vieira, E., Salehi, A. & Gylfe, E. 2007. Glucose inhibits glucagon secretion by a direct effect on mouse pancreatic alpha cells. *Diabetologia,* 50**,** 370-9.

Walker, J. N., Ramracheya, R., Zhang, Q., Johnson, P. R., Braun, M. & Rorsman, P. 2011. Regulation of glucagon secretion by glucose: paracrine, intrinsic or both? *Diabetes Obes Metab,* 13 Suppl 1**,** 95-105.

Wang, J., Ma, M., Locovei, S., Keane, R. W. & Dahl, G. 2007. Modulation of membrane channel currents by gap junction protein mimetic peptides: size matters. *Am J Physiol Cell Physiol,* 293**,** C1112-9.

Wass, J. A., Penman, E., Medbak, S., Dawson, A. M., Tsiolakis, D., Marks, V., Besser, G. M. & Rees, L. H. 1980. Immunoreactive somatostatin changes during insulin-induced hypoglycaemia and operative stress in man. *Clin Endocrinol (Oxf),* 12**,** 269-75.

Webb, S., Levy, I., Wass, J. A., Llorens, A., Penman, E., Casamitjana, R., Wu, P., Gaya, J., Martinez, M. J. & Rivera, F. 1984. Studies on the mechanisms of somatostatin release after insulin induced hypoglycaemia in man. *Clin Endocrinol (Oxf),* 21**,** 667-75.

Weidmann, S. 1952. The electrical constants of Purkinje fibres. *J Physiol,* 118**,** 348-60.

Wellershaus, K., Degen, J., Deuchars, J., Theis, M., Charollais, A., Caille, D., Gauthier, B., Janssen-Bienhold, U., Sonntag, S., Herrera, P., Meda, P. & Willecke, K. 2008. A new conditional mouse mutant reveals specific expression and functions of connexin36 in neurons and pancreatic beta-cells. *Exp Cell Res,* 314**,** 997-1012.

Willecke, K., Eiberger, J., Degen, J., Eckardt, D., Romualdi, A., Guldenagel, M., Deutsch, U. & Sohl, G. 2002. Structural and functional diversity of connexin genes in the mouse and human genome. *Biol Chem,* 383**,** 725-37.

Xu, E., Kumar, M., Zhang, Y., Ju, W., Obata, T., Zhang, N., Liu, S., Wendt, A., Deng, S., Ebina, Y., Wheeler, M. B., Braun, M. & Wang, Q. 2006. Intra-islet insulin suppresses glucagon release via GABA-GABAA receptor system. *Cell Metab,* 3**,** 47-58.

Yue, J. T., Burdett, E., Coy, D. H., Giacca, A., Efendic, S. & Vranic, M. 2012. Somatostatin receptor type 2 antagonism improves glucagon and corticosterone counterregulatory responses to hypoglycemia in streptozotocin-induced diabetic rats. *Diabetes,* 61**,** 197-207.

Yue, J. T., Riddell, M. C., Burdett, E., Coy, D. H., Efendic, S. & Vranic, M. 2013. Amelioration of hypoglycemia via somatostatin receptor type 2 antagonism in recurrently hypoglycemic diabetic rats. *Diabetes,* 62**,** 2215-22.

Zariwala, H. A., Borghuis, B. G., Hoogland, T. M., Madisen, L., Tian, L., De Zeeuw, C. I., Zeng, H., Looger, L. L., Svoboda, K. & Chen, T. W. 2012. A Cre-dependent GCaMP3 reporter mouse for neuronal imaging in vivo. *J Neurosci,* 32**,** 3131-41.

Zhang, J., Dublin, P., Griemsmann, S., Klein, A., Brehm, R., Bedner, P., Fleischmann, B. K., Steinhauser, C. & Theis, M. 2013a. Germ-line recombination activity of the widely used hGFAP-Cre and nestin-Cre transgenes. *Plos One,* 8.

Zhang, Q., Bengtsson, M., Partridge, C., Salehi, A., Braun, M., Cox, R., Eliasson, L., Johnson, P. R., Renström, E., Schneider, T., Berggren, P. O., Göpel, S., Ashcroft, F. M. & Rorsman, P. 2007. R-type Ca^{2+}-channel-evoked CICR regulates glucose-induced somatostatin secretion. *Nat Cell Biol,* 9**,** 453-60.

Zhang, Q., Ramracheya, R., Lahmann, C., Tarasov, A., Bengtsson, M., Braha, O., Braun, M., Brereton, M., Collins, S., Galvanovskis, J., Gonzalez, A., Groschner, L. N., Rorsman, N. J., Salehi, A., Travers, M. E., Walker, J. N., Gloyn, A. L., Gribble, F., Johnson, P. R., Reimann, F., Ashcroft, F. M. & Rorsman, P. 2013b. Role of KATP channels in glucose-regulated glucagon secretion and impaired counterregulation in type 2 diabetes. *Cell Metab,* 18**,** 871-82.

Zimanyi, I., Buck, E., Abramson, J. J., Mack, M. M. & Pessah, I. N. 1992. Ryanodine induces persistent inactivation of the Ca^{2+} release channel from skeletal muscle sarcoplasmic reticulum. *Mol Pharmacol,* 42**,** 1049-57.